UiT
THE ARCTIC
UNIVERSITY
OF NORWAY

Department of Mathematics and Statistics

The EOS Formulation for Linear and Nonlinear Transient Scattering Problems

Aihua Lin

A dissertation for the degree of Philosophiae Doctor – December 2018

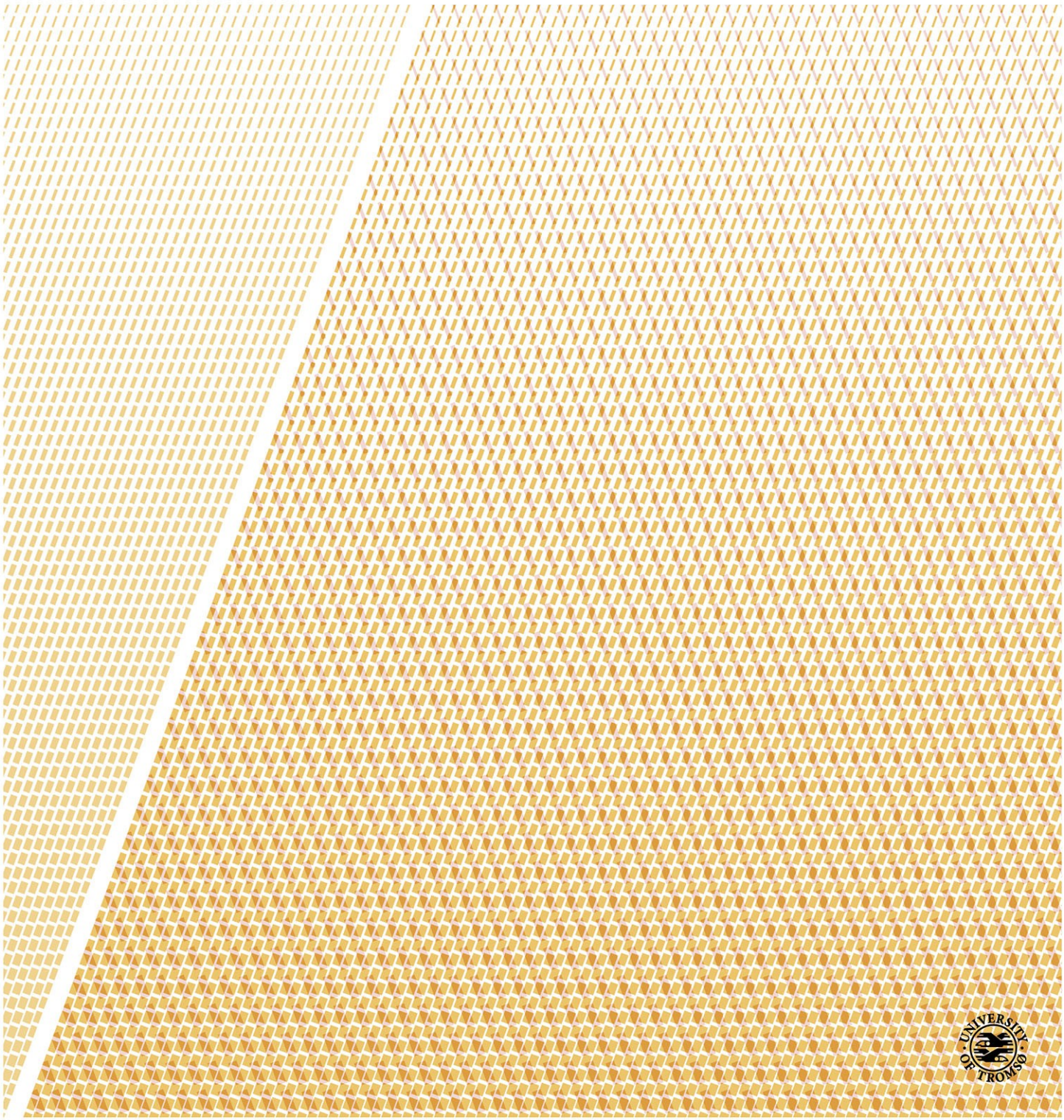

The EOS Formulation for Linear and Nonlinear Transient Scattering Problems

Aihua Lin

December, 2018

Acknowledgements

I would like to express my sincere gratitude to my supervisor Prof. Per Kristen Jakobsen. This thesis would never come into being without his guidance. Thanks for continuous support and patience to help me grow both academically and personally. Thanks for offering me the opportunity to start a new life in Norway. Words are far from expressing my thanks.

I am deeply thankful to Prof. Einar Mjølhus for all his help and guidance at my first course. Thanks to Tor Flå for kind and nice talks and for his care. I greatly appreciate it.

Many thanks to Elinor Ytterstad for all the joyful memories we have shared together. Many thanks to Hugues Verdure for always being available to help me with IT problems no matter where I was located. Deep thanks to them for their generous help in my daily life.

My sincere thanks go to Trygve Johnsen, Martin Rypdal and Helge Johansen for their kind understanding and financial support.

Many thanks to Jan Nyquist Roksvold, Ragnar Soleng, Sigrunn Holbek Sørbye, Marius Overholt and Boris Kruglikov for a lot of interesting conversations.

Great thanks to my parents, my husband and my sister for all their support and for being by my side all the time. I am particularly grateful to having my lovely son, Oliver, without whom I may have been suffering from depression during this long period of doctoral study.

Last but not least, my infinite heartfelt gratitude goes to my grandma, for everything.

Thank you all very much!

Contents

1 Introductions

1.1 Background and motivations

The formulation of partial differential equations in unbounded domains in terms of boundary integral equations has a long history. The roots stretch back at least to the ground breaking publication of a certain set of integral identities by George Green in 1828 [1]. These ideas, which became well known only after his death, became generalized into the notion of Green's functions which are the key elements in all investigations involving boundary integral equations, and many other places in pure and applied science. It would for example be hard to imagine solid state physics and particle physics without Green's functions.

Using computational methods to solve PDEs by solving their corresponding boundary integral equations, also has fairly deep roots, but not nearly as deep as the boundary integral equations themselves. This is because such methods only became feasible in the 1960s after the invention and widespread availability of electronic computers. This approach to solving PDEs numerically became known as the Boundary Element method(BEM) [2].

The boundary element method has several attractive features that makes it well suited to take on any computational problem involving some kind of wave scattering from compact objects in an infinite domain. Many modeling problems in science and engineering are of this type.

First and foremost, the solution of the original PDEs is changed to the solution of an integral equation defined only on the boundaries of the scattering objects. Thanks to this, one whole space dimension is removed from the problem, and no numerical grids outside the scattering objects are needed. This greatly reduces the computational cost and complexity, and therefore BEM is more efficient compared to a traditional domain-based method. The reduction of the number spatial dimensions in the problem is the main advantage of the BEM. For a domain-based method, all spatial dimensions are retained and must be discretize in a numerical solutions algorithm. The discretizations of the outside domain is usually resolved by introducing a box big enough to include all the scattering objects. This domain can easily become very large and thus the computational box will have to be very large. For 3D scattering problems this translates into a large memory requirement for the numerical implementation. In addition, boundary conditions have to be imposed at the boundary of the computational box in such a way that reflections are minimized. For the case of electromagnetic scattering this problem was solved by the introduction of a perfectly matched layer(PML) [3,4]. This is a key element of the finite difference time domain method(FDTD) [5–7], which is the method of choice for simulating electromagnetic scattering. The introduction of PML however does not come free. There are both an increased computational cost, because the PML layer has to be thick enough in order to ensure minimal reflection, and an increased implementional complexity needed to counter the numerical instabilities that are originating from the PML layer. The PML approach has subsequently been simplified and generalized to all kinds of scattering problems [8, 9] using an approach where the physical space outside the computational box is complexified.

Secondly, there is usually a big difference in the material properties between the scattering objects and their surroundings, which in the mathematical model appears as discontinuous, or near-discontinuous, coefficients in the PDEs

defining the model. It is not easy to represent this difference accurately using a domain-based method, like FDTD or the Finite Element method (FEM) [10–12]. This is usually resolved by introducing multiple, interlinked grids. However it is challenging to design accurate and stable numerical algorithm on such grids and it also adds to computation cost of these methods.

Thirdly, the surface localization of boundary integral equations also means that the boundary discretization, which leads to the BEM equations, can be optimized with respect to the geometry of each surface separately when there are more than one scattering object, which there usually is. For domain-based methods like Finite Element methods(FEM) [10–12] and FDTD, such an optimization can only be achieved by using non-uniform or multiple grids tailored to the geometrical shape of the objects. These kinds of efforts have met with some degree of success, but it does add new layers of complexity. Methods such as these, combined with Transformational Optics(TO) [13, 14] have an intuitive appeal and have recently met with some amount of success [15], but numerical stability issues are a major concern.

Lastly, BEM, is exceptionally well suited for modeling scattering problems where the sources are slow on relevant timescales. In this setting the boundary integral equations are derived in the spectral domain and the discretized equations defining BEM only needs to be solved for the small set of discrete frequencies that are required for an accurate representation of the time dependent source. For a domain-based method like FDTD, near-stationary sources are the worst possible case since FDTD is, as the name indicate, a time domain method, and slow sources mean that Maxwell's equations have to be solved for a long interval of time, which is costly in terms of computational resources. FEM, on the other hand, originated in the context of stationary problems in elasticity [16, 17], and as such is well suited to frequency domain problems. However for fast sources in 3D electromagnetic scattering the computational load builds quickly.

Given all these attractive features of BEM for solving scattering problems in electromagnetics, it is somewhat surprising that in a popularity contest, FEM and FDTD beats BEM hands down [2]. The reason for this is that in addition to all its attractive features, BEM has some real drawbacks too.

Firstly, reformulating the scattering problem for a system of PDEs in terms of boundary integral equations typically will involve classical but fairly intricate mathematical tools, as will the discretization of the resulting integral equations. In particular one will need to content with singularities which appear in the limits that always must be taken while deriving the boundary equations from the PDEs. Accurately representing these singularities in the ensuing discretization leading to BEM, is a major issue. FEM have some of the same issues, whereas FDTD is much simpler to implement using mathematical tools that are straight forward and known to all.

Secondly, BEM relies on Green's functions and such functions can only be defined for linear systems of PDEs. In our opinion this is one of the major reasons why BEM is significantly less popular than the major contenders FEM and FDTD. Nonlinearities are common in most areas of pure and applied science, and having to change your whole computational approach when nonlinearities are added to your model is a major nuisance. In some areas of application nonlinearities dominate and hence a computational approach based on Green's functions is out of the question, fluid mechanics is such an area. However in

other areas one can frequently disregard nonlinearities and a computational approach based on Green's functions is feasible. Scattering of electromagnetic waves, where nonlinearities only come into play at very high field intensities, is such an area.

Thirdly, BEM, which is simplest to formulate in the spectral domain, is at it's best when we are looking at a near stationary situation with narrow band sources. For transient scattering with broad band sources one needs to formulate BEM in the time domain and this involves space-time Green's functions that in general tends to be more singular than the frequency domain ones. However, for the specific case of electromagnetic scattering, an integral formulation has been derived [18] whose singularities are fairly weak. This integral formulation of electromagnetics is the foundation of all time dependent BEM formulations to date, and is also the basis for our approach. However, the progress in developing these time dependent BEM schemes has been slow due to several drawbacks.

The time-domain integral equations are retarded and this means that in order to compute the solutions at a certain time, one needs to retain the solutions for an interval of previous times that in some cases can be very large. This leads to a large memory requirement that needs to be met using parallel processing. In today's computational environment parallel implementation of time dependent BEM is fairly standard, but the possibly limited efficiency due to the problem of load balancing is something that always must be contended with.

However the major obstacle that has prevented this method from being widely applied for electromagnetic scattering is the occurrence of numerical instabilities. These instabilities, whose source is not fully understood, occur not at early times, but at later times and have become known as the late time instability. Many efforts have been made and several techniques have been developed in order to improve the stabilities of BEM schemes for time dependent electromagnetics in the last several decades. Basically there are two directions that are pursued. One direction is focused on delaying or removing the late time instability by applying increasing accurate spatial integrations [19–25]. The other direction is aimed at designing more stable time discretization schemes [24, 25]. Some researches were reported to mitigate the instability by both making better approximations of the integrals and applying improved time derivatives [26, 27].

In this thesis we have developed a new hybrid approach for solving linear and nonlinear scattering problems, an approach which is aimed at a situation where a collection of compact scattering objects are located in a homogeneous unbounded space and where the scattering objects can have an inhomogeneous and/or nonlinear response. The basic idea is to combine a domain-based method and a boundary integral method in such a way that the domain-based method is used to propagate the equations governing the wave field inside the scattering objects forward in time while the boundary integral method is used to supply the domain-based method with the required boundary values. The boundary integral method is derived from a space-time integral formulation of the PDEs such that all the scattering and re-scattering outside the scattering objects will be taken into account automatically. As a result, for the numerical implementations, there is no need for grids outside the scattering objects, only grids on the inside and the boundaries of the scattering objects are needed. Thus the new approach combines the best features of both methods; the response inside the scattering objects, which can be caused by both material inhomogeneity

and nonlinearities, is easily taken into account using the domain-based method, and the boundary conditions supplied by the boundary integral method makes it possible to confine the domain based method to the inside of each scattering object.

This kind of idea was firstly proposed in 1972 by E. Wolf and D. N. Pattanyak [28] for the stationary linear scattering of electromagnetic waves in frequency space. The approach was based on the Ewald-Oseen optical extinction theorem, and because of this we call our method the Ewald-Oseen Scattering(EOS) formulation.

In this thesis our aim is to calculate the scattering of waves from objects that are in general inhomogeneous and, additionally, may have a nonlinear response. Thus a space-time integral formulation of the PDEs of interest is needed.

Firstly, we explored the viability of our approach by applying it to two toy models of 1D linear and nonlinear transient wave scattering. These two problems are set up to be analogs of the 3D scattering of electromagnetic waves, whose mathematical incarnation are Maxwell's equations . Our investigation of these two 1D problems is detailed in Paper 1.

Secondly, after confirming the viability of our approach in Paper 1, we extended our approach to the real world highly relevant, but also mathematically highly complex, case of 3D electromagnetic scattering. This extension of our method was successful, and we take this as proof that our EOS formulation is a general approach that is applicable to a wide array of linear and nonlinear wave scattering problems. In Paper 2 we report on the main features of this extension and the problems that needed to be addressed in order for us to succeed in the application of our EOS formulation to the 3D Maxwell's equations.

In paper 3 we discuss, in the context of electromagnetic scattering, two issues that are relevant for the application of our EOS formulation to any wave scattering problem of real world relevance and complexity. This is the issues of stability of the numerically implemented EOS formulation, and the issue of how to handle the singular integrals that occurs as matrix elements in the numerical implementation of the boundary part of the EOS formulation.

1.2 Summary of the papers

This section summarizes the work and the main results of the three papers that are the core of the current thesis.

1.2.1 Paper 1

In this paper, we introduce a new method, which we have called the EOS formulations, for solving linear and nonlinear transient wave scattering problems. As stated in section 1, the method has been developed by combining a boundary integral representations and a domain-based method. This is done in such a way that the inside fields will be propagated forward in time by the domain-based method, while the needed boundary values will supplied by the boundary integral representations. The method is illustrated on two 1D toy models which are chosen as analogs of electromagnetic wave scattering.

Model 1 is governed by equations

$$\begin{aligned} \varphi_t &= c_1\varphi_x + j, \\ \rho_t &= -j_x, \\ j_t &= (\alpha - \beta\rho)\varphi - \gamma j, \quad a_0 < x < a_1, \end{aligned} \tag{1.1}$$

and model 2 is governed by

$$\begin{aligned} \varphi_t &= \mu_1\psi_x + j, \\ \psi_t &= \nu_1\varphi_x, \\ \rho_t &= -j_x, \\ j_t &= (\alpha - \beta\rho)\varphi - \gamma j, \quad a_0 < x < a_1, \end{aligned} \tag{1.2}$$

where α, β and γ are constants, $\varphi = \varphi(x,t)$ is the "electric field", $\psi(x,t)$ is the "magnetic" field, $j = j(x,t)$ is the "current density" and ρ is the "charge density", c_1 is the propagation speed inside the "material". μ_1, ν_1 are "material" parameters and under the translations of $\mu = \frac{1}{\varepsilon}$ and $\nu = \frac{1}{\mu}$, μ and ν are the analog of the electric permittivity and magnetic permeability. The charge density and current density are confined to the interval $[a_0, a_1]$, which is an analog to a compact scattering object in the electromagnetic situation. The fields φ and ψ are defined on the whole real axis. The equation for the "current density", j is a simplification of a real electromagnetic current density model [29].

Outside the interval the two models are respectively governed by

$$\varphi_t = c_0\varphi_x + j_s,$$

and

$$\begin{aligned} \varphi_t &= \mu_0\psi_x + j_s, \\ \psi_t &= \nu_0\varphi_x, \end{aligned}$$

where $j_s(x,t)$ is a given source that has its support in interval $x > a_1$. Model 1 describes a one way propagation with its speed c_0 outside the interval $[a_1, a_1]$ and model 2 describes a two way propagation with its speed $c_0 = \sqrt{\mu_0\nu_0}$ outside the interval. In order to derive the space-time integral formulation of the EOS formulations, we firstly need to derive an integral identity involving the operator

$$L_1 = \partial_t - v\partial_x,$$

for model 1 and

$$L_2 = \begin{pmatrix} \partial_t & -\mu\partial_x \\ -\nu\partial_x & \partial_t \end{pmatrix},$$

for model 2 and the needed advanced Green's functions of their adjoint operators. The integral identities on different intervals will be obtained by inserting the corresponding advanced Green's functions. Finally the integral representations on the boundaries are reached by taking the limit of the integral identities with x approaching the boundaries a_0 and a_1 of the interval. However, the boundary integral representations and the boundary conditions compose an overdetermined system for both model 1 and model 2. This is a general situation

occurring when the EOS formulation is applied to systems of PDEs. An general approach to handling this kind of problem is introduced in this paper. This approach is subsequently applied to the case of Maxwells equations in paper2.

Equations (1.1) or (1.2) together with their corresponding boundary integral representations, by definition, is the EOS formulations of toy model 1 and toy model 2 respectively.

In order to get a second order accuracy numerical solution, we apply the Lax-Wendroof method to the first two equations of (1.1) and the first three equations of (1.2) and we apply the modified Euler's method to the equations of the current density j for the inside interval. For the boundary integrals, we use the mid-point rule. A space grid for the inside of the scattering objects, (a, b), need to support both this mid-point integration rule and also finite difference formulas for the partial derivatives, and it will for this reason be nonuniform close to the boundary. This occurrence of nonuniform internal spatial grids also occur for the case of electromagnetic scattering in paper 2 and is generic if one discretize the EOS formulation using finite difference methods.

For the two models in this paper we use the following spatial grid for the inside of the scattering object

$$x_i = a_0 + (i + \frac{1}{2})\frac{a_1 - a_0}{N},\ i = 0, 1, \cdots, N-1. \tag{1.3}$$

The "electric field" and the "magnetic field" are continuous through the boundaries of the scattering objects. Their space derivatives are therefore approximated by finite difference formulas which involve values both from the inside and the outside of the scattering object. The current density j_1, and the charge density ρ_1, are entirely supported inside the scattering object, and for these quantities it is thus appropriate to approximate their space derivatives using only values from inside the scattering object. For the discretizations of the boundary values that is located between the grid points for the time grid, we choose to use a quadratic interpolation in order to maintain overall second order accuracy for our scheme.

For both toy models we verify the stability and accuracy of our EOS formulations using an approach based on the use of artificial sources. The idea is motivated by a fact that adding an arbitrary source to all the governing equations of the system normally will lead to only minor changes to the numerical scheme. The introduction does however change the model equations in an interesting and useful way. Extending the model equations by the addition of arbitrary sources means that *any* function is a solution to the extended equations for *some* choice of sources.

For example, model 1 extended by the addition of artificial sources is of the form

$$\begin{aligned} \varphi_t &= c_1\varphi_x + j + g_1, \\ \rho_t &= -j_x + g_2, \\ j_t &= (\alpha - \beta\rho)\varphi - \gamma j + g_3, \end{aligned} \tag{1.4}$$

where g_1, g_2, g_3, are the artificial sources. If we choose some functions $\hat{\varphi}, \hat{j}$ and

$\hat{\rho}$ and let

$$\hat{g}_1 = \hat{\varphi}_t - c_1\hat{\varphi}_x - \hat{j},$$
$$\hat{g}_2 = \hat{\rho}_t + \hat{j}_x,$$
$$\hat{g}_3 = \hat{j}_t - (\alpha - \beta\hat{\rho})\hat{\varphi} + \gamma\hat{j},$$

then model 1 with these source functions will have the functions $\hat{\varphi}, \hat{j}$ and $\hat{\rho}$ as solution. If we now use these sources in our numerical discretization of model 1, we *know* that the correct solution is given by $\hat{\varphi}, \hat{j}$ and $\hat{\rho}$, and we can now validate our numerical solution by comparing it to the known correct solution

The comparison between the EOS formulations and the exact solutions of the two toy models show that discretization of our EOS formulation give accurate numerical solutions, and thus shows that our new approach to wave scattering is viable. The solutions of a general scattering where the source is located outside the interval are also implemented for both toy models. The implementations of both the artificial source test and the general scattering are stable with a proper choice of the time step. We observe in this paper that the numerical implementation of the EOS formulations for model 1 and model 2 is stable if the time step is bounded both above and below, and thus belong to a bounded interval. We show in the paper that this stability interval is a consequence of the nonuniform spatial grid used inside the scattering object.

1.2.2 Paper 2

This paper is a continuation and extension of Paper 1 where we explore the possibility of applying the EOS formulations to 3D electromagnetic scattering problems. The goal of this paper is to derive, and implement numerically, the EOS formulation for the scattering of electromagnetic waves from a single scattering object. The extension to several such objects is conceptually trivial, although with respect to computational load, the extension will of course be nontrivial. The basic equations for the situation discussed in this paper are the Maxwell's equations

$$\nabla \times \mathbf{E}_j + \partial_t \mathbf{B}_j = 0, \tag{1.5a}$$
$$\nabla \times \mathbf{B}_j - \frac{1}{c_j^2}\partial_t \mathbf{E}_j = \mu_j \mathbf{J}, \tag{1.5b}$$
$$\partial_t \rho_j + \nabla \cdot \mathbf{J}_j = 0, \tag{1.5c}$$

with the index $j = 0$ representing the outside of the scattering object and $j = 1$ representing the inside of the object. $\mathbf{E}_j$ is the electric field, $\mathbf{B}_j$ is the magnetic field, $\mathbf{J}_j$ and ρ_j are the current density and the charge density respectively. The speed of light in a material with electric permittivity ε_j and magnetic permeability μ_j is given by $c_j = 1/(\varepsilon_j\mu_j)$. For the inside of the object, the dynamics of the current density is determined by the equation

$$\partial_t \mathbf{J}_1 = (\alpha - \beta\rho_1)\mathbf{E}_1 - \gamma\mathbf{J}_1 = F(\mathbf{E}_1, \rho_1, \mathbf{J}_1), \tag{1.6}$$

where α, β, γ are some constants. For the outside of the object, the current density J_0 and the electric density ρ_0 are some given sources that satisfy the continuity equation (1.5c).

The principle of the EOS formulations for 3D electromagnetic scattering is the same as in the 1D case in Paper 1. We solve the inside domain of the model using a domain-based method and use a integral identity on the surface to support the surface values needed by the inside updating in time. In order to derive the boundary integral representations, we firstly need to derive a space-time integral identities for the electric field and the magnetic field. The required integral identities can be derived by noting that each component of the electric and magnetic fields satisfy scalar wave equations. From the integral identities satisfied by solutions to the 3D wave equations one can, after highly nontrivial vector calculus manipulations, derive the integral representations of the electric field and the magnetic field in the form

$$\begin{aligned}
\mathbf{E}_j(\mathbf{x},t) &= -\partial_t \frac{\mu_j}{4\pi}\int_{V_j} \mathrm{d}V' \frac{\mathbf{J}_j(\mathbf{x}',T)}{|\mathbf{x}'-\mathbf{x}|} - \nabla \frac{1}{4\pi\varepsilon_j}\int_{V_j} \mathrm{d}V' \frac{\rho_j(\mathbf{x}',T)}{|\mathbf{x}'-\mathbf{x}|} \\
&\mp \partial_t [\frac{1}{4\pi}\int_S \mathrm{d}S' \{\frac{1}{c_j|\mathbf{x}'-\mathbf{x}|}(\mathbf{n}'\times\mathbf{E}_j(\mathbf{x}',T))\times\nabla'|\mathbf{x}'-\mathbf{x}| \\
&+ \frac{1}{c_j|\mathbf{x}'-\mathbf{x}|}(\mathbf{n}'\cdot\mathbf{E}_j(\mathbf{x}',T))\nabla'|\mathbf{x}'-\mathbf{x}| + \frac{1}{|\mathbf{x}'-\mathbf{x}|}\mathbf{n}'\times\mathbf{B}_j(\mathbf{x}',T)\}] \qquad (1.7)\\
&\pm \frac{1}{4\pi}\int_S \mathrm{d}S' \{(\mathbf{n}'\times\mathbf{E}_j(\mathbf{x}',T))\times\nabla'\frac{1}{|\mathbf{x}'-\mathbf{x}|} \\
&+ (\mathbf{n}'\cdot\mathbf{E}_j(\mathbf{x}',T))\nabla'\frac{1}{|\mathbf{x}'-\mathbf{x}|}\},
\end{aligned}$$

$$\begin{aligned}
\mathbf{B}_j(\mathbf{x},t) &= \nabla\times\frac{\mu_j}{4\pi}\int_{V_j}\mathrm{d}V'\frac{\mathbf{J}_j(\mathbf{x}',T)}{|\mathbf{x}'-\mathbf{x}|} \\
&+ \partial_t[\frac{1}{4\pi}\int_S \mathrm{d}S'\{\frac{1}{c_j|\mathbf{x}'-\mathbf{x}|}(\mathbf{n}'\times\mathbf{B}_j(\mathbf{x}',T))\times\nabla'|\mathbf{x}'-\mathbf{x}| \\
&\mp \frac{1}{c_j|\mathbf{x}'-\mathbf{x}|}(\mathbf{n}'\cdot\mathbf{B}_j(\mathbf{x}',T))\nabla'|\mathbf{x}'-\mathbf{x}| - \frac{1}{c_j^2}\frac{1}{|\mathbf{x}'-\mathbf{x}|}\mathbf{n}'\times\mathbf{E}_j(\mathbf{x}',T)\}] \qquad (1.8)\\
&\pm \frac{1}{4\pi}\int_S \mathrm{d}S'\{(\mathbf{n}'\times\mathbf{B}_j(x',T))\times\nabla'\frac{1}{|\mathbf{x}'-\mathbf{x}|} \\
&+ (\mathbf{n}'\cdot\mathbf{B}_j(\mathbf{x}',T))\nabla'\frac{1}{|\mathbf{x}'-\mathbf{x}|}\},
\end{aligned}$$

for $\mathbf{x}\in V_j$. These are however not the only integral identities that follows from this procedure. We also find that from the two outer identities we get two additional inner identities and similarly from the two inner we get two additional outer identities. In optics, which is a subfield of electromagnetics, these extra identities are called the Ewald-Oseen extinction theorem. From a mathematical point of view they follow from a defining property of Dirac delta functions. The

extra pair of integral identities are

$$
\begin{aligned}
0 = & -\partial_t \frac{\mu_{1-j}}{4\pi} \int_{V_{1-j}} \mathrm{d}V' \frac{\mathbf{J}_{1-j}(\mathbf{x}', T)}{|\mathbf{x}' - \mathbf{x}|} - \nabla \frac{1}{4\pi\varepsilon_{1-j}} \int_{V_{1-j}} \mathrm{d}V' \frac{\rho_{1-j}(\mathbf{x}', T)}{|\mathbf{x}' - \mathbf{x}|} \\
& \pm \partial_t [\frac{1}{4\pi} \int_S \mathrm{d}S' \{ \frac{1}{c_{1-j}|\mathbf{x}' - \mathbf{x}|} (\mathbf{n}' \times \mathbf{E}_{1-j}(\mathbf{x}', T)) \times \nabla' |\mathbf{x}' - \mathbf{x}| \\
& + \frac{1}{c_{1-j}|\mathbf{x}' - \mathbf{x}|} (\mathbf{n}' \cdot \mathbf{E}_{1-j}(\mathbf{x}', T)) \nabla' |\mathbf{x}' - \mathbf{x}| + \frac{1}{|\mathbf{x}' - \mathbf{x}|} \mathbf{n}' \times \mathbf{B}_{1-j}(\mathbf{x}', T) \}] \\
& \mp \frac{1}{4\pi} \int_S \mathrm{d}S' \{ (\mathbf{n}' \times \mathbf{E}_{1-j}(\mathbf{x}', T)) \times \nabla' \frac{1}{|\mathbf{x}' - \mathbf{x}|} \\
& + (\mathbf{n}' \cdot \mathbf{E}_{1-j}(\mathbf{x}', T)) \nabla' \frac{1}{|\mathbf{x}' - \mathbf{x}|} \},
\end{aligned}
\tag{1.9}
$$

and

$$
\begin{aligned}
0 = & \nabla \times \frac{\mu_{1-j}}{4\pi} \int_{V_{1-j}} \mathrm{d}V' \frac{\mathbf{J}_{1-j}(\mathbf{x}', T)}{|\mathbf{x}' - \mathbf{x}|} \\
& \pm \partial_t [\frac{1}{4\pi} \int_S \mathrm{d}S' \{ \frac{1}{c_{1-j}|\mathbf{x}' - \mathbf{x}|} (\mathbf{n}' \times \mathbf{B}_{1-j}(\mathbf{x}', T)) \times \nabla' |\mathbf{x}' - \mathbf{x}| \\
& + \frac{1}{c_{1-j}|\mathbf{x}' - \mathbf{x}|} (\mathbf{n}' \cdot \mathbf{B}_{1-j}(\mathbf{x}', T)) \nabla' |\mathbf{x}' - \mathbf{x}| \\
& - \frac{1}{c_{1-j}^2|\mathbf{x}' - \mathbf{x}|} \mathbf{n}' \times \mathbf{E}_{1-j}(\mathbf{x}', T) \}] \\
& \mp \frac{1}{4\pi} \int_S \mathrm{d}S' \{ (\mathbf{n}' \times \mathbf{B}_{1-j}(x', T)) \times \nabla' \frac{1}{|\mathbf{x}' - \mathbf{x}|} \\
& + (\mathbf{n}' \cdot \mathbf{B}_{1-j}(\mathbf{x}', T)) \nabla' \frac{1}{|\mathbf{x}' - \mathbf{x}|} \},
\end{aligned}
\tag{1.10}
$$

for $\mathbf{x} \in V_j$. After taking the limits of (1.7)-(1.10) when $\mathbf{x}$ approaches the surfaces from both the inside and the outside of the scattering objects, we get four integral representations on the surfaces. We also have four electromagnetic interface conditions at the boundary of the scattering object.boundary conditions for the usual electromagnetics. We have thus four unknowns and six interface conditions, which is overdetermined. The technique for solving this overdetermined problem is explained in the main text of Paper 2. The final boundary integral identities takes the following compact form

$$
(I + \frac{1}{2}(\frac{\varepsilon_1}{\varepsilon_0} - 1)\mathbf{n}\ \mathbf{n})\mathbf{E}_+(\mathbf{x}, t) = \mathbf{I}_e + \mathbf{O}_e + \mathbf{B}_e, \tag{1.11a}
$$

$$
(I + \frac{1}{2}(1 - \frac{\mu_0}{\mu_1})\mathbf{n}\ \mathbf{n})\mathbf{B}_+(\mathbf{x}, t) = \mathbf{I}_b + \mathbf{O}_b + \mathbf{B}_b, \tag{1.11b}
$$

where I is a 3×3 identity matrix, $\mathbf{E}_+$ and $\mathbf{B}_+$ are the limits of the electric field and the magnetic field by letting $\mathbf{x}$ approach the surface from the inside of the scattering object, $\mathbf{I}_e$ and $\mathbf{I}_b$ are volume integrals of the inside current density and the charge density, $\mathbf{O}_e$ and $\mathbf{O}_b$ are fields on the surfaces generated by the source in the absence of the scattering objects, $\mathbf{B}_e$ and $\mathbf{B}_b$ are surface integrals of the historical values of the fields on the surface. Expressions of these integrals are presented in Paper 2. Equations (1.5) and (1.6) together with the boundary

integral identities (1.11a) and (1.11b) compose the EOS formulations of the 3D model.

In Paper 2, our aim is focused on illustrating the EOS formulations with respect to its complexity and numerical stability, thus we choose a scattering object of the simplest possible shape.set the shape , a rectangular box. In order to get a second order accuracy numerical solutions, we use the Lax-Wendroff method on (1.5) and the modified Euler's method on (1.6). For the boundary integral identities, we use the mid-point rules for second order accuracy. Inside the scattering object we introduce, for the reasons explained in paper 1, a non-uniform spatial grid of the form

$$\begin{aligned} x_i &= x_a + (i+0.5)\Delta x, \qquad i = 0, 1, \cdots N_x - 1, \\ y_j &= y_a + (j+0.5)\Delta y, \qquad j = 0, 1, \cdots N_y - 1, \\ z_k &= z_a + (k+0.5)\Delta z, \qquad k = 0, 1, \cdots N_z - 1, \end{aligned} \tag{1.12}$$

with

$$\Delta x = \frac{x_b - x_a}{N_x},$$

$$\Delta y = \frac{y_b - y_a}{N_y},$$

$$\Delta z = \frac{z_b - z_a}{N_z},$$

where N_x, N_y and N_z are the number of grid points in x, y and z directions respectively.

For the inside grids, the discretized solutions of (1.5) at grid point (x_i, y_j, z_k) at time t_{n+1} are calculated by

$$\phi_{i,j,k}^{n+1} = \phi_{i,j,k}^{n} + \Delta t (\frac{\partial \phi}{\partial t})_{i,j,k}^{n} + \frac{1}{2}(\Delta t)^2 (\frac{\partial^2 \phi}{\partial t^2})_{i,j,k}^{n}, \tag{1.13}$$

where ϕ represents e_i, b_i, ρ_1, $i = 1, 2, 3$. The expressions of $\frac{\partial \phi}{\partial t}$ and $\frac{\partial^2 \phi}{\partial t^2}$ will be expressed by the space derivatives through Lax-Wendroff method. The same as for the 1D models, due to the sharp changes of the properties of the material on the boundaries of the scattering objects, the space derivatives of the electric field and the magnetic field involve both the inside values and the outside values while the space derivatives of the current density and the charge density only involve the inside values.

After discretization the current equation (1.6), using the modified Euler's method, we get a numerical scheme defined by the difference equation

$$\begin{aligned} (\bar{j}_l)_{i,j,k}^{n+1} &= (j_l)_{i,j,k}^{n} + \Delta t \cdot F((e_l)_{i,j,k}^{n}, (\rho_1)_{i,j,k}^{n}, (j_l)_{i,j,k}^{n}), \\ (j_l)_{i,j,k}^{n+1} &= \frac{1}{2}((j_l)_{i,j,k}^{n} + (\bar{j}_l)_{i,j,k}^{n+1} + \Delta t \cdot F((e_l)_{i,j,k}^{n+1}, (\rho_1)_{i,j,k}^{n+1}(\bar{j}_l)_{i,j,k}^{n+1})), \end{aligned} \tag{1.14}$$

where $l = 1, 2, 3$, representing the three components of the current density.

For the discretizations of the boundary integral identities, the final formulas takes the form

$$\begin{pmatrix} M_{11} & M_{12} \\ M_{21} & M_{22} \end{pmatrix} \begin{pmatrix} \mathbf{E}_p^n \\ \mathbf{B}_p^n \end{pmatrix} = \begin{pmatrix} \mathbf{E}_R \\ \mathbf{B}_R \end{pmatrix}, \tag{1.15}$$

where $\mathbf{E}_p^n$ and $\mathbf{B}_p^n$ are the numerical solutions at grid point $\mathbf{x}_p$ at time t_n. $\mathbf{E}_R$ and $\mathbf{B}_R$ are the right hand of (1.11a) and (1.11b) respectively after moving the unknown into the right side of the equations. M_{11} and so on are 3×3 matrices. The numerical solution for a general case where the sources are located outside the scattering domain is implemented. In order to be easily integrated in space, we have set up the outside source J_0 and ρ_0 as a combination of a smooth localized function in time and a delta function in space.

In order to validate our method, we solve an extended system with artificial sources described by

$$\partial_t \mathbf{B} + \nabla \times \mathbf{E} = 0, \tag{1.16a}$$

$$\frac{1}{c_1^2}\partial_t \mathbf{E} - \nabla \times \mathbf{B} = -\mu_1 \mathbf{J}, \tag{1.16b}$$

$$\nabla \cdot \mathbf{E} = \frac{1}{\varepsilon_1}\rho, \tag{1.16c}$$

$$\partial_t \mathbf{J} = (\alpha - \beta\rho)\mathbf{E} - \gamma \mathbf{J} + \boldsymbol{\varphi}. \tag{1.16d}$$

If we choose some functions for $\tilde{\mathbf{E}}, \tilde{\mathbf{B}}$, then these choices will be a solution to model (1.16), if the artificial source are chosen to be

$$\boldsymbol{\varphi} = \partial_t \tilde{\mathbf{J}} - (\alpha - \beta\tilde{\rho})\tilde{\mathbf{E}} - \gamma \tilde{\mathbf{J}}, \tag{1.17}$$

with

$$\tilde{\mathbf{J}} = \frac{1}{\mu_1}(\nabla \times \tilde{\mathbf{B}} - \frac{1}{c_1^2}\partial_t \tilde{\mathbf{E}}),$$

and

$$\tilde{\rho} = \varepsilon_1 \nabla \cdot \tilde{\mathbf{E}}.$$

The comparison between the numerical implementations and the exact solutions show high accuracy without instabilities with proper choices of parameters and restricted time step. It's also noted in Paper 2 that the numerical solution is stable if the time step is contained in a certain bounded interval. This interval is determined by both the inside domain-based method and the boundary integral identities.

1.2.3 Paper 3

In this paper we discuss the three major issues involved in solving the 3D Maxwell's equations using the EOS formulations. We believe that these issues are representative for the kind of problems that must be overcome while using the EOS formulation to calculate transient scattering of waves.

The first issue to be discussed in this paper is numerical stability. As mentioned above, the numerical scheme for the EOS formulation derived in paper2 is stable for time steps in a certain bounded interval. In the two 1D toy models, this interval is purely determined by the domain-based method, namely the Lax-Wendroff method, in our case. For the 3D model of Maxwell's equations, our finding is that the instability, when it occur, shows up at late times and comes from two sources. One source is the domain-based method applied inside the scattering object and the other source is the integral identities applied on the surfaces of the scattering object which are supplying the boundary conditions that are needed by the domain-based method. Specifically, the lower limit of

this interval comes from the boundary integral identities and are determined by the material of the scattering object through the relative electric permittivity and the relative magnetic permeability, while the upper limit is determined by the domain-based method applied inside the scattering object. Our conclusions are based on two tests.

In the first test we assume that there is no current density and the charge density inside the object, and that the inside and outside has the same material parameters. Thus $\mu_1 = \mu_0$, $\varepsilon_1 = \varepsilon_0$, $\mathbf{J}_1 = 0$ and $\rho_1 = 0$. In other words, there is no scattering object present in the material sense. Under these assumptions, the electric field inside the scattering object $\mathbf{E}_1$ can be calculated by three methods.

In method 1, the field inside the scattering object is produced directly by the outside sources, thus the exact solution is calculated by

$$\mathbf{E}_1(\mathbf{x},t) = -\partial_t \frac{\mu_0}{4\pi}\int_{V_0} \mathrm{d}V' \frac{\mathbf{J}_0(\mathbf{x}',T)}{|\mathbf{x}'-\mathbf{x}|} - \nabla \frac{1}{4\pi\varepsilon_0}\int_{V_0} \mathrm{d}V' \frac{\rho_0(\mathbf{x}',T)}{|\mathbf{x}'-\mathbf{x}|}, \tag{1.18}$$

where V_0 denotes the outside domain of the scattering object while $\mathbf{x}$ is located inside of the object.

Note that by using the formula (1.18), for the electric field, and the corresponding one for the magnetic field, we find that the boundary values for the electric and magnetic field are given by

$$\mathbf{E}_+(\mathbf{x},t) = -\partial_t \frac{\mu_0}{4\pi}\int_{V_0} \mathrm{d}V' \frac{\mathbf{J}_0(\mathbf{x}',T)}{|\mathbf{x}'-\mathbf{x}|} - \nabla \frac{1}{4\pi\varepsilon_0}\int_{V_0} \mathrm{d}V' \frac{\rho_0(\mathbf{x}',T)}{|\mathbf{x}'-\mathbf{x}|}, \tag{1.19}$$

and

$$\mathbf{B}_+(\mathbf{x},t) = \nabla \times \frac{\mu_0}{4\pi}\int_{V_0} \mathrm{d}V' \frac{\mathbf{J}_0(\mathbf{x}',T)}{|\mathbf{x}'-\mathbf{x}|}, \tag{1.20}$$

where $\mathbf{x}$ is located on the surface S of the scattering object. $\mathbf{E}_+(\mathbf{x},t)$ and $\mathbf{B}_+(\mathbf{x},t)$ respectively represent the limits of the electric filed $\mathbf{E}_+$ and the magnetic field $\mathbf{B}_+$ by letting $\mathbf{x}$ approach the surface from the inside of the scattering object.

Based on this we can now calculate the inside electric field $\mathbf{E}_+$ by two methods more.

In method 2, we calculate the inside electric field using the boundary integral identity of the inside solution,

$$\begin{aligned}
\mathbf{E}_1(\mathbf{x},t) = \partial_t [& \frac{1}{4\pi}\int_S \mathrm{d}S' \{ \frac{1}{c_1|\mathbf{x}'-\mathbf{x}|}(\mathbf{n}'\times\mathbf{E}_+(\mathbf{x}',T))\times\nabla'|\mathbf{x}'-\mathbf{x}| \\
& + \frac{1}{c_1|\mathbf{x}'-\mathbf{x}|}(\mathbf{n}'\cdot\mathbf{E}_+(\mathbf{x}',T))\nabla'|\mathbf{x}'-\mathbf{x}| \\
& + \frac{1}{|\mathbf{x}'-\mathbf{x}|}\mathbf{n}'\times\mathbf{B}_+(\mathbf{x}',T)\}] \\
& - \frac{1}{4\pi}\int_S \mathrm{d}S' \{(\mathbf{n}'\times\mathbf{E}_+(\mathbf{x}',T))\times\nabla'\frac{1}{|\mathbf{x}'-\mathbf{x}|} \\
& + (\mathbf{n}'\cdot\mathbf{E}_+(\mathbf{x}',T))\nabla'\frac{1}{|\mathbf{x}'-\mathbf{x}|}\},
\end{aligned} \tag{1.21}$$

which involves the surface values $\mathbf{E}_+$ and $\mathbf{B}_+$ expressed by (1.19) and (1.20).

In method 3, we update the inside values using the Lax-Wendroff method with boundary values given by the same surface values $\mathbf{E}_+$ and $\mathbf{B}_+$ as in method 2.

The comparison of the results from these three method show high accuracy and no instabilities if the time step is confined in the stable interval.

If we break the upper limit, Method 2 works well but Method 3 has late time instabilities. Thus the upper limit is controlled by the domain-based part of the EOS method.

The second test is based on the artificial source model (1.16). Given exact solutions of $\mathbf{E}_1$ and $\mathbf{B}_1$, the artificial source can be calculated by (1.17). Then we numerically calculate $\mathbf{E}_1$ and $\mathbf{B}_1$ by two methods.

In method 1 we apply the EOS formulations developed in this thesis which combines a domain based method and the boundary integral representation.

In method 2 we update the inside values of the fields using the Lax-Wendroff method with boundary values given explicitly by our choice of the electric $\mathbf{E}_1$ field and magnetic $\mathbf{B}_1$ field. Results show that for time steps that breaks the lower limit of the stable interval, Method 1 shows the late time instability while Method 2 works perfectly. Thus the lower limit is determined by the boundary integral part of the EOS method

Considering test 1 together with test 2, we come to the conclusion that the lower limit is determined the boundary integral representations while the upper limit is determined by the inside domain-based method. Specifically, the lower limit is directly determined by the relative electric permittivity and magnetic permeability and the upper limit is determined by the introduction of the non-uniform grids of the inside domain-based method.

The second issue is how to handle the singular integrals that appear in matrix elements when we discretize the EOS formulation. These singular integrals come from the process taking limits of the integral representations when the observing point moves from the inside or the outside onto the surfaces of the scattering object. The integrals are calculated by splitting them in a regular part and a singular core. The regular part we calculate using midpoint rule or 3D Gaussian integration and the singular core we calculate exactly using certain integral theorems.

The third issue is parallelization. Because of the retardation in time which is an integral part of the EOS formulation, or any formulation using dimensional reduction based on space-time Greens functions, there is a large memory requirement for the algorithm. Implementation in a parallel computational environment will therefore be necessary for most nontrivial application of our method.

1.3 Discussions and future work

A new hybrid method for solving linear and nonlinear transient scattering problems is introduced in this thesis. The hybrid method combines a domain based method and boundary integral representations in the time domain.

In this thesis, our focus has been to provide proof of principle that our new method is viable as an approach to the numerical calculation of transient wave scattering. By detailing the mathematical formulation and numerical implementation of our approach for two models of 1D transient wave scattering, and

the 3D transient scattering of electromagnetic waves, we have achieved what the goal of this thesis.

Beyond the proof of viability of our new approach, there are several topics relating to this new method that needs to be investigated.

Firstly, it would be very useful if an unconditional stable numerical implementation of our EOS formulation could be found. The numerical implementations we have introduced, through our proof of principle studies, are all only conditionally stable. For all cases the numerical implementations are only stable for the time step in a bounded interval. For the 1D case this interval is entirely determined by the inner domain based method whereas for the 3D electromagnetic case the upper limit is determined by the domain based part of the method whereas the lower limit is determined by the boundary part of the method. Specifically the lower limit depends on the difference in material properties outside and inside the scattering object. If this difference is too large, the lower limit become larger than the higher limit and thus the numerical implementation is unstable for all sizes of the step length and thus the scheme is useless. In applications of our scheme to antenna theory this situation is realized and this might be the whole explanation, or part of the explanation, for the late time instability that always, in one way or another, seems to appear in this area of application of boundary methods. A fully implicit implementation of the EOS formulation , if it can be found, would remove restriction on the time step for stable operation and, inn all probability, may remove the late time instability for good. During this thesis work we briefly investigated the possibility of an implicit implementation of the EOS formulation, but did not achieve anything worth reporting here. We did however gain enough insight into the problem to realize that this is a difficult, perhaps even impossible, thing to achieve. This is certainly a topic worth looking into in any future investigation of the EOS formulation.

Secondly, the fundamental integral equations underlying both the BEM and the EOS formulations, developed in this work, are always retarded in time. This is because the underlying equations can only be derived using space-time Green's functions. Thus the solutions at a specific grid point at a certain time will depend on a series of historical solutions of all other grid points of the scattering object. Therefore, these methods are memory intensive. This is in particular true for the EOS formulation, because it grids the inside of the scattering object as well as it boundary. Although this can be solved by parallel computing, whenever large scale parallel processing is needed, there are always the issues of load balancing and saturation to take into account. In our work, the EOS formulation of 3D Maxwell's model was implemented on a large cluster, but we were not focused on parallel issues in any systematic way and have not reported on any parallelization issues that came up during our investigations. Because of the memory intensive nature of the EOS formulation these are however important issues, and therefore must form the part of any future work aimed at making our approach to transient wave scattering into at practical and efficient tool in the toolbox of scientific computing.

Thirdly, there is the issue how the EOS formulation compare to other, more conventional approaches to transient wave scattering. The main contenders here are FDTD and FEM. On the surface of it, it would appear that the EOS formulation is a clear front runner in any such comparison. After all, using this method removes the need to grid most of the physical domain, only the

inside and the boundaries of the actual scattering objects need to be discretized. Thus the EOS formulation requires much fewer spatial grid points than either of FDTD and FEM. However, the retardation of the equations defining the boundary part of the EOS formulation means that this method require many more temporal grid points than the two main contenders. It is appropriate to ask if anything has been gained with respect to memory usage compared to a fully domain-based method like the FDTD method?

The outcome of comparing the memory usage of FDTD and FEM with the EOS formulation is anything but obvious. The outcome of such an investigation most likely will not present us with a clear winner. The ranking will almost surely depend on the nature of the problems under investigation. If the EOS formulation is going to take its place in the toolbox of scientific computing investigations like the one described in this section is sorely needed.

However, even if the memory usage for purely domain based methods and our EOS approach are roughly the same for many problems of interest, our approach avoid many of the sources of problems that need to be considered while using purely domain based methods. These are problems like stair-casing at sharp interfaces defining the scattering objects, issues of accuracy, stability and complexity associated with the use of multiple grids in order to accommodate the possibly different geometric shapes of the scattering objects, and the need to minimize the reflection from the boundary of the finite computational box. The EOS approach is not subject to any of these problems.

2 Paper 1

Submitted to PLOS ONE and revised in the fall of 2018.

A boundary integral approach to linear and nonlinear transient wave scattering

Aihua Lin, Anastasiia Kuzmina and Per Kristen Jakobsen

Department of Mathematics and Statistics, UIT the Arctic University of Norway, 9019 Tromsø, Norway

Abstract

In this work, we introduce a method for solving linear and nonlinear scattering problems for wave equations using a new hybrid approach. This new approach consists of a reformulation of the governing equations into a form that can be solved by a combination of a domain-based method and a boundary-integral method. Our reformulation is aimed at a situation in which we have a collection of compact scattering objects located in an otherwise homogeneous unbounded space.

The domain-based method is used to propagate the equations governing the wave field inside the scattering objects forward in time. The boundary integral method is used to supply the domain-based method with the required boundary values for the wave field.

In this way, the best features of both methods come into play. The response inside the scattering objects, which can be caused by both material inhomogeneity and nonlinearities, is easily considered using the domain-based method, and the boundary conditions supplied by the boundary integral method makes it possible to confine the domain-method to the inside of each scattering object.

1 Introduction

Boundary integral formulations are well known in all areas of science and technology and lead to highly efficient numerical algorithms for solving partial differential equations (PDEs). Particularly, their utility is evident for scattering waves from objects located in an unbounded space. For these situations, one whole space dimension is taken out of the problem by reducing the solution of the original PDEs to the solution of an integral equation located on the boundaries of the scattering objects.

However, this reduction relies on the use of Green's functions and is therefore only possible if the PDEs are linear. For computational reasons, one is also usually restricted to situations in which Green's functions are given by explicit formulas, which rules out most situations in which the materials are inhomogeneous. Since many problems of interest involve scattering waves from objects that display both material inhomogeneity and nonlinearity, boundary integral methods have appeared to be of limited utility in computational science. Adding to the limited scope of the method, the fact that somewhat advanced

mathematical machinery is needed to formulate PDEs in terms of boundary integral equations, it is perhaps not difficult to understand why the method is that popular.

Domain-based methods, like the finite difference method and finite element method, appear to have much wider utility. Their simple formulation and wide applicability to many types of PDEs, both linear and nonlinear, have made them extremely popular in the scientific computing community. In the context of scattering problems, they have problems of their own to contend with. These problems are of two quite distinct types.

The first type of problem is related to the fact that the scattering objects frequently represent abrupt changes in material properties compared to the properties of the surrounding homogeneous space. This abrupt change leads to PDEs with discontinuous or near-discontinuous coefficients. Such features are hard to represent accurately using the finite element or finite difference methods. The favored approach is to introduce multiple, interlinked grids that are adjusted so that they conform to the boundaries of the scattering objects. Generating such grids, tailored to the possibly complex shape of the scattering objects, linking them together in the correct way and designing them in such a way that the resulting numerical algorithm is accurate and stable, is challenging. The approach has been refined over many years and in general works quite well, but it certainly adds to the implementation complexity of these methods.

The second type of problem is related to the fact that one cannot grid the domain where the scattering objects are located for the simple reason, that in almost all situations of interest, this domain is unbounded. This problem is well known in the research community and the way it is resolved is to grid a computational box that is large enough to contain all scattering objects of interest. This can easily become a very large domain, leading to a very large number of degrees of freedom in the numerical algorithm. However, most of the time, the numerical algorithm associated with the domain has a simple structure for which it is possible to design very fast implementations. However, the introduction of the finite computational box in what is an unbounded domain leads to the question of designing boundary conditions on the boundary of the box so that it is fully transparent to waves. This is not easy to achieve, as most approaches will introduce inhomogeneity that will partly reflect the waves hitting the boundary. This problem was first solved satisfactorily for the case of scattering electromagnetic waves. The domain-based method of choice for electromagnetic waves is the finite difference time domain method (FDTD) [1],[2],[3]. As the name indicates, this is a finite difference method that has been designed to consider the special structure of Maxwell's equations. The removal of reflections from the finite computational box was achieved by the introduction of a perfectly matched layer (PML)[4],[5]. This amounts to adding a narrow layer of a specially constructed artificial material to the outside of the computational box. The PML layer is only perfectly transparent to wave propagation if the grid has infinite resolution. For any finite grid there is still a small reflection from the boundary of the computational box. This can be reduced by making the PML layer thicker, but this leads to more degrees of freedom and thus an increasing computational load. However, overall PML works well and certainly much better than anything that came before it. There is no doubt that the introduction of PML was a breakthrough.

The use of PML was closely linked to the special structure of Maxwell's

equations. However, it was soon realized that the same effect could be achieved by complexifying the physical space outside the computational box and analytically continuing the fields into this complex spatial domain[6],[7]. Significantly, this realization made the benefits of a reflection-less boundary condition available to all kinds of scattering problems. However, the use of these reflection less boundary conditions certainly leads to an increased computational load, increased implementation complexity, and numerical stability issues that must be resolved. It is at this point worth recalling that the boundary of the computational box is not part of the original physical problem, and all the added implementation complexity and computational cost is spent trying to make it invisible after the choice of a domain method forced us to put it there in the first place.

In this paper, we are dedicated to developing an efficient new method to solve transient wave scattering in two 1D models in which the scattering objects have a nonlinear response where we only apply the domain-based method inside each scattering object. First, this will reduce the size of the computational grid enormously since we now need only to grid the inside of the scattering objects. Second, our approach makes it possible to use different computational grids for each scattering object, with each grid tailored to the corresponding object's geometric shape, without having to worry about the inherent complexity caused by letting the different grids meet up. Third, it makes the introduction of a large computational box, with its artificial boundary, redundant. In this way, the computational load is substantially reduced, and we remove the implementation complexity and instabilities associated with the boundary of the computational box.

However, the domain based-method restricted to the inside of each scattering object requires field values on the boundaries of the scattering objects to propagate the fields forward in time. These boundary values will be supplied by a boundary integral method derived from a space-time integral formulation of the PDEs to be solved. This boundary integral method will consider all the scattering and re-scattering of the solution to the PDEs in the unbounded domain outside the scattering objects. Since the boundary integral method explicitly considers the radiation condition at infinity, no finite computational box with its artificial boundary conditions is needed.

This kind of idea for solving scattering problems was, to our knowledge, first proposed in 1972 by Pattanayak and Wolf [8] for the case of electromagnetic waves. They discussed their ideas in the context of a generalization of the Ewald-Oseen optical extinction theorem; therefore, we will refer to our method as the Ewald-Oseen Scattering(EOS) formulation.

However, Pattanayak and Wolf only discussed stationary linear scattering of electromagnetic waves and they therefore did their integral formulation in frequency space. This approach is not the right one when one is interested in transient scattering from objects that are generally inhomogeneous and additionally may have a nonlinear response. What is needed for our approach is a space-time integral formulation of the PDEs of interest.

In sections 2 and 3, we illustrate our approach by implementing our EOS formulation for two different 1D scattering problems. Both cases can be thought of as toy models for scattering electromagnetic waves. This should not be taken to mean that only models that in some way are related to electromagnetic scattering can be subject to our approach. It merely reflects our particular interest

in electromagnetic scattering. The way we see it, only one essential requirement must be fulfilled for our method to be applicable. It must be possible to derive an explicit integral formulation for the PDEs of interest. This means that at some point one needs to find the explicit expression for Green's function for some differential operator related to our PDEs. In general, it is difficult to find explicit expressions for Green's function belonging to nontrivial differential operators. However, the Green's function needed for our EOS formulation will always be of the infinite, homogeneous space type, and explicit expressions for such Green's functions can frequently be found.

The two toy models presented in this work have been chosen for their simplicity, which makes them well suited for illustrating our EOS approach for scattering of waves. For more general and consequently more complicated cases, there are no new ideas beyond the technical details that must be mastered for each case to derive the EOS formulation and implement it numerically. To explore the feasibility of our approach for more realistic and useful PDEs, we have implemented our approach for several other cases, both 2D and 3D. Particularly we have derived and implemented our EOS approach for the full 3D vector Maxwell's equations. The results of these investigations will be reported elsewhere.

For both models we use an approach for testing the stability and accuracy of our implementations that involves what is known as *artificial sources*. This method has probably been around for a long time but apart from an application to the Navier-Stokes equations [9], we are not aware of any published work using this method. The method is based on the simple observation that, if arbitrary source terms are added to any system of PDEs then any function is a solution for some choice of the source. Adding a source term typically introduce only trivial modifications to whichever numerical method was used to solve the PDEs. This essentially means that for any PDEs of interest, we can design particular functions to test various critical aspects of the numerical method related to numerical stability and accuracy.

This is a very simple approach to validating numerical implementations for PDEs that deserves to be much better known than it is.

2 The first scattering model; one way propagation

Our first toy model, model 1, is

$$\begin{aligned} \varphi_t &= c_1\varphi_x + j, \\ \rho_t &= -j_x, \\ j_t &= (\alpha - \beta\rho)\varphi - \gamma j \quad a_0 < x < a_1, \end{aligned} \tag{2.1}$$

where α, β and γ are real parameters determining the "material response" part model 1 and where $\varphi = \varphi(x,t)$ is the "electric field", $j = j(x,t)$ the "current density" and ρ the "charge density". These quantities are analogs for the corresponding quantities in Maxwell's equations. With this in mind, we observe that the second equation in the model (2.1) is a 1D version of the equation of continuity from electromagnetics, and c_1 is the analog of the speed of light inside

the "material" scattering object residing inside the interval $[a_0, a_1]$. The charge density and current density are the material degrees of freedom and are therefore assumed to be confined to the interval $[a_0, a_1]$ on the real axis, whereas φ is a field defined on the whole real axis. Thus the interval $[a_0, a_1]$ is the analog of a compact scattering object in the electromagnetic situation. Outside the scattering object the model takes the form

$$\varphi_t = c_0\varphi_x + j_s \quad x < a_0 \text{ or } x > a_1, \tag{2.2}$$

where c_0 is the propagation speed for the electric field in the "vacuum" outside the scattering object and the function $j_s(x,t)$ is a fixed source that has its support in a compact set in the interval $x > a_1$. For the field φ we impose the condition of continuity at the points a_0 and a_1. The equation for the current density, j is a radical simplification of a real current density model used to describe second harmonic generation in nonlinear optics [10].

2.1 The EOS formulation

In order to derive the EOS formulation for the model (2.1), we will firstly need a space-time integral identity involving the operator

$$L = \partial_t - v\partial_x,$$

where v is some constant. Using integration by parts it is easy to see that the following integral identity holds

$$\begin{aligned}&\int_{S\times T} \mathrm{d}x\mathrm{d}t\{L\varphi(x,t)\psi(x,t) - \varphi(x,t)L^\dagger\psi(x,t)\}\\ &= \int_S \mathrm{d}x\varphi(x,t)\psi(x,t)|_{t_0}^{t_1} - v\int_T \mathrm{d}t\varphi(x,t)\psi(x,t)|_{x_0}^{x_1},\end{aligned} \tag{2.3}$$

where $L^\dagger = -\partial_t + v\partial_x$ is the formal adjoint of L and where $S = (x_0, x_1)$ and $T = (t_0, t_1)$ are open space and time intervals.

The second item we need in order to derive the EOS formulation for model (2.1), is the advanced Green's function for the operator $L^\dagger$. This is a function $G = G(x,t,x',t')$ which is a solution to the equation

$$L^\dagger G(x,t,x',t') = \delta(t-t')\delta(x-x'),$$

and that vanishes when $t > t'$. Since the operator $\mathcal{L}^+$ is invariant under time and space translations we can without loss of generality assume that

$$G(x,t,x',t') = G(x-x', t-t').$$

Thus it is sufficient to solve the equation

$$L^\dagger G(x,t) = \delta(x)\delta(t). \tag{2.4}$$

After performing the Fourier transform

$$\hat{f}(k,\omega) = \int_{-\infty}^{\infty}\int_{-\infty}^{\infty} f(x,t)e^{-i(kx-\omega t)}\,\mathrm{d}x\,\mathrm{d}t, \tag{2.5}$$

on (2.4), we get

$$\hat{G}(k,\omega) = \frac{-i}{\omega + vk}.$$

It is noticed that there's a single pole at $\omega = -vk$ on the real axis, we need to find the advanced Green's function. It is defined by shifting the integral contour from the real ω-axis to a contour below and parallel to the real axis at a distance $c_\epsilon : z = \omega - i\epsilon, \epsilon > 0$. Using the inverse Fourier transform

$$f(x,t) = \frac{1}{4\pi^2} \int_{-\infty}^{\infty} \int_{-\infty}^{\infty} \hat{f}(k,\omega) e^{i(kx-\omega t)} \, \mathrm{d}k \, \mathrm{d}\omega, \tag{2.6}$$

we get the representation

$$G(x,t) = \frac{1}{4\pi^2} \int_{-\infty}^{+\infty} g(k,t) e^{ikx} \, \mathrm{d}k,$$

with

$$g(k,t) = \int_{c_\epsilon} \frac{-i}{z + vk} e^{-izt} \, \mathrm{d}z.$$

For $t < 0$, we close the contour c_ϵ in the upper half plane and get by Cauchy's residue theorem

$$g(k,t) = 2\pi e^{ivkt},$$

and for $t > 0$, we close the contour c_ϵ in the lower half plane and get $g(k,t) = 0$. This gives for $t < 0$

$$G(x,t) = \frac{1}{4\pi^2} \int_{-\infty}^{+\infty} 2\pi e^{ivkt} e^{ikx} \mathrm{d}k = \delta(x + vt),$$

and for $t > 0$,

$$G(x,t) = 0.$$

In the end G is given by

$$G(x,t,x',t') = \theta(t' - t)\delta(x' - x + v(t' - t)), \tag{2.7}$$

where θ is the Heaviside step function with $\theta(x) = 1$ for $x > 0$ and zero otherwise.

We will now apply the integral identity (2.3) to each space interval $(-\infty, a_0)$, (a_0, a_1) and (a_1, ∞). For the function ψ we will substitute the advanced Green's function (2.7) and we will let φ be the solution to equation (2.2) with vanishing initial condition, $\varphi(x, t_0) = 0$. We thus have a problem where all solutions are purely source-generated. For the first interval, $(-\infty, a_0)$, we let ψ be the Green's function

$$G_0(x,t,x',t') \equiv \theta(t' - t)\delta(x' - x + c_0(t' - t)), \tag{2.8}$$

and $\varphi = \varphi_0$ be the solution to the equation

$$\begin{gathered} \varphi_{0t} = c_0 \varphi_{0x}, \\ \Updownarrow \\ L_0 \varphi_0 = 0. \end{gathered} \tag{2.9}$$

Inserting (2.8), (2.9) and $S = (-\infty, a_0)$ into the integral identity (2.3), using the initial condition and the fact that the Green's function is advanced, we get for x in $(-\infty, a_0)$

$$\begin{aligned}
&\int_{S\times T} \{\mathcal{L}\varphi_0(x',t')G(x',t',x,t) - \varphi_0(x',t')\mathcal{L}^+G(x',t',x,t)\}\,\mathrm{d}x'\,\mathrm{d}t' \\
&= \int_{-\infty}^{a_0} \varphi_0(x',t_1)\theta(t-t_1)\delta(x-x'+c_0(t-t_1))\,\mathrm{d}x' \\
&- \int_{-\infty}^{a_0} \varphi_0(x',t_0)\theta(t-t_0)\delta(x-x'+c_0(t-t_0))\,\mathrm{d}x' \\
&- c_0\int_{t_0}^{t_1} \varphi_0(a_0,t')\theta(t-t')\delta(x-a_0+c_0(t-t'))\,\mathrm{d}t' \\
&+ c_0 \lim_{x'\to-\infty}\int_{t_0}^{t_1} \varphi_0(x',t')\theta(t-t')\delta(x-x'+c_0(t-t'))\,\mathrm{d}t',
\end{aligned}$$

after interchanging the primed and unprimed variables. The initial condition and $t_0 < t < t_1$ imply that the integrals on S vanish. The last integral vanishes also because $x - x' + c_0(t-t') > 0$ when $x' < x$ for all t' in the integration interval (t_0, t). So we finally get

$$\varphi_0(x,t) = c_0\int_{t_0}^{t} \mathrm{d}t'\varphi_0(a_0,t')\delta(x-a_0+c_0(t-t')). \tag{2.10}$$

Note that when writing formula (2.10) we have made the substitution

$$\varphi_0(a_0,\cdot) \equiv \lim_{x\to a_0^-} \varphi_0(x,\cdot).$$

Similar substitutions will be made without comment later in the following sections.

For the second interval, (a_0, a_1), we let ψ be the Green's function

$$G_1(x,t,x',t') \equiv \theta(t'-t)\delta(x'-x+c_1(t'-t)), \tag{2.11}$$

and $\varphi = \varphi_1$ be the solution to the equation

$$\begin{aligned}
&\varphi_{1t} = c_1\varphi_{1x} + j, \\
&\Updownarrow \\
&L_1\varphi = j,
\end{aligned} \tag{2.12}$$

with vanishing initial conditions. Inserting (2.11),(2.12) and $S = (a_0, a_1)$ into the integral identity (2.3), using the initial condition and the fact that the

Green's function is advanced, we get for x in (a_0, a_1)

$$\begin{aligned}\varphi_1(x,t) &= \int_{a_0}^{a_1} \mathrm{d}x' \int_{t_0}^{t} \mathrm{d}t' j(x',t')\delta(x-x'+c_1(t-t')) \\ &+ c_1 \int_{t_0}^{t} \mathrm{d}t' \varphi_1(a_1,t')\delta(x-a_1+c_1(t-t')) \\ &- c_1 \int_{t_0}^{t} \mathrm{d}t' \varphi_1(a_0,t')\delta(x-a_0+c_1(t-t')) \\ &= \int_{a_0}^{a_1} \mathrm{d}x' \int_{t_0}^{t} \mathrm{d}t' j(x',t')\delta(x-x'+c_1(t-t')) \\ &+ c_1 \int_{t_0}^{t} \mathrm{d}t' \varphi_1(a_1,t')\delta(x-a_1+c_1(t-t')), \end{aligned} \tag{2.13}$$

after interchanging primed and unprimed variables. The last equality sign follows because $x - a_0 + c_1(t-t') > 0$ for all t' in the integration interval when $a_0 < x < a_1$.

Finally, for the third integration interval, (a_1, ∞), we let ψ be the Green's function

$$G_0(x,t,x',t') \equiv \theta(t'-t)\delta(x'-x+c_0(t'-t)), \tag{2.14}$$

and $\varphi = \varphi_2$ be the solution to the equation

$$\begin{aligned} \varphi_{2t} &= c_0\varphi_{2x} + j_s, \\ &\Updownarrow \\ L_0\varphi_2 &= j_s, \end{aligned} \tag{2.15}$$

with vanishing initial conditions. Inserting (2.14),(2.15) and $S = (a_1, \infty)$ into the integral identity (2.3), using the initial conditions and the fact that the Green's function is advanced, we get for x in (a_1, ∞)

$$\begin{aligned}\varphi_2(x,t) &= \int_{a_1}^{\infty} \mathrm{d}x' \int_{t_0}^{t} \mathrm{d}t' j_s(x',t')\delta(x-x'+c_0(t-t')) \\ &+ c_0 \lim_{x'\to\infty} \int_{t_0}^{t} \mathrm{d}t' \varphi_2(x',t')\delta(x-x'+c_0(t-t')) \\ &- c_0 \int_{t_0}^{t} \mathrm{d}t' \varphi_2(a_1,t')\delta(x-a_1+c_0(t-t')) \\ &= \int_{a_1}^{\infty} \mathrm{d}x' \int_{t_0}^{t} \mathrm{d}t' j_s(x',t')\delta(x-x'+c_0(t-t')), \end{aligned} \tag{2.16}$$

after interchanging primed and unprimed variables. The third term vanishes because $x - a_1 + c_0(t-t') > 0$ for all t' in the integration interval when $x > a_1$. The second term vanishes because $x - x' + c_0(t-t') < 0$ for all fixed $x > a_1$, $t > t_0$ and all t' in the integration interval (t_0, t) when x' is large enough.

We now investigate the limit of these integral identities as x approaches the boundary points $\{a_0, a_1\}$ of the open interval (a_0, a_1) from inside and outside the interval. This will give us four equations for the four quantities

$$\varphi_0(a_0,t), \varphi_1(a_0,t), \varphi_1(a_1,t), \varphi_2(a_1,t).$$

However, by assumption, acceptable solutions of model 1 are continuous across the boundary points $\{a_0, a_1\}$. Therefore, we have two additional equations

$$\varphi_0(a_0, t) = \varphi_1(a_0, t),$$
$$\varphi_1(a_1, t) = \varphi_2(a_1, t).$$

At this point we are faced with a problem. The four unknown quantities must satisfy six linear equations. The problem is thus overdetermined and we would not normally expect any nontrivial solutions to exist.

On the other hand, the equations, boundary conditions and source function j_s that define model 1 do determine a unique function φ. This function satisfies by construction the integral identities (2.10),(2.13) and (2.16), whose limits yielded the overdetermined system. Thus the overdetermined linear system does have a solution.

There is a more direct way to see why the overdetermined system will have a solution. Let us consider the inside of the scattering object, thus $x \in (a_0, a_1)$. Here, the field φ is determined in terms of the current $j(x, t)$, and the boundary value $\varphi(a_1, t)$ by identity (2.13)

$$\begin{aligned}\varphi_1(x,t) = &\int_{a_0}^{a_1} \mathrm{d}x' \int_{t_0}^{t} \mathrm{d}t' j(x', t')\delta(x - x' + c_1(t - t')) \\ &+ c_1 \int_{t_0}^{t} \mathrm{d}t' \varphi_1(a_1, t')\delta(x - a_1 + c_1(t - t')).\end{aligned} \tag{2.17}$$

Naively, one would expect that we would obtain an equation determining the unknown boundary value $\varphi(a_1, t)$, by taking the limit of (2.17) as x approaches a_1 from below. However, this would make the field inside the scattering object independent of the outside source, which must be wrong from a scattering point of view. After all, it is the outside source $j_s(x, t)$ that determines the field both outside and inside the scattering object. If this source is turned off the field would simply be zero everywhere. So what is going on?

Note that if we actually take the limit of (2.17) we get the equation

$$0\ \varphi_1(a_1, t) = 0,$$

which leaves the boundary value entirely arbitrary. If we analyze the rest of the overdetermined system in the same way, we find that one more equation for the boundary data is redundant, and that the two unknown boundary values, $\varphi_1(a_0, t)$ and $\varphi(a_1, t)$, are uniquely determined by the following two equations

$$\begin{aligned}\varphi_1(a_0,t) = &\int_{a_0}^{a_1} \mathrm{d}x' \theta(a_0 - x' + c_1(t - t_0)) j(x', t - \frac{a_1 - a_0}{c_1}) \\ &+ \theta(a_0 - a_1 + c_1(t - t_0))\varphi(a_1, t - \frac{a_1 - a_0}{c_1}),\end{aligned} \tag{2.18}$$

$$\varphi_1(a_1,t) = \frac{1}{c_0} \int_{a_1}^{\infty} \mathrm{d}x' \theta(a_1 - x' + c_0(t - t_0)) j_s(x', t - \frac{x' - a_1}{c_0}). \tag{2.19}$$

We emphasize the fact that we end up with an overdetermined system of linear equations for the boundary values because this is a generic outcome when we derive the EOS formulation for any given system of PDEs. We see that this

very same problem will appear when we discuss the second toy model in Section 3.

This problem has been recognized by the research community in the context of space-time boundary integral formulation for Maxwell's equations, and a simple fix has been invented to resolve it.

However, as far as we know, the universal nature of this problem in the area of space-time integral formulations of linear and nonlinear scattering problems has not been recognized.

Observe that equation (2.19) determines the value of the field at the boundary point a_1 in terms of the given external source j_s, and the equation (2.18) determines the value of the field at the boundary point a_0 in terms of the current density j inside the scattering object and the field values at the boundary point a_1.

Equations (2.1) restricted to the the open interval (a_0, a_1) together with the integral identities (2.18) and (2.19) define the EOS formulation for model 1.

2.2 Numerical implementation of the EOS formulation

In this section, a numerical implementation of the EOS formulation for model 1 is presented. Many different numerical implementations are possible. The EOS formulation itself does not in any way dictate the use of a particular implementation. However it does put some constraints on how we proceed with our method of choice.

If our problem was to calculate the free-space propagation according to the first equation in (2.1) with vanishing j the obvious choice would be to use the standard Lax-Wendroff method[11] on a uniform space grid. However, the EOS formulation presents us with an integro-differential equation because the boundary update rule is defined in terms of integrals of the current density over the scattering domain (a_0, a_1). Thus our grid must also give a good approximation for the integrals (2.18) and (2.19) that define the update rule. We will be looking for second-order accuracy and would like to use the midpoint rule to approximate the integrals and thus introduce the following nonuniform space grid inside the scattering object, (a_0, a_1),

$$x_i = a_0 + (i + 0.5)\Delta x,\ i = 0, 1, \cdots, N-1, \tag{2.20}$$

where $\Delta x = \frac{a_1 - a_0}{N}$. The grid points (2.20) will be called internal nodes. We also introduce a discrete time grid

$$t^n = n\Delta t,\ n = 0, 1, \cdots .$$

The values of the parameter Δt will, as usual, be bounded by the requirement of stability for the scheme. We will say a few words about this bound later.

To obtain a numerical scheme of second-order accuracy, we apply the Lax-Wendroff method to the first two equations of (2.1) and apply the modified Euler's method to the last equation of (2.1). Because of these choices the nu-

merical scheme for iteration at the internal nodes takes the form

$$\begin{aligned}
\varphi_i^{n+1} =& \varphi_i^n + \Delta t\ (c_1 \frac{\partial \varphi}{\partial x} + j)_i^n + \frac{1}{2}(\Delta t)^2 (c_1^2 \frac{\partial^2 \varphi}{\partial x^2} + c_1 \frac{\partial j}{\partial x} + f)_i^n, \\
\rho_i^{n+1} =& \rho_i^n + \Delta t\ (-\frac{\partial j}{\partial x})_i^n + \frac{1}{2}(\Delta t)^2 (-\frac{\partial f}{\partial x})_i^n, \\
\bar{j}_i^{n+1} =& j_i^n + \Delta t\ f_i^n, \\
j_i^{n+1} =& \frac{1}{2}(j_i^n + \bar{j}_i^{n+1} + \Delta t\ f(\rho_i^{n+1}, \varphi_i^{n+1}, \bar{j}_i^{n+1})),
\end{aligned} \tag{2.21}$$

for $i = 0, 1, \cdots, N$ and where $f = (\alpha - \beta\rho)\varphi - \gamma j$. Except for the two internal nodes closest to the boundary points a_0 and a_1, the space derivatives are approximated to second-order accuracy by the following standard finite difference formulas

$$\begin{aligned}
(\frac{\partial \phi}{\partial x})_i^n &= \frac{\phi_{i+1}^n - \phi_{i-1}^n}{2\Delta x}, \\
(\frac{\partial^2 \phi}{\partial x^2})_i^n &= \frac{\phi_{i+1}^n - 2\phi_i^n + \phi_{i-1}^n}{(\Delta x)^2},\ \phi = \varphi, j, f, \text{and } i = 1, 2, \cdots, N-2.
\end{aligned} \tag{2.22}$$

For the two internal nodes closest to the boundary, the standard, second-order accurate difference formulas, cannot be used because the internal nodes are non-uniformly distributed in this part of the domain. For the field, φ, we must rather use the following second-order accurate difference formulas for these two nodes

$$\begin{aligned}
(\frac{\partial \varphi}{\partial x})_0^n &= -\frac{1}{3\Delta x}(4\varphi_{a_0}^n - 3\varphi_0^n - \varphi_1^n), \\
(\frac{\partial^2 \varphi}{\partial x^2})_0^n &= \frac{4}{3(\Delta x)^2}(2\varphi_{a_0}^n - 3\varphi_0^n + \varphi_1^n), \\
(\frac{\partial \varphi}{\partial x})_{N-1}^n &= \frac{1}{3\Delta x}(4\varphi_{a_1}^n - 3\varphi_{N-1}^n - \varphi_{N-2}^n), \\
(\frac{\partial^2 \varphi}{\partial x^2})_{N-1}^n &= \frac{4}{3(\Delta x)^2}(2\varphi_{a_1}^n - 3\varphi_{N-1}^n + \varphi_{N-2}^n).
\end{aligned} \tag{2.23}$$

The boundary value $\varphi_{a_0}^n$ needed in formulas (2.23) can be calculated from the discretized form of the integral update rules (2.18)

$$\begin{aligned}
\varphi_{a_0}^{n+1} = \frac{\Delta x}{c_1} \sum_{i=0}^{N-1} & \theta(t_{n+1} - t_0 - \frac{x_i - a_0}{c_1}) j(x_i, t_{n+1} - \frac{x_i - a_0}{c_1}), \\
& + \theta(t_{n+1} - t_0 - \frac{a_1 - a_0}{c_1}) \varphi(a_1, t_{n+1} - \frac{a_1 - a_0}{c_1}),
\end{aligned} \tag{2.24}$$

while $\varphi_{a_1}^n$ is determined by the outside source using (2.19).

The current density, j, is entirely supported inside the scattering object and in general would be discontinuous at a_0 and a_1 if extended to the whole domain by making it zero external to the scattering object. Because of this, we need difference rules for j at the nodes closest to the boundary points a_0 and a_1 that only depend on the values of j on internal nodes. The following second-order

accurate difference rules for j are of this type

$$
\begin{aligned}
(\frac{\partial j}{\partial x})_0^n &= \frac{1}{2\Delta x}(4j_1^n - 3j_0^n - j_2^n), \\
(\frac{\partial j}{\partial x})_{N-1}^n &= -\frac{1}{2\Delta x}(4j_{N-2}^n - 3j_{N-1}^n - j_{N-3}^n).
\end{aligned} \tag{2.25}
$$

It is evident that the discretized boundary update rule (2.24) needs values of the current density that are located between the grid points for the time grid $\{t^n\}$. This situation is general and will always arise when we seek numerical implementations of EOS formulations of PDEs. Some numerical interpolation scheme will always be needed to calculate the field values and/or the material variables between the time grid locations. We use a quadratic interpolation for values of the current density located between two time levels to maintain overall second-order accuracy for our scheme.

The iteration (2.21) with the boundary update rule (2.24) supplemented by the finite difference rules (2.22),(2.23) and (2.25) constitute our numerical implementation of the EOS formulation for model 1.

2.3 Artificial source test

The basic idea behind the artificial source test, of some numerical scheme designed for a system of PDEs, is to slightly modify the system by adding an arbitrary source to all the equations in the system. This modification typically leads to minimal modifications to the numerical scheme, where most of the effort and complexity are usually spent on the derivatives and nonlinear terms. For the equations, however, the presence of the sources changes the situation completely. This is because the presence of the added sources implies that *any* function is a solution to the equations for *some* choice of sources.

With the risk of expanding on perhaps an already obvious idea, what we are saying is that, if we have developed a numerical scheme for some system of differential equations $\mathscr{L}\psi = 0$, we can with small modifications extend our scheme to the extended equation $\mathscr{L}\psi = g$ where g is any given function. Given this, we test the numerical scheme by picking a function ψ_0, then use the equation to calculate the source function $g_0 = \mathscr{L}\psi_0$ that ensures that our chosen function is a solution to the extended equation. Finally, we run the numerical scheme with the calculated source function and find an approximate solution that we compare with the exact solution ψ_0.

Mode 1 extended with artificial sources takes the form

$$
\begin{aligned}
\varphi_t &= c_1\varphi_x + j + g_1, \\
\rho_t &= -j_x + g_2, \\
j_t &= (\alpha - \beta\rho)\varphi - \gamma j + g_3,
\end{aligned} \tag{2.26}
$$

where g_1, g_2, g_3, are the artificial source functions. For some choice of functions $\hat{\varphi}, \hat{j}$ and $\hat{\rho}$ the corresponding source functions are computed by

$$
\begin{aligned}
\hat{g}_1 &= \hat{\varphi}_t - c_1\hat{\varphi}_x - \hat{j}, \\
\hat{g}_2 &= \hat{\rho}_t + \hat{j}_x, \\
\hat{g}_3 &= \hat{j}_t - (\alpha - \beta\hat{\rho})\hat{\varphi} + \gamma\hat{j}.
\end{aligned}
$$

As our exact solution we choose

$$\begin{aligned}\hat{\varphi}(x,t) =& \frac{2A_1}{\pi}\arctan(b^2t^2)e^{-\alpha_1(x-x_o+\beta_1(t-t_s))^2},\\ \hat{j}(x,t) =& A_2 e^{-\frac{(x-x_j)^2}{\delta_1^2}-\frac{(t-t_j)^2}{\delta_2^2}},\\ \hat{\rho}(x,t) =& A_3 e^{-\frac{(x-x_\rho)^2}{\delta_3^2}-\frac{(t-t_\rho)^2}{\delta_4^2}},\end{aligned} \tag{2.27}$$

which is nowhere near a solution to the equations (2.2) defining the unmodified model 1. Note that the chosen exact solution satisfies the vanishing of the initial data $\hat{\varphi}(x,t_0=0)=0$, as it must in order to be consistent with the EOS formulation. The boundary update rule for the source extended model (2.26) is changed into

$$\begin{aligned}\varphi_{a_0}^{n+1} =& \frac{\Delta x}{c_1}\sum_{i=0}^{N-1}\theta(t_{n+1}-t_0-\frac{x_i-a_0}{c_1})j(x_i,t_{n+1}-\frac{x_i-a_0}{c_1}),\\ &+\frac{\Delta x}{c_1}\sum_{i=0}^{N-1}\theta(t_{n+1}-t_0-\frac{x_i-a_0}{c_1})\hat{g}_1(x_i,t_{n+1}-\frac{x_i-a_0}{c_1}),\\ &+\theta(t_{n+1}-t_0-\frac{a_1-a_0}{c_1})\hat{\varphi}(a_1,t_{n+1}-\frac{a_1-a_0}{c_1}),\end{aligned}$$

while $\hat{\varphi}_{a_1}^n$ is given explicitly by the exact solution $\hat{\varphi}(x,t)$. The comparison

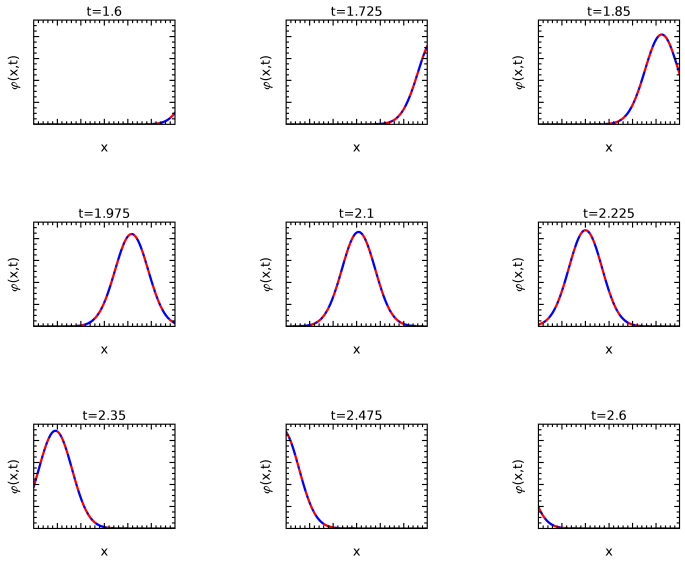

Figure 2.1: Comparison between the numerical solution and the exact solution for the source extended model 1. Parameter values used are $a_0=0.0, a_1=3.0, N=1600$, $\alpha=-1.0$, $\beta=0.3$, $\gamma=8.0$, $c=2.0$, $c_0=1.0$, $A_1=1.0$, $A_2=1.0$, $A_3=1.0$, $b=1.0$, $\alpha_1=4.0, \beta_1=4.0, x_o=6.0, t_s=1.0$, $x_j=1.1, x_\rho=1.3, t_j=1.2, t_\rho=1.3, \delta_1=0.3, \delta_2=0.32, \delta_3=1.0, \delta_4=0.33$.

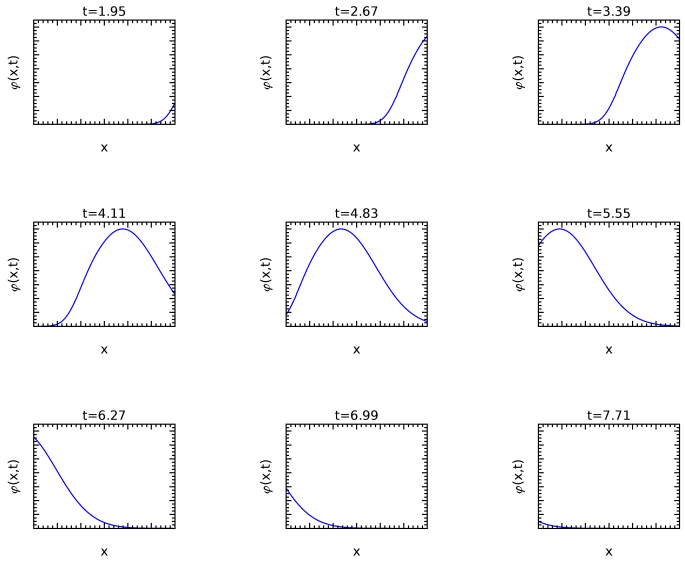

Figure 2.2: A numerical solution of the EOS formulation for model 1 generated by an external source. The parameter values used are $a_0 = 0.0, a_1 = 3.0, N = 1600, c = 2.0, c_0 = 1.0$, $\alpha = -1.0$, $\beta = 0.3$, $\gamma = 8.0$.

between the exact solution (2.27) and the approximative solution generated by our numerical implementation of the EOS formulation of the source extended model 1, (2.26), is shown in Fig 2.1 for some choice of the parameters. As we can see, the correspondence between the exact and approximative solution is excellent. After having established that our implementation is accurate using the artificial source test, we show in Fig 2.2 the numerical solution φ of model 1, (2.1), where the system is driven by an outside source of the form

$$j_s = 5e^{-36(x-4)^2-4(t-0.5)^2},$$

which is chosen so that no influence hit the boundary at a_1 before $t = 0$. This will ensure that the initial condition $\varphi(x, t = 0) = 0$, underlying the EOS formulation of model 1, is satisfied.

In these simulations we used a Δt which is in the stable range for the numerical implementation, specifically we used $\Delta t = 0.4\frac{\Delta x}{c}$. Observe that the stability domain for our implementation of the EOS formulation is restricted compared to the stability domain for the underlying Lax-Wendroff method on an infinite domain. The focus of the first two sections is to derive the EOS formulation for two simple illustrative models and show that, using standard finite difference discretization of the EOS formulation, we get an accurate and stable representation of the solution to the scattering problems defined by the two toy models. A discussion of the stability of our schemes for both toy models has been relegated to Appendix A. We have found that stability of our scheme requires that the time step is contained in an interval. This interval is determined by the domain-based method, which is propagating the fields inside the scattering object forward in time. While applying the EOS approach to the

case of 3D electromagnetic scattering, we also found a stability interval for the time step. For this case however, we find that both the domain part and the boundary part of the EOS formulation play a role in determining the interval. We believe that the way that the material parameters for the scattering objects influence the boundaries of the stability interval has some interesting things to say about the occurrence of the late time instability from antenna theory.

3 The second scattering model; two way propagation

Our second toy model, model 2 is

$$\begin{aligned}
\varphi_t &= \mu_1 \psi_x + j, \\
\psi_t &= \nu_1 \varphi_x, \\
\rho_t &= -j_x, \\
j_t &= (\alpha - \beta\rho)\varphi - \gamma j \quad a_0 < x < a_1,
\end{aligned} \tag{3.1}$$

where , like for model 1, $\varphi = \varphi(x,t)$, $j = j(x,t)$ and $\rho(x,t)$ are interpreted as "electric field", "current density" and "charge density". The additional field, $\psi(x,t)$ is interpreted as the "magnetic" field. The charge density and current density will, as in model 1, be confined to the interval $[a_0, a_1]$ on the real axis whereas the fields φ and ψ are defined on the whole real axis. The interval $[a_0, a_1]$ is, like for model 1, the analog of a compact scattering object in the electromagnetic situation. Outside the interval the model equations are

$$\begin{aligned}
\varphi_t &= \mu_0 \psi_x + j_s, \\
\psi_t &= \nu_0 \varphi_x,
\end{aligned} \tag{3.2}$$

where the function $j_s(x,t)$ is a given source that, like for model 1, has its support on a compact set in the interval $x > a_1$. The parameters μ_1, μ_0, ν_1, ν_0 are "material" parameters. Using the translation $\mu \to \frac{1}{\epsilon}$ and $\nu \to \frac{1}{\mu}$ they are analogous for the electric permittivity, ϵ, and the magnetic permeability, μ, inside and outside the scattering object.

3.1 EOS formulation

In order to derive the EOS formulation for model 2 (3.1),(3.2), we will firstly need a space-time integral identity involving the matrix operator

$$L = \begin{pmatrix} \partial_t & -\mu\partial_x \\ -\nu\partial_x & \partial_t \end{pmatrix},$$

where μ and ν are constants. The operator acts on vector valued functions in the usual way

$$L \begin{pmatrix} \varphi \\ \psi \end{pmatrix} = \begin{pmatrix} \partial_t\varphi - \mu\partial_x\psi \\ \partial_t\psi - \nu\partial_x\varphi \end{pmatrix}.$$

Using integration by parts, it is easy to derive

$$\int_{S\times T} A\mathcal{L}\begin{pmatrix}\varphi\\ \psi\end{pmatrix}(x,t)\,dx\,dt$$

$$=\int_{S\times T}\begin{pmatrix}-\partial_t A_{11}+\nu\partial_x A_{12} & \mu\partial_x A_{11}-\partial_t A_{12}\\ -\partial_t A_{21}+\nu\partial_x A_{22} & \mu\partial_x A_{21}-\partial_t A_{22}\end{pmatrix}\begin{pmatrix}\varphi\\ \psi\end{pmatrix}(x,t)\,dx\,dt$$

$$+\int_S \begin{pmatrix}A_{11} & A_{12}\\ A_{21} & A_{22}\end{pmatrix}\begin{pmatrix}\varphi\\ \psi\end{pmatrix}(x,t)\Big|_{t_0}^{t_1} dx$$

$$+\int_T \begin{pmatrix}-\nu A_{12} & -\mu A_{11}\\ -\nu A_{22} & -\mu A_{21}\end{pmatrix}\begin{pmatrix}\varphi\\ \psi\end{pmatrix}(x,t)\Big|_{x_0}^{x_1} dt,$$

so we get the following integral identity

$$\int_{S\times T} \mathrm{d}x dt\{AL\begin{pmatrix}\varphi\\ \psi\end{pmatrix}(x,t)-L^\dagger A\begin{pmatrix}\varphi\\ \psi\end{pmatrix}(x,t)\}$$

$$=\int_S \mathrm{d}x A\begin{pmatrix}\varphi\\ \psi\end{pmatrix}(x,t)|_{t_0}^{t_1}+\int_T dtB\begin{pmatrix}\varphi\\ \psi\end{pmatrix}(x,t)|_{x_0}^{x_1}, \tag{3.3}$$

where $S=(x_0,x_1)$ and $T=(t_0,t_1)$ are open space and time intervals and where φ and ψ are smooth functions on the space-time interval $S\times T$. Also $A=A(x,t)$ is a 2×2 matrix valued function and $L^\dagger$ is the formal adjoint to the operator L, and acts on the matrix valued function A in the following way

$$L^\dagger A=\begin{pmatrix}-\partial_t A_{11}+\nu\partial_x A_{12} & \mu\partial_x A_{11}-\partial_t A_{12}\\ -\partial_t A_{21}+\nu\partial_x A_{22} & \mu\partial_x A_{21}-\partial_t A_{22}\end{pmatrix}. \tag{3.4}$$

B is the 2×2 matrix valued function

$$B=\begin{pmatrix}-\nu A_{12} & -\mu A_{11}\\ -\nu A_{22} & -\mu A_{21}\end{pmatrix}. \tag{3.5}$$

The second item we need in order to derive the EOS formulation for model (3.1), (3.2), is the advanced Green's function for the operator $L^\dagger$. This is a 2×2 matrix valued function $G(x,t,x',t')$ that satisfies the equation

$$L^\dagger G(x,t,x',t')=\delta(t-t')\delta(x-x')I, \tag{3.6}$$

and that vanishes for $t>t'$. In (3.6), I is the 2×2 identity matrix. Due to the fact that any Green's function, because of translational invariance only depends on $x-x'$ and $t-t'$, we can solve

$$L^\dagger G(x,t)=\delta(t)\delta(x)I,$$

instead. Writing out components we get

$$\begin{aligned}
&\partial_t G_{11}-\nu\partial_x G_{12}=-\delta(t)\delta(x),\\
&\partial_t G_{12}-\mu\partial_x G_{11}=0,\\
&\partial_t G_{21}-\nu\partial_x G_{22}=0,\\
&\partial_t G_{22}-\mu\partial_x G_{21}=-\delta(t)\delta(x).
\end{aligned} \tag{3.7}$$

Performing Fourier transform (2.5) on the first two equations of (3.7) gives

$$\begin{aligned} -i\omega\hat{G}_{11} - i\nu k\hat{G}_{12} &= -1, \\ -i\omega\hat{G}_{12} - i\nu k\hat{G}_{11} &= 0. \end{aligned} \tag{3.8}$$

The solutions to (3.8) are

$$\begin{aligned} \hat{G}_{11}(k,\omega) &= \frac{-i\omega}{\omega^2 - c^2k^2}, \\ \hat{G}_{12}(k,\omega) &= \frac{i\mu k}{\omega^2 - c^2k^2}, \end{aligned} \tag{3.9}$$

where $c^2 = \mu\nu$. By enforcing the inverse Fourier transform (2.6) on (3.9), we get

$$\begin{aligned} G_{11}(x,t) &= \frac{1}{4\pi^2}\int_{-\infty}^{\infty} g_{11}(k,t)e^{ikx}\,dk, \\ G_{12}(x,t) &= \frac{1}{4\pi^2}\int_{-\infty}^{\infty} g_{12}(k,t)e^{ikx}\,dk, \end{aligned} \tag{3.10}$$

where

$$\begin{aligned} g_{11}(k,t) &= \int_{-\infty}^{\infty} \hat{G}_{11}(k,\omega)e^{-i\omega t}\,d\omega, \\ g_{12}(k,t) &= \int_{-\infty}^{\infty} \hat{G}_{12}(k,\omega)e^{-i\omega t}\,d\omega. \end{aligned}$$

The expressions for g_{11} and g_{12} are not really well defined since the integrands have two poles on the real ω-axis, so we choose the advanced Green's function for our work. It is defined by shifting the integral contour from the real ω-axis to a contour below and parallel to the real axis at a distance $c_\epsilon : z = \omega - i\epsilon, \epsilon > 0$, thus

$$\begin{aligned} g_{11}(k,t) &= \int_{c_\epsilon} \frac{-iz}{z^2 - c^2k^2}e^{-izt}\,dz, \\ g_{12}(k,t) &= \int_{c_\epsilon} \frac{i\mu k}{z^2 - c^2k^2}e^{-izt}\,dz. \end{aligned}$$

If $t > 0$,

$$\lim_{z_i \to -\infty} e^{z_i t} = 0,$$

so we close the contour in the lower half plane and have

$$\begin{aligned} g_{11}(k,t) &= 0, \\ g_{12}(k,t) &= 0. \end{aligned}$$

If $t < 0$,

$$\lim_{z_i \to +\infty} e^{z_i t} = 0,$$

then we close the contour in the upper half plane. There are now two poles $z = \pm ck$ inside the closed contour. Cauchy's residue theorem gives

$$\begin{aligned} g_{11}(k,t) &= \pi\{e^{ikct} + e^{-ikct}\}, \\ g_{12}(k,t) &= \frac{\pi\mu}{c}\{e^{ikct} - e^{-ikct}\}. \end{aligned} \tag{3.11}$$

Inserting (3.11) into (3.10), we obtain

$$\begin{aligned} G_{11}(k,t) &= \frac{\theta(-t)}{2}(\delta(x+ct)+\delta(x-ct)), \\ G_{12}(k,t) &= \frac{\mu\theta(-t)}{2c}(\delta(x+ct)-\delta(x-ct)). \end{aligned}$$

G_{12} and G_{22} are calculated in the same way,

$$\begin{aligned} G_{21}(k,t) &= \frac{\nu\theta(-t)}{2c}(\delta(x+ct)-\delta(x-ct)), \\ G_{22}(k,t) &= \frac{\theta(-t)}{2}(\delta(x+ct)+\delta(x-ct)). \end{aligned}$$

In the end, G is given by

$$G(x,t,x',t') = \frac{\theta(t'-t)}{2c}\{\begin{pmatrix} c & \mu \\ \nu & c \end{pmatrix}\delta(x-x'+c(t-t')) + \begin{pmatrix} c & -\mu \\ -\nu & c \end{pmatrix}\delta(x-x'-c(t-t'))\}, \tag{3.12}$$

where $\theta(s)$ is the Heaviside step function. Note that, using the identifications introduced while describing model 2 at the start of the current section, the formula defining the speed, c, is completely analogous to the one defining the speed of light in electromagnetics.

We will now apply the integral identity (3.3) to each space interval $(-\infty, a_0)$, (a_0, a_1) and (a_1, ∞) with A equal to the advanced Green's function (3.12) for the corresponding interval and where φ and ψ are solutions to the system (3.1),(3.2) with vanishing initial conditions $\varphi(x,t_0) = \psi(x,t_0) = 0$.

For the first interval, $(-\infty, a_0)$, we let A be the Green's function

$$G_0(x,t,x',t') = \frac{\theta(t'-t)}{2c_0}\{\begin{pmatrix} c_0 & \mu_0 \\ \nu_0 & c_0 \end{pmatrix}\delta(x-x'+c_0(t-t')) + \begin{pmatrix} c_0 & -\mu_0 \\ -\nu_0 & c_0 \end{pmatrix}\delta(x-x'-c_0(t-t'))\}, \tag{3.13}$$

where $c_0^2 = \mu_0\nu_0$. In this interval we let $\varphi = \varphi_0, \psi = \psi_0$ be the solution to the system

$$\begin{aligned} \varphi_{0t} &= \mu_0\psi_{0x}, \\ \psi_{0t} &= \nu_0\varphi_{0x}, \\ &\Updownarrow \\ L_0\begin{pmatrix} \varphi_0 \\ \psi_0 \end{pmatrix} &= 0. \end{aligned} \tag{3.14}$$

Inserting (3.13), (3.14) and $S = (-\infty, a_0)$ into the integral identity (3.3), using the initial conditions and the fact that the Green's function is advanced, we get

for x in the interval $(-\infty, a_0)$.

$$\begin{pmatrix} \varphi_0 \\ \psi_0 \end{pmatrix}(x,t) = -\int_{t_0}^{t_1} \mathrm{d}t' B_0(a_0,t',x,t) \begin{pmatrix} \varphi_0 \\ \psi_0 \end{pmatrix}(a_0,t') + \lim_{R\to-\infty} \int_{t_0}^{t_1} \mathrm{d}t' B_0(R,t',x,t) \begin{pmatrix} \varphi_0 \\ \psi_0 \end{pmatrix}(R,t'), \tag{3.15}$$

after interchanging primed and unprimed variables.

The function B_0 is from (3.5)

$$B_0(x',t',x,t) = -\frac{\theta(t-t')}{2}\{\begin{pmatrix} c_0 & \mu_0 \\ \nu_0 & c_0 \end{pmatrix}\delta(x-x'+c_0(t-t')) + \begin{pmatrix} -c_0 & \mu_0 \\ \nu_0 & -c_0 \end{pmatrix}\delta(x-x'-c_0(t-t'))\}. \tag{3.16}$$

From (3.16) it is evident that the last term in (3.15) vanishes. This is because for large enough R, the argument of the delta function does not change sign in the interval of integration. Inserting the expression (3.16) into (3.15) and changing to the variable defining the argument of the delta function in the two integrals, we get that for x in $(-\infty, a_0)$

$$\begin{pmatrix} \varphi_0 \\ \psi_0 \end{pmatrix}(x,t) = \frac{\theta(x-a_0+c_0(t-t_0))}{2c_0} \begin{pmatrix} c_0 & \mu_0 \\ \nu_0 & c_0 \end{pmatrix} \begin{pmatrix} \varphi_0 \\ \psi_0 \end{pmatrix}(a_0, t+\frac{x-a_0}{c_0}). \tag{3.17}$$

For the second interval, (a_0, a_1), we let A be the Green's function

$$G_1(x,t,x',t') = \frac{\theta(t'-t)}{2c_1}\{\begin{pmatrix} c_1 & \mu_1 \\ \nu_1 & c_1 \end{pmatrix}\delta(x-x'+c_1(t-t')) + \begin{pmatrix} c_1 & -\mu_1 \\ -\nu_1 & c_1 \end{pmatrix}\delta(x-x'-c_1(t-t'))\}. \tag{3.18}$$

where $c_1^2 = \mu_1\nu_1$. In this interval, the functions $\varphi = \varphi_1, \psi = \psi_1$ are the solutions to the system

$$\begin{aligned} \varphi_{1t} &= \mu_1\psi_{1x} + j, \\ \psi_{1t} &= \nu_1\varphi_{1x}, \\ &\Updownarrow \\ L_1 \begin{pmatrix} \varphi_1 \\ \psi_1 \end{pmatrix} &= \begin{pmatrix} j \\ 0 \end{pmatrix}. \end{aligned} \tag{3.19}$$

Inserting (3.18), (3.19) and $S = (a_0, a_1)$ in the integral identity (3.3), using the vanishing initial conditions and the fact that the Green's function is advanced,

we get for x in the interval (a_0, a_1).

$$\begin{pmatrix} \varphi_1 \\ \psi_1 \end{pmatrix}(x,t) = \int_{S\times T} \mathrm{d}x'\mathrm{d}t' G_1(x',t',x,t) \begin{pmatrix} j \\ 0 \end{pmatrix}(x',t') \\ - \int_{t_0}^{t_1} \mathrm{d}t' B_1(a_1,t',x,t) \begin{pmatrix} \varphi_1 \\ \psi_1 \end{pmatrix}(a_1,t) \\ + \int_{t_0}^{t_1} \mathrm{d}t' B_1(a_0,t',x,t) \begin{pmatrix} \varphi_1 \\ \psi_1 \end{pmatrix}(a_0,t), \tag{3.20}$$

after interchanging primed and unprimed variables.

The function B_1 is from (3.5)

$$B_1(x',t',x,t) = -\frac{\theta(t-t')}{2}\{\begin{pmatrix} c_1 & \mu_1 \\ \nu_1 & c_1 \end{pmatrix}\delta(x-x'+c_1(t-t')) \\ + \begin{pmatrix} -c_1 & \mu_1 \\ \nu_1 & -c_1 \end{pmatrix}\delta(x-x'-c_1(t-t'))\}. \tag{3.21}$$

Inserting (3.18) and (3.21) into (3.20), we get after changing variables to the arguments in the delta functions that for x in (a_0, a_1)

$$\begin{pmatrix} \varphi_1 \\ \psi_1 \end{pmatrix}(x,t) =$$

$$\frac{1}{2c_1^2}\begin{pmatrix} c_1 & -\mu_1 \\ -\nu_1 & c_1 \end{pmatrix}\int_{a_0}^{x}\mathrm{d}x'\theta(c_1(t-t_0)-(x-x'))\binom{j}{0}(x',t-\frac{x-x'}{c_1})$$

$$+\frac{1}{2c_1^2}\begin{pmatrix} c_1 & \mu_1 \\ \nu_1 & c_1 \end{pmatrix}\int_{x}^{a_1}\mathrm{d}x'\theta(c_1(t-t_0)-(x'-x))\binom{j}{0}(x',t-\frac{x'-x}{c_1})$$

$$+\theta(c_1(t-t_0)-(a_1-x))\frac{1}{2c_1}\begin{pmatrix} c_1 & \mu_1 \\ \nu_1 & c_1 \end{pmatrix}\begin{pmatrix} \varphi_1 \\ \psi_1 \end{pmatrix}(a_1,t-\frac{a_1-x}{c_1})$$

$$-\theta(c_1(t-t_0)-(x-a_0))\frac{1}{2c_1}\begin{pmatrix} -c_1 & \mu_1 \\ \nu_1 & -c_1 \end{pmatrix}\begin{pmatrix} \varphi_1 \\ \psi_1 \end{pmatrix}(a_0,t-\frac{x-a_0}{c_1}). \tag{3.22}$$

For the third interval, (a_1, ∞), we let A be the Green's function

$$G_0(x,t,x',t') = \frac{\theta(t'-t)}{2c_0}\{\begin{pmatrix} c_0 & \mu_0 \\ \nu_0 & c_0 \end{pmatrix}\delta(x-x'+c_0(t-t')) \\ + \begin{pmatrix} c_0 & -\mu_0 \\ -\nu_0 & c_0 \end{pmatrix}\delta(x-x'-c_0(t-t'))\}. \tag{3.23}$$

In this interval, the functions $\varphi = \varphi_2, \psi = \psi_2$ are the solutions to the system

$$\begin{aligned} \varphi_{2t} &= \mu_0 \psi_{2x} + j_s, \\ \psi_{2t} &= \nu_0 \varphi_{2x}, \\ &\Updownarrow \\ L_0 \begin{pmatrix} \varphi_2 \\ \psi_2 \end{pmatrix} &= \begin{pmatrix} j_s \\ 0 \end{pmatrix}. \end{aligned} \tag{3.24}$$

Inserting (3.23), (3.24) and $S = (a_1, \infty)$ in the integral identity (3.3), using the initial conditions and the fact that the Green's function is advanced, we get for x in the interval (a_1, ∞).

$$\begin{aligned} \begin{pmatrix} \varphi_2 \\ \psi_2 \end{pmatrix}(x,t) = &\int_{S\times T} \mathrm{d}x'\mathrm{d}t' G_0(x',t',x,t) \begin{pmatrix} j_s \\ 0 \end{pmatrix}(x',t') \\ &- \lim_{R\to\infty} \int_{t_0}^{t_1} \mathrm{d}t' B_0(R,t',x,t) \begin{pmatrix} \varphi_2 \\ \psi_2 \end{pmatrix}(R,t) \\ &+ \int_{t_0}^{t_1} \mathrm{d}t' B_0(a_1,t',x,t) \begin{pmatrix} \varphi_2 \\ \psi_2 \end{pmatrix}(a_1,t), \end{aligned} \tag{3.25}$$

after interchanging primed and unprimed variables.

Since the arguments of the delta functions in B_0 does not change sign in the interval of integration, for R big enough, it is clear that the second term in (3.25) will vanish. Inserting (3.23) and (3.16) into the remaining terms of (3.25), we get after changing variables to the arguments in the delta functions that for x in (a_1, ∞)

$$\begin{pmatrix} \varphi_2 \\ \psi_2 \end{pmatrix}(x,t) =$$

$$\begin{aligned} &- \theta(c_0(t-t_0) - (x-a_1)) \frac{1}{2c_0} \begin{pmatrix} -c_0 & \mu_0 \\ \nu_0 & -c_0 \end{pmatrix} \begin{pmatrix} \varphi_2 \\ \psi_2 \end{pmatrix}(a_1, t - \frac{x-a_1}{c_0}) \\ &+ \begin{pmatrix} \varphi_i \\ \psi_i \end{pmatrix}(x,t), \end{aligned} \tag{3.26}$$

where φ_i and ψ_i are fields that are entirely determined by the given source j_s

$$\begin{pmatrix} \varphi_i \\ \psi_i \end{pmatrix}(x,t) =$$

$$\frac{1}{2c_0^2} \begin{pmatrix} c_0 & -\mu_0 \\ -\nu_0 & c_0 \end{pmatrix} \int_{a_1}^{x} \mathrm{d}x' \theta(c_0(t-t_0) - (x-x')) \begin{pmatrix} j_s \\ 0 \end{pmatrix}(x', t - \frac{x-x'}{c_0})$$

$$+ \frac{1}{2c_0^2} \begin{pmatrix} c_0 & \mu_0 \\ \nu_0 & c_0 \end{pmatrix} \int_{x}^{\infty} \mathrm{d}x' \theta(c_0(t-t_0) - (x'-x)) \begin{pmatrix} j_s \\ 0 \end{pmatrix}(x', t - \frac{x'-x}{c_0}).$$

Taking the limit of the integral identities (3.17),(3.22) and (3.26) as x approaches

the boundary points $\{a_0, a_1\}$ from inside and outside the interval (a_0, a_1) we get

$$\begin{pmatrix} c_0 & -\mu_0 \\ -\nu_0 & c_0 \end{pmatrix} \begin{pmatrix} \varphi_0 \\ \psi_0 \end{pmatrix} (a_0, t) = 0, \tag{3.27}$$

$$\begin{pmatrix} c_1 & \mu_1 \\ \nu_1 & c_1 \end{pmatrix} \begin{pmatrix} \varphi_1 \\ \psi_1 \end{pmatrix} (a_0, t) =$$

$$\frac{1}{c_1} \begin{pmatrix} c_1 & \mu_1 \\ \nu_1 & c_1 \end{pmatrix} \int_{a_0}^{a_1} \mathrm{d}x' \theta(c_1(t - t_0) - (x' - a_0)) \binom{j}{0} (x', t - \frac{x' - a_0}{c_1})$$

$$+ \theta(c_1(t - t_0) - (a_1 - a_0)) \begin{pmatrix} c_1 & \mu_1 \\ \nu_1 & c_1 \end{pmatrix} \begin{pmatrix} \varphi_1 \\ \psi_1 \end{pmatrix} (a_1, t - \frac{a_1 - a_0}{c_1}), \tag{3.28}$$

$$\begin{pmatrix} c_1 & -\mu_1 \\ -\nu_1 & c_1 \end{pmatrix} \begin{pmatrix} \varphi_1 \\ \psi_1 \end{pmatrix} (a_1, t) =$$

$$\frac{1}{c_1} \begin{pmatrix} c_1 & -\mu_1 \\ -\nu_1 & c_1 \end{pmatrix} \int_{a_0}^{a_1} \mathrm{d}x' \theta(c_1(t - t_0) - (a_1 - x')) \binom{j}{0} (x', t - \frac{a_1 - x'}{c_1})$$

$$- \theta(c_1(t - t_0) - (a_1 - a_0)) \begin{pmatrix} -c_1 & \mu_1 \\ \nu_1 & -c_1 \end{pmatrix} \begin{pmatrix} \varphi_1 \\ \psi_1 \end{pmatrix} (a_0, t - \frac{a_1 - a_0}{c_1}), \tag{3.29}$$

$$\begin{pmatrix} c_0 & \mu_0 \\ \nu_0 & c_0 \end{pmatrix} \begin{pmatrix} \varphi_2 \\ \psi_2 \end{pmatrix} (a_1, t) = 2c_0 \begin{pmatrix} \varphi_i \\ \psi_i \end{pmatrix} (a_1, t). \tag{3.30}$$

Continuity of the fields at the boundary points $\{a_0, a_1\}$, gives us two additional equations,

$$\begin{pmatrix} \varphi_0 \\ \psi_0 \end{pmatrix} (a_0, t) = \begin{pmatrix} \varphi_1 \\ \psi_1 \end{pmatrix} (a_0, t), \tag{3.31}$$

$$\begin{pmatrix} \varphi_1 \\ \psi_1 \end{pmatrix} (a_1, t) = \begin{pmatrix} \varphi_2 \\ \psi_2 \end{pmatrix} (a_1, t). \tag{3.32}$$

Altogether we have six linear equations for the four vectors

$$\begin{pmatrix} \varphi_0 \\ \psi_0 \end{pmatrix} (a_0, t), \begin{pmatrix} \varphi_1 \\ \psi_1 \end{pmatrix} (a_0, t), \begin{pmatrix} \varphi_1 \\ \psi_1 \end{pmatrix} (a_1, t), \begin{pmatrix} \varphi_2 \\ \psi_2 \end{pmatrix} (a_1, t).$$

Thus our system (3.27)-(3.32) is overdetermined just like it was for model 1. And just like for model 1, the system (3.27)-(3.32) contains equations that are redundant. Mathematically this is reflected in the fact that the determinant of the matrices

$$\begin{pmatrix} c_j & \pm\mu_j \\ \pm\nu_j & c_j \end{pmatrix}, \quad j = 0, 1 \ ,$$

are all zero. For the first toy model, it was obvious which two equations were redundant. Here it is not immediately clear which equations we can remove, and

this will also be the case if we write down the EOS formulation for more general systems of PDEs, like for example Maxwell's equations. For the system (3.27)-(3.32), it is not very difficult to identify the redundant equations, but we would rather introduce a different approach that is generally quite useful when working with the EOS formulations of PDEs. This is the method that has been used by the research community to calculate electromagnetic scattering from linear homogeneous scattering objects using a time dependent integral formulation of Maxwell's equations. The *reason* that this method has been used for Maxwell's equations has not been clearly stated in the research literature. It has taken the form of a trick that is needed to achieve stability and accuracy for the numerical implementation of the boundary formulation of electromagnetic scattering.

The point is that, although the system (3.27)-(3.32) is singular, we know from its construction that it has a solution consisting boundary values coming from the unique solution to the system (3.1),(3.2).

In terms of linear algebra, the situation is that for two given singular matrices A and B, the system

$$\begin{aligned} A\mathbf{x} &= \mathbf{b}_1, \\ B\mathbf{x} &= \mathbf{b}_2, \end{aligned} \tag{3.33}$$

has a solution, $\mathbf{x}$. Let us assume that there are numbers a and b such that

$$\det(aA + bB) \neq 0.$$

Given (3.33) it is clear that $\mathbf{x}$ is a solution to the linear system

$$(aA + bB)\mathbf{x} = a\mathbf{b}_1 + b\mathbf{b}_2, \tag{3.34}$$

and since the system (3.34) is nonsingular, $\mathbf{x}$ is the unique solution to the system. Finding numbers such that $aA + bB$ is nonsingular is in general not difficult.

Let us apply this approach to the system (3.27)-(3.32). Simply adding together the equations give us a matrix

$$\begin{pmatrix} c_0 & -\mu_0 \\ -\nu_0 & c_0 \end{pmatrix} + \begin{pmatrix} c_1 & \mu_1 \\ \nu_1 & c_1 \end{pmatrix} = \begin{pmatrix} c_1 + c_0 & \mu_1 - \mu_0 \\ \nu_1 - \nu_0 & c_1 + c_0 \end{pmatrix},$$

and

$$\det \begin{pmatrix} c_1 + c_0 & \mu_1 - \mu_0 \\ \nu_1 - \nu_0 & c_1 + c_0 \end{pmatrix} = 2c_1c_0 + \mu_0\nu_1 + \mu_1\nu_0,$$

which is nonzero since all the numbers ν_i, μ_j, c_j are positive by assumption. In a similar way, adding together (3.29) and (3.30) will result in a nonsingular system. Thus from the singular system (3.27)-(3.32) we get the nonsingular system

$$\begin{pmatrix} c_1 + c_0 & \mu_1 - \mu_0 \\ \nu_1 - \nu_0 & c_1 + c_0 \end{pmatrix} \begin{pmatrix} \varphi_1 \\ \psi_1 \end{pmatrix} (a_0, t) =$$

$$\frac{1}{c_1} \begin{pmatrix} c_1 & \mu_1 \\ \nu_1 & c_1 \end{pmatrix} \int_{a_0}^{a_1} \mathrm{d}x' \theta(c_1(t - t_0) - (x' - a_0)) \begin{pmatrix} j \\ 0 \end{pmatrix} (x', t - \frac{x' - a_0}{c_1})$$

$$+ \theta(c_1(t - t_0) - (a_1 - a_0)) \begin{pmatrix} c_1 & \mu_1 \\ \nu_1 & c_1 \end{pmatrix} \begin{pmatrix} \varphi_1 \\ \psi_1 \end{pmatrix} (a_1, t - \frac{a_1 - a_0}{c_1}), \tag{3.35}$$

$$\begin{pmatrix} c_0+c_1 & \mu_0-\mu_1 \\ \nu_0-\nu_1 & c_1+c_0 \end{pmatrix}\begin{pmatrix} \varphi_1 \\ \psi_1 \end{pmatrix}(a_1,t) =$$

$$\frac{1}{c_1}\begin{pmatrix} c_1 & -\mu_1 \\ -\nu_1 & c_1 \end{pmatrix}\int_{a_0}^{a_1} \mathrm{d}x'\theta(c_1(t-t_0)-(a_1-x'))\binom{j}{0}(x', t-\frac{a_1-x'}{c_1})$$

$$-\theta(c_1(t-t_0)-(a_1-a_0))\begin{pmatrix} -c_1 & \mu_1 \\ \nu_1 & -c_1 \end{pmatrix}\begin{pmatrix} \varphi_1 \\ \psi_1 \end{pmatrix}(a_0, t-\frac{a_1-a_0}{c_1})$$
$$+2c_0\begin{pmatrix} \varphi_i \\ \psi_i \end{pmatrix}(a_1,t). \tag{3.36}$$

The system (3.35),(3.36), which determine the boundary values of the fields in term of internal and external current densities, together with the differential equations (3.1), restricted to the inside the scattering object (a_0, a_1), constitute the EOS formulation for model 2.

3.2 Numerical implementation of the EOS formulation

The numerical implementation of model 2 contains the same elements as the ones we introduced for model 1. Thus we first define a nonuniform space grid inside the scattering object, (a_0, a_1),

$$x_i = a_0 + (i+0.5)\Delta x,\ i = 0, 1, \cdots, N-1, \tag{3.37}$$

where $\Delta x = \frac{a_1-a_0}{N}$. The grid points (3.37) are the internal nodes for model 2. We also introduce the discrete time grid

$$t^n = n\Delta t,\ n = 0, 1, \cdots.$$

The values of the parameter Δt will of course, like for model 1, be bounded by the requirement of stability for the scheme. We apply the Lax-Wendroff method to the first three equations of (3.1) and the modified Euler's method to the last equation of (3.1). For interval (a_0, a_1), the numerical iteration can be written as

$$\begin{aligned}
\varphi_i^{n+1} =& \varphi_i^n + \Delta t\ (\mu_1\frac{\partial\psi}{\partial x} + j)_i^n + \frac{1}{2}(\Delta t)^2(\mu_1\nu_1\frac{\partial^2\varphi}{\partial x^2} + f)_i^n, \\
\psi_i^{n+1} =& \psi_i^n + \Delta t\ (\nu_1\frac{\partial\varphi}{\partial x})_i^n + \frac{1}{2}(\Delta t)^2(\mu_1\nu_1\frac{\partial^2\psi}{\partial x^2} + \nu_1\frac{\partial j}{\partial x})_i^n, \\
\rho_i^{n+1} =& \rho_i^n + \Delta t\ (-\frac{\partial j}{\partial x})_i^n + \frac{1}{2}(\Delta t)^2(-\frac{\partial f}{\partial x})_i^n, \\
\bar{j}_i^{n+1} =& j_i^n + \Delta t\ f_i^n, \\
j_i^{n+1} =& \frac{1}{2}(j_i^n + \bar{j}_i^n + \Delta t\ f(\rho_i^{n+1}, \varphi_i^{n+1}, \bar{j}_i^{n+1})),
\end{aligned} \tag{3.38}$$

where $f = (\alpha - \beta\rho)\varphi - \gamma j$. The finite difference approximations for the fields and the current density at all internal nodes, except the two nodes closest to

the boundary points a_0 and a_1, are given by the standard expressions

$$\begin{aligned}(\frac{\partial\phi}{\partial x})_i^n &= \frac{\phi_{i+1}^n - \phi_{i-1}^n}{2\Delta x},\\ (\frac{\partial^2\phi}{\partial x^2})_i^n &= \frac{\phi_{i+1}^n - 2\phi_i^n + \phi_{i-1}^n}{(\Delta x)^2},\ \phi = \varphi, \psi, j,\end{aligned} \tag{3.39}$$

for $i = 1, 2, \cdots, N-2,$. For the two internal nodes closest to the boundary points, we need to use alternative difference rules because the grid is nonuniform in the domain around these nodes

$$\begin{aligned}(\frac{\partial\phi}{\partial x})_0^n &= -\frac{1}{3\cdot\Delta x}(4\phi_{a_0}^n - 3\phi_0^n - \phi_1^n),\\ (\frac{\partial^2\phi}{\partial x^2})_0^n &= \frac{4}{3\cdot(\Delta x)^2}(2\phi_{a_0}^n - 3\phi_0^n + \phi_1^n),\\ (\frac{\partial\phi}{\partial x})_{N-1}^n &= \frac{1}{3\cdot\Delta x}(4\phi_{a_1}^n - 3\phi_{N-1}^n - \phi_{N-2}^n),\\ (\frac{\partial^2\phi}{\partial x^2})_{N-1}^n &= \frac{4}{3\cdot(\Delta x)^2}(2\phi_{a_1}^n - 3\phi_{N-1}^n + \phi_{N-2}^n),\\ (\frac{\partial j}{\partial x})_0^n &= \frac{1}{2\Delta x}(4j_1^n - 3j_0^n - j_2^n),\\ (\frac{\partial j}{\partial x})_{N-1}^n &= -\frac{1}{2\Delta x}(4j_{N-2}^n - 3j_{N-1}^n - j_{N-3}^n),\end{aligned} \tag{3.40}$$

where $\phi = \varphi, \psi$. The discretization of the boundary update rules (3.35) and (3.36) are

$$\begin{pmatrix} c_1 + c_0 & \mu_1 - \mu_0 \\ \nu_1 - \nu_0 & c_1 + c_0 \end{pmatrix} \begin{pmatrix} \varphi \\ \psi \end{pmatrix} (a_0, t_{n+1})$$

$$= \frac{\Delta x}{c_1} \begin{pmatrix} c_1 & \mu_1 \\ \nu_1 & c_1 \end{pmatrix} \sum_{i=0}^{N-1} \theta(t_{n+1} - t_0 - \frac{x_i - a_0}{c_1}) \begin{pmatrix} j \\ 0 \end{pmatrix} (x_i, t_{n+1} - \frac{x_i - a_0}{c_1}) \tag{3.41}$$

$$+ \begin{pmatrix} c_1 & \mu_1 \\ \nu_1 & c_1 \end{pmatrix} \theta(t_{n+1} - t_0 - \frac{a_1 - a_0}{c_1}) \begin{pmatrix} \varphi \\ \psi \end{pmatrix}_- (a_1, t_{n+1} - \frac{a_1 - a_0}{c_1}),$$

$$\begin{pmatrix} c_1 + c_0 & \mu_0 - \mu_1 \\ \nu_0 - \nu_1 & c_1 + c_0 \end{pmatrix} \begin{pmatrix} \varphi \\ \psi \end{pmatrix} (a_1, t_{n+1}) =$$

$$\frac{\Delta x}{c_1} \begin{pmatrix} c_1 & -\mu_1 \\ -\nu_1 & c_1 \end{pmatrix} \sum_{i=0}^{N-1} \theta(t_{n+1} - t_0 - \frac{a_1 - x_i}{c_1}) \begin{pmatrix} j \\ 0 \end{pmatrix} (x_i, t_{n+1} - \frac{a_1 - x_i}{c_1})$$

$$- \begin{pmatrix} -c_1 & \mu_1 \\ \nu_1 & -c_1 \end{pmatrix} \theta(t_{n+1} - t_0 - \frac{a_1 - a_0}{c_1}) \begin{pmatrix} \varphi \\ \psi \end{pmatrix}_+ (a_0, t_{n+1} - \frac{a_1 - a_0}{c_1}) \tag{3.42}$$

$$+ 2c_0 \begin{pmatrix} \varphi_i \\ \psi_i \end{pmatrix} (a_1, t_{n+1}).$$

where $\begin{pmatrix} \varphi_i \\ \psi_i \end{pmatrix}(a_1, t_{n+1})$ are determined by the external source. The iteration (3.38) with the boundary update rules (3.41), (3.42) supplemented by the finite difference rules (3.39) and (3.40) constitute our numerical implementation of the EOS formulation for model 2.

3.3 Artificial source test

The source extended model 2, is given by

$$\begin{aligned}
\varphi_t &= \mu_1 \psi_x + j + g_1, \\
\psi_t &= \nu_1 \varphi_x + g_2, \\
\rho_t &= -j_x + g_3, \\
j_t &= (\alpha - \beta\rho)\varphi - \gamma j + g_4.
\end{aligned}$$

For the source extended model 2, any given set of functions $\hat{\varphi}$, $\hat{\psi}$, $\hat{j}$ and $\hat{\rho}$ is a solution if the sources are chosen to be

$$\begin{aligned}
\hat{g}_1 &= \hat{\varphi}_t - \mu_1 \hat{\psi}_x - \hat{j}, \\
\hat{g}_2 &= \hat{\psi}_t - \nu_1 \hat{\varphi}_x, \\
\hat{g}_3 &= \hat{\rho}_t + \hat{j}_x, \\
\hat{g}_4 &= \hat{j}_t - (\alpha - \beta\hat{\rho})\hat{\varphi} + \gamma\hat{j}.
\end{aligned}$$

The boundary update rules for the source extended model 2 are changed into

$$\begin{pmatrix} c_1 + c_0 & \mu_1 - \mu_0 \\ \nu_1 - \nu_0 & c_1 + c_0 \end{pmatrix} \begin{pmatrix} \varphi_1 \\ \psi_1 \end{pmatrix}(a_0, t) =$$

$$\frac{1}{c_1} \begin{pmatrix} c_1 & \mu_1 \\ \nu_1 & c_1 \end{pmatrix} \int_{a_0}^{a_1} \mathrm{d}x' \theta(c_1(t - t_0) - (x' - a_0)) \begin{pmatrix} j + \hat{g}_1 \\ \hat{g}_2 \end{pmatrix}(x', t - \frac{x' - a_0}{c_1})$$

$$+ \theta(c_1(t - t_0) - (a_1 - a_0)) \begin{pmatrix} c_1 & \mu_1 \\ \nu_1 & c_1 \end{pmatrix} \begin{pmatrix} \varphi_1 \\ \psi_1 \end{pmatrix}(a_1, t - \frac{a_1 - a_0}{c_1}),$$

$$\begin{pmatrix} c_0 + c_1 & \mu_0 - \mu_1 \\ \nu_0 - \nu_1 & c_1 + c_0 \end{pmatrix} \begin{pmatrix} \varphi_1 \\ \psi_1 \end{pmatrix}(a_1, t) =$$

$$\frac{1}{c_1} \begin{pmatrix} c_1 & -\mu_1 \\ -\nu_1 & c_1 \end{pmatrix} \int_{a_0}^{a_1} \mathrm{d}x' \theta(c_1(t - t_0) - (a_1 - x')) \begin{pmatrix} j + \hat{g}_1 \\ \hat{g}_2 \end{pmatrix}(x', t - \frac{a_1 - x'}{c_1})$$

$$- \theta(c_1(t - t_0) - (a_1 - a_0)) \begin{pmatrix} -c_1 & \mu_1 \\ \nu_1 & -c_1 \end{pmatrix} \begin{pmatrix} \varphi_1 \\ \psi_1 \end{pmatrix}(a_0, t - \frac{a_1 - a_0}{c_1})$$

$$+ 2c_0 \begin{pmatrix} \varphi_i \\ \psi_i \end{pmatrix}(a_1, t).$$

In Fig 3.1 we compare the numerical and exact solution of the EOS formulation

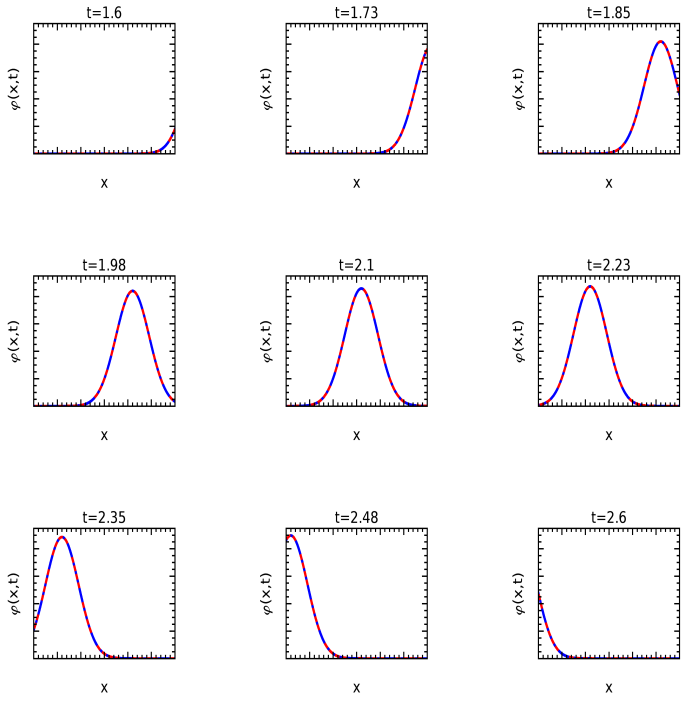

Figure 3.1: Comparison between the numerical solution and the exact solution for the source extended model 2. Parameter values used are $a_0 = 0.0, a_1 = 3.0, N = 1600$, $\alpha = -1.0$, $\beta = 0.3$, $\gamma = 8.0$, $\mu = 2.0, \nu = 2.0$, $\mu_0 = 1.0, \nu_0 = 1.0$, $A_1 = 1.0$, $A_2 = 1.0$, $A_3 = 1.0$, $A_4 = 1.0$, $b_1 = 1.0$, $b_2 = 1.0$, $\alpha_1 = 4.0, \beta_1 = 4.0, \alpha_2 = 4.0, \beta_2 = 4.0, x_o = 6.0, t_s = 1.0$, $x_j = 1.1, x_\rho = 1.3, t_j = 1.2, t_\rho = 1.3, \delta_1 = 0.3, \delta_2 = 0.32, \delta_3 = 1.0, \delta_4 = 0.33$.

for the source extended model 2. The exact solution we used for this test is

$$\hat{\varphi}(x,t) = \frac{2A_1}{\pi}\arctan(b_1^2t^2)e^{-\alpha_1(x-x_o+\beta_1(t-t_s))^2},$$
$$\hat{\psi}(x,t) = \frac{2A_2}{\pi}\arctan(b_2^2t^2)e^{-\alpha_2(x-x_o+\beta_2(t-t_s))^2},$$
$$\hat{j}(x,t) = A_3e^{-\frac{(x-x_j)^2}{\delta_1^2}-\frac{(t-t_j)^2}{\delta_2^2}},$$
$$\hat{\rho}(x,t) = A_4e^{-\frac{(x-x_\rho)^2}{\delta_3^2}-\frac{(t-t_\rho)^2}{\delta_4^2}}.$$

Our implementation clearly passes the artificial source test with flying colors. Fig 3.2 shows scattering of a wave generated by an external source calculated from our numerical implementation of the EOS formulation for model 2. The source we used is given by

$$j_s = Ae^{-\alpha_1(x-x_o)^2-\beta_1(t-ts)^2}.$$

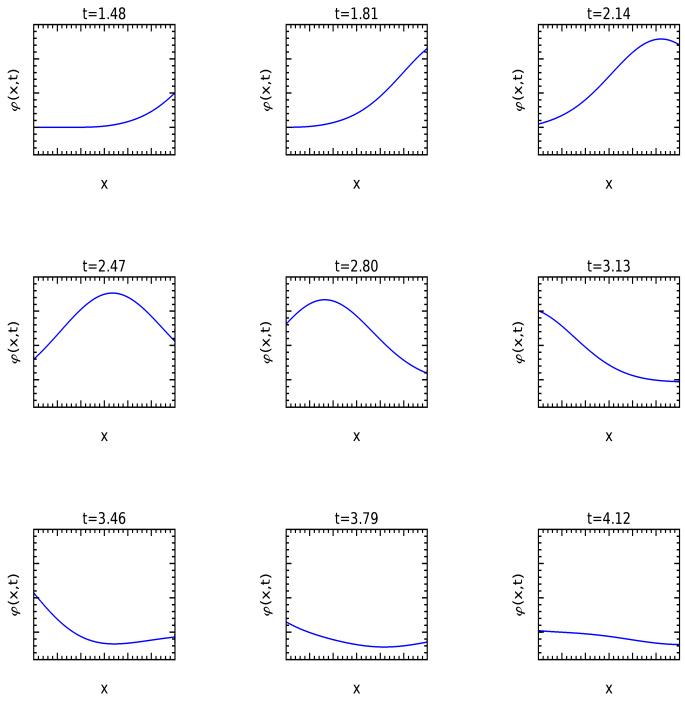

Figure 3.2: A numerical solution of the EOS formulation for model 2 generated by an external source. The parameter values used are $a_0 = 0.0, a_1 = 3.0, N = 1600$, $\alpha = -1.0$, $\beta = 0.3$, $\gamma = 8.0$, $\mu = 2.0$, $\nu = 2.0$, $\mu_0 = 1.0$, $\nu_0 = 1.0, A = 1.0, \alpha_1 = 36, \beta_1 = 4, t_s = 1.0, x_o = 4.0$.

A Stability of the numerical schemes for model 1 and model 2

As mentioned in the main text, we do not expect the two 1D models to be representative for stability issues pertaining to numerical implementation to EOS formulations in general. However, there is an issue that is worth discussing here. From the EOS formulation of model 1, one might expect that there would be severe stability issues associated with any numerical approximation. The reason is that the basic equation for the field inside the domain (a_0, a_1)

$$\varphi_t = c_1 \varphi_x, \tag{A.1}$$

uncoupled for simplicity from the internally generated current density j, can only satisfy the boundary condition at the right boundary a_1 induced by the external source. This is because equation (A.1) is of order one in space derivatives. Consequently, one cannot impose any additional boundary condition at a_0 that is independent of the one imposed at a_1. The EOS formulation evades this problem in this simplified setting by imposing the boundary condition

$$\varphi_1(a_0, t) = \theta(a_0 - a_1 + c_1(t - t_0))\varphi(a_1, t - \frac{a_1 - a_0}{c_1}), \tag{A.2}$$

which depends on the boundary condition at a_1 in exactly the way it needs for a solution, for the boundary value problem for (A.1) on the interval (a_0, a_1), to exist. However, this existence seems precarious. If we miss the right value by even a small amount in a numerical scheme, are we not then solving a boundary value problem for (A.1) where the two boundary conditions are *not* related in the right way, and is there not a danger that this non-existence will manifest itself in a numerical instability? In fact, could it be that the restricted domain of stability of the EOS formulation, as noted in the main text, is a result of the very particular delay-boundary conditions imposed because of the EOS formulation? If this was true it would be important because such delay boundary conditions are a general feature of EOS formulations. We will however now show that the restricted domain of stability for the 1D models are in fact caused by nonuniformity rather than delayed type boundary conditions.

For this purpose we introduce a family of grids of the interval (a_0, a_1) that are parametrized by ϵ. The grid is uniform for $\epsilon = 0$ and is equal to the nonuniform grid we used for our numerical implementations for model 1 and 2 when $\epsilon = 1$.

$$x_i = a_0 + (i + 1 - 0.5\epsilon)\Delta x, \;\; i = 0, 1, \cdots, N - 1,$$

where $\epsilon \in [0, 1]$ and

$$\Delta = \frac{N + \epsilon}{N(N + 1)}(a_1 - a_0).$$

To derive a finite difference scheme for (A.1), using the Lax-Wendroff approach, as in the main text, we must to impose some boundary conditions. In the end, these conditions do not influence the stability of the scheme. Therefor, for simplicity, we impose fixed boundary conditions. Given this the numerical scheme takes the form

$$\mathbf{U}_{n+1} = M_1 \mathbf{U}_n + \mathbf{b}, \tag{A.3}$$

where $\mathbf{U} = (\varphi)$ is a N vector, M_1 is a matrix of order $N \times N$ given by

$$M_1 = \begin{bmatrix} \eta_1 + c_1\,\eta_2 & \gamma_1 + c_1\,\gamma_2 & 0 & 0 & 0 & \dots & 0 \\ \kappa_1 - c_1\,\kappa_2 & \chi & \kappa_1 + c_1\,\kappa_2 & 0 & 0 & \dots & 0 \\ 0 & \kappa_1 - c_1\,\kappa_2 & \chi & \kappa_1 + c_1\,\kappa_2 & 0 & \dots & 0 \\ \vdots & \vdots & \vdots & \vdots & \vdots & \vdots & \vdots \\ 0 & \dots & 0 & 0 & \kappa_1 - c_1\,\kappa_2 & \chi & \kappa_1 + c_1\,\kappa_2 \\ 0 & \dots & 0 & 0 & 0 & \gamma_3 - c_1\,\gamma_4 & \eta_3 - c_1\,\eta_4 \end{bmatrix}$$

where the entries of the matrix depend on the discrete grid but not on the boundary conditions and where $\mathbf{b}$ is determined by the boundary values. For

the numerical schemes in toy model 1,

$$\eta_1 = 1 - \frac{\Delta^2 + \Delta_1\,\Delta}{\delta_1}\tau^2, \qquad \eta_2 = \frac{\Delta^2 - \Delta_1^2}{\delta_1}D,$$
$$\eta_3 = 1 - \frac{\Delta^2 + \Delta_2\,\Delta}{\delta_2}\tau^2, \qquad \eta_4 = \frac{\Delta^2 - \Delta_2^2}{\delta_2}D,$$
$$\gamma_1 = \frac{\Delta_1\,\Delta}{\delta_1}\tau^2, \qquad \gamma_2 = \frac{\Delta_1^2}{\delta_1}D,$$
$$\gamma_3 = \frac{\Delta_2\,\Delta}{\delta_2}\tau^2, \qquad \gamma_4 = \frac{\Delta_2^2}{\delta_2}D,$$
$$\kappa_1 = \frac{1}{2}\tau^2, \qquad \kappa_2 = \frac{1}{2}D,$$
$$\chi = 1 - \tau^2,$$

where

$$\Delta t = \tau\frac{\Delta}{c_1}, \qquad D = \frac{\Delta t}{\Delta},$$
$$\Delta_1 = (1 - \frac{1}{2}\epsilon)\Delta, \qquad \Delta_2 = \frac{N - \frac{1}{2}N\epsilon + \frac{1}{2}\epsilon^2}{N + \epsilon}\Delta,$$
$$\delta_1 = \Delta_1^2 + \Delta_1\,\Delta, \qquad \delta_2 = \Delta_2^2 + \Delta_2\,\Delta.$$

Let us look for a constant solution to (A.3), $\mathbf{U} = \mathbf{U}^*$. For $\mathbf{U}^*$ to be a solution, we must have

$$(M_1 - I)\mathbf{U}^* = \mathbf{b}, \tag{A.4}$$

where I is identity matrix of order $N \times N$. In order to have a unique solution for (A.4), $\lambda = 1$ must not be an eigenvalue for M. Thus, the unique solution will be given by

$$\mathbf{U}^* = (M_1 - I)^{-1}\mathbf{b}.$$

Define now $\mathbf{y}_n$ by

$$\mathbf{U}_n = \mathbf{y}_n + \mathbf{U}^*.$$

$$\begin{aligned} \mathbf{y}_{n+1} + \mathbf{U}^* &= M_1(\mathbf{y}_n + \mathbf{U}^*) + \mathbf{b}, \\ &\Updownarrow \\ \mathbf{y}_{n+1} &= M_1\mathbf{y}_n. \end{aligned} \tag{A.5}$$

The matrix M_1 is not symmetric, but numerical investigations show that it in general has N different eigenvalues, $\lambda_i, i = 1, 2, \cdots, N$. Then the corresponding eigenvectors, $\mathbf{y}_i$, are then independent and form a basis for $\mathbb{R}$. Let now $\mathbf{y}_0 \in \mathbb{R}$ be an initial value for (A.5). Then we have

$$\begin{aligned} \mathbf{y}_0 &= \sum_i d_i\mathbf{y}_i, \\ &\Updownarrow \\ \mathbf{y}_n = M_1^n\mathbf{y}_0 &= \sum_i d_i\lambda_i^n\mathbf{y}_i. \end{aligned}$$

We can see that if there exists any eigenvalue that is located outside the unit circle, then $\|\mathbf{y}_n\| \to \infty$. To obtain a stable numerical solution to model (A.1), the eigenvalues of M_1 must satisfy

$$\max_i \ |\lambda_i \ | < 1.$$

Using this result we find that the stability domain as a function of ϵ is of the form

$$\tau_1(\epsilon)\frac{\Delta x}{c_1} < \Delta t < \tau_2(\epsilon)\frac{\Delta x}{c_1}. \tag{A.6}$$

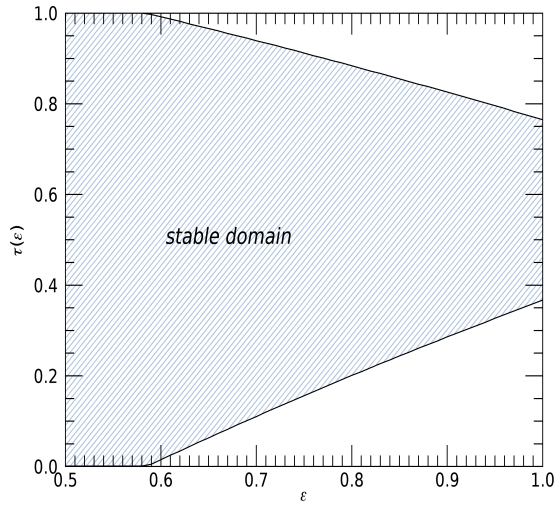

Figure A.1: The stability domain for the EOS formulation of (A.1).

It is evident from Fig A.1 that the restriction on the stability domain for the EOS formulation of (A.1), as compared to the Lax-Wendroff scheme for the case of free space propagation, is caused by the introduction of a nonuniform grid for the EOS formulation.

For model 2 we find the same stability domain as illustrated in Fig A.1 for model 1. That there should be some relation between the stability of these two models is perhaps not very surprising at the level of PDEs. After all, if we decouple the fields in model 2 from the current, the resulting system is equivalent to the wave equation and the solutions of that equation are sums of left and right going waves of the type described by Model 1. However, at the level of numerical schemes the coinciding of the stability domains for the two models is somewhat less obvious. Note that we can write the matrix M_1, determining the stability for model 1, in the form

$$M_1 = m_1 + c\, m_1,$$

where m_1 and m_2 are $N \times N$ matrices given by,

$$m_1 = \begin{bmatrix} \eta_1 & \gamma_1 & 0 & 0 & 0 & \dots & 0 \\ \kappa_1 & \chi & \kappa_1 & 0 & 0 & \dots & 0 \\ 0 & \kappa_1 & \chi & \kappa_1 & 0 & \dots & 0 \\ \vdots & \vdots & \vdots & \vdots & \vdots & \vdots & \vdots \\ 0 & \dots & 0 & 0 & \kappa_1 & \chi & \kappa_1 \\ 0 & \dots & 0 & 0 & 0 & \gamma_3 & \eta_3 \end{bmatrix},$$

$$m_2 = \begin{bmatrix} \eta_2 & \gamma_2 & 0 & 0 & 0 & \dots & 0 \\ -\kappa_2 & 0 & \kappa_2 & 0 & 0 & \dots & 0 \\ 0 & -\kappa_2 & 0 & \kappa_2 & 0 & \dots & 0 \\ \vdots & \vdots & \vdots & \vdots & \vdots & \vdots & \vdots \\ 0 & \dots & 0 & 0 & -\kappa_2 & 0 & \kappa_2 \\ 0 & \dots & 0 & 0 & 0 & -\gamma_4 & -\eta_4 \end{bmatrix}.$$

Given this, the $2N \times 2N$ matrix determining the stability of model 2 is given by

$$M_2 = \begin{bmatrix} m_1 & \mu_1 m_2 \\ -\nu_1 m_2 & m_1 \end{bmatrix}.$$

The matrix M_2 clearly has a block structure and the same blocks give a linear decomposition of M_1 into a sum of two terms. However, we were not able use these commonalities between M_1 and M_2 to explain the fact that model 1 and model 2 have, not approximately, but exactly the same domain of stability as far as we can determine. Note that the occurence of a stability domain like (A.6) might be a universal feature of EOS formulations. We have for example found a stability domain of this type in the EOS formulation of 3D Maxwell's equations. There, however, it is clear that the delay boundary conditions is at least partly responsible for the width of the stability domain.

References

[1] K. Yee. Numerical solution of initial boundary value problems involving Maxwell's equations in isotropic media. IEEE Transactions on Antennas and Propagation. 1966 May, 14(3):302-307.

[2] A. Taflove. Application of the finite-difference time-domain method to sinusoidal steady state electromagnetic penetration problems. IEEE Transactions on Electromagnetic Compatibility. 1980, 22(3): 191-202.

[3] A. Taflove et. al. Computational Electrodynamics: the Finite-Difference Time-Domain Method, 3rd Ed. Artech House Publishers, 2005.

[4] J. Berenger. A perfectly matched layer for the absorption of electromagnetic waves. Journal of computational physics. 1994, 114(2): 185-200.

[5] S. Gedney. An anisotropic perfectly matched layer absorbing media for the truncation of FDTD lattices. IEEE Transactions on Antennas and Propagation. 1996, 44(12): 1630-1639.

[6] W. C. Chew and W. H. Weedon. A 3d perfectly matched medium from modified Maxwell's equations with stretched coordinates. Microwave and Optical Tech. Lett. 1994, 7(13): 599-604.

[7] Steven G. Johnson. Notes on Perfectly Matched Layers. Technical report, MIT, 2007.

[8] D. N. Pattanayak and E. Wolf. General form and new interpretation of the Ewald-Oseen extincition theorem. Optics communications. 1972, 6(3): 217-220.

[9] H. F. C. Brehm. Immersed interface method for solving the incompressible Navier-Stokes equations with moving boundaries. 49th AIAA Aerospace Science meeting Including the New Horizons Forum and Aerospace Science Exposition 2011.

[10] Yong Zeng and Walter Hoyer and Jinjie Liu and Stephan W. Koch and Jerome V. Moloney. Classical theory for second-harmonic generation from metallic nanoparticles. Physical Review B. 2009, 79: 235109.

[11] P. D. Lax and B. Wendroff. Systems of conservation laws. Communications in pure and applied mathematics. 1960, 13(2): 217-237.

3 Paper 2

Submitted to Physica Scripta in the fall of 2018.

A 3D Nonlinear Maxwell's Equations Solver Based On A Hybrid Numerical Method

Aihua Lin and Per Kristen Jakobsen

Department of Mathematics and Statistics, UIT the Arctic University of Norway, 9019 Tromsø, Norway

Abstract

In this paper we explore the possibility for solving the 3D Maxwell's equations in the presence of nonlinear and/or inhomogeneous material response. We propose using a hybrid approach which combines a boundary integral representation with a domain-based method. This hybrid approach has previously been successfully applied to 1D linear and nonlinear transient wave scattering problems. The basic idea of the approach is to propagate the Maxwell's equations inside the scattering objects forward in time by using a domain-based method, while a boundary integral representation of the electromagnetic field is used to supply the domain-based method with the required surface values. Thus no grids outside the scattering objects are needed and this greatly reduces the computational cost and complexity.

1 Introduction

Boundary Element method (BEM), as a tool for solving scattering problems, has several attractive features. First and foremost, BEM is well suited to treating scattering problems in unbounded domains because the boundary integral equations are located on the surfaces of the scattering objects and thus one whole dimension is taken out of the problem. Secondly, the scattering objects are usually defined by sharp material boundaries and thus a domain-based method must seek to resolve the fast variation in the corresponding solutions generated by the boundaries. This is a well known problem in the most popular domain-based method for electromagnetic scattering, the Finite Difference Time Domain method(FDTD) [1–3]. This method like all domain-based methods must also struggle with reducing wave reflection from the boundary of the finite computational box which is added in order to discretize the outside domain. This problem has been more or less solved by using perfectly matched layers [4, 5], but the solution comes with additional cost and complexity. While the BEM takes this radiation condition into account automatically.

However BEM has some drawbacks too. Firstly, singularities always appear during the deriving of the boundary equations from the PDEs. How to accurately calculate these integrals with singularities is an issue of the subject especially for irregular scattering objects. While the domain-based method is much simpler to implement. Secondly, the derivation of the BEM relies on Green's

functions which is only defined for linear systems of PDEs. For some applications where the nonlinearity dominates, the BEM cannot be derived. However for the applications where the nonlinearity can be discarded, a computational approach based on Green's functions is feasible. Scattering of electromagnetic waves, where nonlinearities only come into play at very high field intensities, is such an area. Thirdly, the time-domain integral equations are retarded and there is large memory requirement. Also the matrix resulted from the BEM is dense and nonsymmetrical, thus it is usually not easy to solve. However the major obstacle that has prevented BEM from being popular is the late time instabilities. Although the sources of these instabilities are not fully recognized, many remedies have been made to improve the stabilities of BEM schemes for time dependent electromagnetics [6–12].

Our work has not been aimed at joining in or improving on any of the efforts pursued by these research groups. Our major aim has been to generalize boundary approaches to electromagnetic scattering for cases where the scattering objects have an inhomogeneous and/or nonlinear response. Most work in the area of time dependent BEM has been focused on metallic objects with linear response whose dimensions are large with respect to the wave length, antennas is a major example of the kind of structure one has been interested in. The kind of problem we have in mind is scattering from very small objects, from micron to nanometer scale, objects who might have engineered inhomogeneities in their structure and strong, also engineered, nonlinear response. At this scale, the standard simplifying assumption of disregarding the inside of the scattering objects and modeling them using surface charges and currents, is not applicable. The skin depth at this microscopic scale can easily be as large as the scattering objects themselves, which is a marked difference to what is true for macroscopic antenna theory. For this reason, and also because of the complex inner structure of these microscopic scattering objects, a different approach is needed. The traditional BEM can not be used here.

Our approach is based on the same integral representation of the electromagnetic field [13] as the traditional BEM, however, we use the integral representation in a way that is different from what one does in BEM. We solve the Maxwell's equations on the inside of each scattering object, as an initial boundary value problem, and use the integral identities to supply the boundary values needed in order to make the initial boundary value problem for Maxwell, well posed. This kind of approach for solving electromagnetic scattering problems was first proposed in 1972 by E. Wolf and D. N. Pattanyak [14] in the context of stationary linear scattering and was based on the Ewald-Oseen optical extinction theorem. For this reason we call this particular way of reformulating the electromagnetic scattering problem for the Ewald Oseen Scattering(EOS) formulation. This reformulation can be applied to any kind of wave scattering situation. It has previously been applied to two toy models of 1D linear and nonlinear transient wave scattering by the authors [15] where the EOS formulations work perfectly well with high accuracy and low computational load and without any instabilities, even at very late times.

In section 2 we show some of the details of the derivation of our EOS formulation for Maxwell's equations and in section 3 we discuss some tests we have run on our numerical implementation of the EOS formulation of Maxwell's equations. In this paper we do not describe the numerical implementational details, like how we handle the singular integrals and issues of numerical stability.

These, mainly very technical considerations, would cloud the main message of the current paper, which is that our EOS formulation of scattering problems works. The technical details pertaining to our choise of implementation, some of which are probably relevant for most numerical implementations of the EOS formulation, will be reported elsewhere in a paper soon to appear [16]. Here we will just note that, just like for the 1D case, the internal numerical scheme, Lax-Wendroff for our case, determines a stability interval for the time step. The difference is that, in the 1D case, the stability interval is purely determined by the internal numerical scheme while in 3D case, there is another lower limit of the stability interval determined by the integral part of the scheme. We also find that the late time instability is highly depended on the features of the scattering materials. Section 4 summarizes what we have achieved and discuss extensions of our work that could be of interest to pursue.

2 EOS formulations of the 3D Maxwell's equations

In this paper, we investigate an electromagnetic scattering problem described by the 3D Maxwell's equations

$$\begin{aligned} \nabla \times \mathbf{E} + \partial_t \mathbf{B} &= 0, \\ \nabla \times \mathbf{H} - \partial_t \mathbf{D} &= \mathbf{J}, \\ \nabla \cdot \mathbf{D} &= \rho, \\ \nabla \cdot \mathbf{B} &= 0, \end{aligned}$$

where $\mathbf{J}$ and ρ are the current density and the charge density of free charges. Bound charges and currents determine $\mathbf{D}$ and $\mathbf{H}$ as functionals of $\mathbf{E}$ and $\mathbf{B}$,

$$\begin{aligned} \mathbf{D} &= \mathbf{D}[\mathbf{E}, \mathbf{B}], \\ \mathbf{H} &= \mathbf{H}[\mathbf{E}, \mathbf{B}]. \end{aligned}$$

In the simplest situation, where the response from the bound charges and currents is linear, isotropic, homogeneous and instantaneous, we have

$$\mathbf{D} = \varepsilon \mathbf{E}, \ \mathbf{H} = \frac{1}{\mu} \mathbf{B},$$

where $\sqrt{\frac{1}{\varepsilon \mu}} = c$ is the speed of light in the material. For this particular situation, we have

$$\begin{aligned} \nabla \times \mathbf{E} + \partial_{\mathbf{t}} \mathbf{B} &= 0, \\ \nabla \times \mathbf{B} - \frac{1}{c^2} \partial_t \mathbf{E} &= \mu \mathbf{J}, \\ \nabla \cdot \mathbf{E} &= \frac{1}{\varepsilon} \rho, \\ \nabla \cdot \mathbf{B} &= 0. \end{aligned} \tag{2.1}$$

We now rewrite the Maxwell's equations into a form that is a suitable starting point for our EOS formulation of the elctromagnetic wave scattering problem.

First, observe that

$$\begin{aligned} \partial_t \nabla \cdot \mathbf{B} &= 0, \\ \partial_t \nabla \cdot \mathbf{E} &= -\frac{1}{\varepsilon} \nabla \cdot \mathbf{J}. \end{aligned} \tag{2.2}$$

Equations (2.1) and (2.2) lead to

$$\partial_t (\nabla \cdot \mathbf{E} - \frac{1}{\varepsilon}\rho) = -\frac{1}{\varepsilon}(\partial_t \rho + \nabla \cdot \mathbf{J}). \tag{2.3}$$

All fields we consider will be driven by the source that will operate for some finite time interval. This means that at some time in the past $t = t_0$, we have

$$\begin{aligned} \nabla \cdot \mathbf{B}(\mathbf{x}, t_0) &= 0, \\ \nabla \cdot \mathbf{E}(\mathbf{x}, t_0) &= \frac{1}{\varepsilon}\rho(\mathbf{x}, t_0) = 0, \end{aligned}$$

and this together with (2.2) and (2.3) imply that for any t

$$\nabla \cdot \mathbf{B}(\mathbf{x}, t) = 0$$

holds true. If we now use the equation of charge conservation

$$\partial_t \rho + \nabla \cdot \mathbf{J} = 0$$

then

$$\nabla \cdot \mathbf{E}(\mathbf{x}, t) = \frac{1}{\varepsilon}\rho(\mathbf{x}, t)$$

also holds true at all time. Taking these considerations into account, Maxwell's equations can be written in the following equivalent form

$$\nabla \times \mathbf{E} + \partial_t \mathbf{B} = 0, \tag{2.4a}$$

$$\nabla \times \mathbf{B} - \frac{1}{c^2}\partial_t \mathbf{E} = \mu \mathbf{J}, \tag{2.4b}$$

$$\partial_t \rho + \nabla \cdot \mathbf{J} = 0. \tag{2.4c}$$

In order to complete the model, we must supply an equation of motion for the current $\mathbf{J}$

$$\partial_t \mathbf{J} = F[\mathbf{J}, \rho, \mathbf{E}, \mathbf{B}].$$

The specific form for the functional F is determined by what kind of material response we are considering. In order for the system to lead to an efficient numerical method it is important that the sources $\rho, \mathbf{J}$ are confined to some small region. In this paper, in order to be specific, we look at the case of a small metallic object interacting with light. We are not seeking to make a detailed computational investigation of this system, but is rather focused on testing our computational approach with respect to implementational complexity and numerical stability. For this reason we choose the following simple nonlinear model for the metal response of such a system

$$\partial_t \mathbf{J} = (\alpha - \beta\rho)\mathbf{E} - \gamma \mathbf{J}, \tag{2.5}$$

where α, β and γ are constants.

Following the usual approach, it is easy to show that the electric field satisfy the following equation

$$\frac{1}{c^2}\partial_{tt}\mathbf{E} - \nabla^2\mathbf{E} = -\frac{1}{\varepsilon}\nabla\rho - \mu\partial_t\mathbf{J}. \tag{2.6}$$

Each vector component of equation (2.6) is an inhomogeneous wave equation. Let's suppose the scattering object is confined in a compact homogeneous domain denoted by V_1 while the light source is located in an unbounded domain outside the object which is denoted by V_0. μ, ε are the magnetic permeability and the electric permittivity with their values μ_1, ε_1 inside and μ_0, ε_0 outside respectively. c represents the speed of light, with value c_1 inside and c_0 outside the scattering object V_1. The sources $\mathbf{J_0}$ and ρ_0 are given and $\mathbf{J_1}$, ρ_1 are the response sources generated by the metallic object interacting with the light field.

We are now ready to start the construction of the EOS formulations of this scattering problem.

Applying the integral relation for the wave equation (A.6) derived in Appendix A on equation (2.6) in domain V_0 and V_1 respectively, we get

$$\begin{aligned}\mathbf{E}_j(\mathbf{x},t) = &-\int_{V_j} \mathrm{d}V' h_j(\mathbf{x}',\mathbf{x})\{\mu_j\partial_{t'}\mathbf{J}_j + \frac{1}{\varepsilon_j}\nabla'\rho_j\}(\mathbf{x}',T)\\ &\mp\int_S \mathrm{d}S'\{h_j(\mathbf{x}',\mathbf{x})(\partial_{\mathbf{n}'}\mathbf{E}_j)(\mathbf{x}',T) - \partial_{\mathbf{n}'}h_j(\mathbf{x}',\mathbf{x})\mathbf{E}_j(\mathbf{x}',T)\\ &+\frac{1}{c_j}h_j(\mathbf{x}',\mathbf{x})\partial_{\mathbf{n}'}|\mathbf{x}'-\mathbf{x}|(\partial_{t'}\mathbf{E}_j)(\mathbf{x}',T)\},\end{aligned} \tag{2.7}$$

where

$$h_j(\mathbf{x}',\mathbf{x}) = \frac{c_j}{4\pi|\mathbf{x}'-\mathbf{x}|},$$

with $j=0$ representing the outside domain V_0 and $j=1$ representing the inside domain V_1. Here $\mathbf{x}\in V_j$ and $\mathbf{n}'$ is the unit normal to the boundary, S of V_1, at the point $\mathbf{x}'\in S$, pointing out of the domain V_1. The upper sign applies to the case $j=0$ and the lower sign for the case $j=1$. The same convention applies to all the following expressions in this section.

After a series of algebraic manipulations, starting with (2.7), we obtain

$$\begin{aligned}\mathbf{E}_j(\mathbf{x},t) = &-\partial_t\frac{\mu_j}{4\pi}\int_{V_j}\mathrm{d}V'\frac{\mathbf{J}_j(\mathbf{x}',T)}{|\mathbf{x}'-\mathbf{x}|} - \nabla\frac{1}{4\pi\varepsilon_j}\int_{V_j}\mathrm{d}V'\frac{\rho_j(\mathbf{x}',T)}{|\mathbf{x}'-\mathbf{x}|}\\ &\mp\partial_t[\frac{1}{4\pi}\int_S \mathrm{d}S'\{\frac{1}{c_j|\mathbf{x}'-\mathbf{x}|}(\mathbf{n}'\times\mathbf{E}_j(\mathbf{x}',T))\times\nabla'|\mathbf{x}'-\mathbf{x}|\\ &+\frac{1}{c_j|\mathbf{x}'-\mathbf{x}|}(\mathbf{n}'\cdot\mathbf{E}_j(\mathbf{x}',T))\nabla'|\mathbf{x}'-\mathbf{x}| + \frac{1}{|\mathbf{x}'-\mathbf{x}|}\mathbf{n}'\times\mathbf{B}_j(\mathbf{x}',T)\}]\\ &\pm\frac{1}{4\pi}\int_S\mathrm{d}S'\{(\mathbf{n}'\times\mathbf{E}_j(\mathbf{x}',T))\times\nabla'\frac{1}{|\mathbf{x}'-\mathbf{x}|}\\ &+(\mathbf{n}'\cdot\mathbf{E}_j(\mathbf{x}',T))\nabla'\frac{1}{|\mathbf{x}'-\mathbf{x}|}\}.\end{aligned} \tag{2.8}$$

These manipulations are detailed in Appendix B.
Like the electric field, the magnetic field also satisfies a wave equation

$$\frac{1}{c^2}\partial_{tt}\mathbf{B} - \nabla^2\mathbf{B} = \mu\nabla\times\mathbf{J}. \tag{2.9}$$

After a set of algebraic manipulations, similar to the ones we did for the electric field, we obtain

$$
\begin{aligned}
&\mathbf{B}_j(\mathbf{x},t) = \nabla \times \frac{\mu_j}{4\pi}\int_{V_j} \mathrm{d}V' \frac{\mathbf{J}_j(\mathbf{x}',T)}{|\mathbf{x}'-\mathbf{x}|} \\
&+ \partial_t[\frac{1}{4\pi}\int_S \mathrm{d}S'\{\frac{1}{c_j|\mathbf{x}'-\mathbf{x}|}(\mathbf{n}'\times\mathbf{B}_j(\mathbf{x}',T))\times\nabla'|\mathbf{x}'-\mathbf{x}| \\
&\mp \frac{1}{c_j|\mathbf{x}'-\mathbf{x}|}(\mathbf{n}'\cdot\mathbf{B}_j(\mathbf{x}',T))\nabla'|\mathbf{x}'-\mathbf{x}| - \frac{1}{c_j^2}\frac{1}{|\mathbf{x}'-\mathbf{x}|}\mathbf{n}'\times\mathbf{E}_j(\mathbf{x}',T)\}] \\
&\pm \frac{1}{4\pi}\int_S \mathrm{d}S'\{(\mathbf{n}'\times\mathbf{B}_j(x',T))\times\nabla'\frac{1}{|\mathbf{x}'-\mathbf{x}|} \\
&+ (\mathbf{n}'\cdot\mathbf{B}_j(\mathbf{x}',T))\nabla'\frac{1}{|\mathbf{x}'-\mathbf{x}|}\}.
\end{aligned}
\tag{2.10}
$$

The identities (2.8) and (2.10), for the electric and magnetic field, are our version of the general integral identities for the electromagnetic field derived by D.S.Jones [13]. In addition to these two identities we get, in a very similar way, two additional integral identities [16],

$$
\begin{aligned}
0 &= -\partial_t\frac{\mu_{1-j}}{4\pi}\int_{V_{1-j}} \mathrm{d}V' \frac{\mathbf{J}_{1-j}(\mathbf{x}',T)}{|\mathbf{x}'-\mathbf{x}|} - \nabla\frac{1}{4\pi\varepsilon_{1-j}}\int_{V_{1-j}} \mathrm{d}V' \frac{\rho_{1-j}(\mathbf{x}',T)}{|\mathbf{x}'-\mathbf{x}|} \\
&\pm \partial_t[\frac{1}{4\pi}\int_S \mathrm{d}S'\{\frac{1}{c_{1-j}|\mathbf{x}'-\mathbf{x}|}(\mathbf{n}'\times\mathbf{E}_{1-j}(\mathbf{x}',T))\times\nabla'|\mathbf{x}'-\mathbf{x}| \\
&+ \frac{1}{c_{1-j}|\mathbf{x}'-\mathbf{x}|}(\mathbf{n}'\cdot\mathbf{E}_{1-j}(\mathbf{x}',T))\nabla'|\mathbf{x}'-\mathbf{x}| + \frac{1}{|\mathbf{x}'-\mathbf{x}|}\mathbf{n}'\times\mathbf{B}_{1-j}(\mathbf{x}',T)\}] \\
&\mp \frac{1}{4\pi}\int_S \mathrm{d}S'\{(\mathbf{n}'\times\mathbf{E}_{1-j}(\mathbf{x}',T))\times\nabla'\frac{1}{|\mathbf{x}'-\mathbf{x}|} \\
&+ (\mathbf{n}'\cdot\mathbf{E}_{1-j}(\mathbf{x}',T))\nabla'\frac{1}{|\mathbf{x}'-\mathbf{x}|}\},
\end{aligned}
\tag{2.11}
$$

and

$$
\begin{aligned}
0 &= \nabla\times\frac{\mu_{1-j}}{4\pi}\int_{V_{1-j}} \mathrm{d}V' \frac{\mathbf{J}_{1-j}(\mathbf{x}',T)}{|\mathbf{x}'-\mathbf{x}|} \\
&\pm \partial_t[\frac{1}{4\pi}\int_S \mathrm{d}S'\{\frac{1}{c_{1-j}|\mathbf{x}'-\mathbf{x}|}(\mathbf{n}'\times\mathbf{B}_{1-j}(\mathbf{x}',T))\times\nabla'|\mathbf{x}'-\mathbf{x}| \\
&+ \frac{1}{c_{1-j}|\mathbf{x}'-\mathbf{x}|}(\mathbf{n}'\cdot\mathbf{B}_{1-j}(\mathbf{x}',T))\nabla'|\mathbf{x}'-\mathbf{x}| - \frac{1}{c_{1-j}^2}\frac{1}{|\mathbf{x}'-\mathbf{x}|}\mathbf{n}'\times\mathbf{E}_{1-j}(\mathbf{x}',T)\}] \\
&\mp \frac{1}{4\pi}\int_S \mathrm{d}S'\{(\mathbf{n}'\times\mathbf{B}_{1-j}(x',T))\times\nabla'\frac{1}{|\mathbf{x}'-\mathbf{x}|} \\
&+ (\mathbf{n}'\cdot\mathbf{B}_{1-j}(\mathbf{x}',T))\nabla'\frac{1}{|\mathbf{x}'-\mathbf{x}|}\},
\end{aligned}
\tag{2.12}
$$

for $\mathbf{x}\in V_j,\ j=0,1$. In the above expressions,

$$
\mathbf{E}_j(\mathbf{x}',t) = \lim_{\mathbf{x}\to\mathbf{x}'}\mathbf{E}_j(\mathbf{x},t)
$$

and

$$\mathbf{B}_j(\mathbf{x}',t) = \lim_{\mathbf{x}\to\mathbf{x}'} \mathbf{B}_j(\mathbf{x},t),$$

where $\mathbf{x} \in V_j$, $j = 0, 1$. In the end, we have a full set of the integral identities of the inside and the outside fields expressed by (2.8), (2.10), (2.11) and (2.12) which can be written compactly as

$$\begin{aligned} \mathbf{E}_1 &= M_1(\mathbf{n}' \times \mathbf{E}_1, \mathbf{n}' \cdot \mathbf{E}_1, \mathbf{n}' \times \mathbf{B}_1), \\ 0 &= M_0(\mathbf{n}' \times \mathbf{E}_0, \mathbf{n}' \cdot \mathbf{E}_0, \mathbf{n}' \times \mathbf{B}_0), \\ \mathbf{B}_1 &= N_1(\mathbf{n}' \times \mathbf{B}_1, \mathbf{n}' \cdot \mathbf{B}_1, \mathbf{n}' \times \mathbf{E}_1), \\ 0 &= N_0(\mathbf{n}' \times \mathbf{B}_0, \mathbf{n}' \cdot \mathbf{B}_0, \mathbf{n}' \times \mathbf{E}_0), \end{aligned} \tag{2.13}$$

for $\mathbf{x} \in V_1$ and

$$\begin{aligned} \mathbf{E}_0 &= M_0(\mathbf{n}' \times \mathbf{E}_0, \mathbf{n}' \cdot \mathbf{E}_0, \mathbf{n}' \times \mathbf{B}_0), \\ 0 &= M_1(\mathbf{n}' \times \mathbf{E}_1, \mathbf{n}' \cdot \mathbf{E}_1, \mathbf{n}' \times \mathbf{B}_1), \\ \mathbf{B}_0 &= N_0(\mathbf{n}' \times \mathbf{B}_0, \mathbf{n}' \cdot \mathbf{B}_0, \mathbf{n}' \times \mathbf{E}_0), \\ 0 &= N_1(\mathbf{n}' \times \mathbf{B}_1, \mathbf{n}' \cdot \mathbf{B}_1, \mathbf{n}' \times \mathbf{E}_1, \end{aligned} \tag{2.14}$$

for $\mathbf{x} \in V_0$.

We will now derive the boundary integral identities of (2.4) by letting $\mathbf{x}$ approach the surface from the inside and the outside of the scattering object V_1, separately. We observe that, in this limit, strong singularities only appear in the last term of the integrals in (2.13) and (2.14). Hence we are faced with a singular term which takes the form of

$$\begin{aligned} \mathbf{I} &= \lim_{\epsilon\to 0} \int_{S_\epsilon} \mathrm{d}S' \{(\mathbf{n}' \times \mathbf{A}(\mathbf{x}',T)) \times \nabla' \frac{1}{|\mathbf{x}'-\mathbf{x}|} + (\mathbf{n}' \cdot \mathbf{A}(\mathbf{x}',T))\nabla' \frac{1}{|\mathbf{x}'-\mathbf{x}|}\} \\ &= \lim_{\epsilon\to 0} \int_{S_\epsilon} \mathrm{d}S' \{(\frac{\mathbf{x}'-\mathbf{x}}{|\mathbf{x}'-\mathbf{x}|^3} \cdot \mathbf{A})\mathbf{n}' - (\frac{\mathbf{x}'-\mathbf{x}}{|\mathbf{x}'-\mathbf{x}|^3} \cdot \mathbf{n}')\mathbf{A} - (\mathbf{n}' \cdot \mathbf{A})\frac{\mathbf{x}'-\mathbf{x}}{|\mathbf{x}'-\mathbf{x}|^3}\}, \end{aligned} \tag{2.15}$$

where $\mathbf{A}(\mathbf{x}',T)$ is a vector function with $\mathbf{x}'$ located on the surface S_ϵ which is an small disk of radius ϵ. If we let $\mathbf{x}$ approach a surface point $\boldsymbol{\xi}$, from the inside of V_1, along a direction

$$\mathbf{x} - \boldsymbol{\xi} = \epsilon\mathbf{a} = -\epsilon\alpha\mathbf{n} - \epsilon\boldsymbol{\beta},$$

where $\mathbf{n}$ is the unit normal vector pointing out of V_1, at the point $\boldsymbol{\xi}$, and $\boldsymbol{\beta}$ is a unit vector along the direction $\mathbf{x}' - \boldsymbol{\xi}$, tangential to S, at the same point $\boldsymbol{\xi}$, we have

$$\lim_{\epsilon\to 0} \int_{S_\epsilon} \frac{\mathbf{x}'-\mathbf{x}}{|\mathbf{x}'-\mathbf{x}|^3}\,\mathrm{d}S = \lim_{\epsilon\to 0} \int_{S_\epsilon} \frac{\boldsymbol{\eta}+\epsilon\alpha\mathbf{n}}{|\boldsymbol{\eta}+\epsilon\alpha\mathbf{n}|^3}\,\mathrm{d}S, \tag{2.16}$$

where $\eta = \mathbf{x}' - \boldsymbol{\xi} + \epsilon\boldsymbol{\beta}$. Using spherical coordinates, (2.16) turns into

$$\lim_{\epsilon\to 0} \int_0^{2\pi} \int_0^{\epsilon} \rho \frac{(\rho\cos\theta, \rho\sin\theta, \epsilon\alpha)}{(\rho^2 + (\epsilon\alpha)^2)^{\frac{3}{2}}}\,\mathrm{d}\theta\,\mathrm{d}\rho = \chi\mathbf{n},$$

where $\chi = 2\pi\alpha(1 - \frac{1}{\sqrt{\alpha^2+1}})$. Similarly, if $\mathbf{x}$ approaches $\boldsymbol{\xi}$ from outside of V_1, we have,

$$\lim_{\epsilon\to 0}\int_{S_\epsilon} \frac{\mathbf{x}' - \mathbf{x}}{|\mathbf{x}' - \mathbf{x}|^3}\,\mathrm{d}S = -\chi\mathbf{n}.$$

So in the end,

$$\begin{aligned} I_+ &= \chi\mathbf{A}, \\ I_- &= -\chi\mathbf{A}, \end{aligned}$$

where I_+ and I_- denote the limit of equation (2.15) by letting $\mathbf{x}$ approach S_ϵ from the inside and the outside of V_1 respectively. After taking these inside and outside limits, we get the following set of equations

$$\begin{aligned} \mathbf{E}_+ &= M_1(\mathbf{n}'\times\mathbf{E}_+, \mathbf{n}'\cdot\mathbf{E}_+, \mathbf{n}'\times\mathbf{B}_+) + \chi\mathbf{E}_+, \\ 0 &= M_0(\mathbf{n}'\times\mathbf{E}_-, \mathbf{n}'\cdot\mathbf{E}_-, \mathbf{n}'\times\mathbf{B}_-) - \chi\mathbf{E}_-, \\ \mathbf{E}_- &= M_0(\mathbf{n}'\times\mathbf{E}_-, \mathbf{n}'\cdot\mathbf{E}_-, \mathbf{n}'\times\mathbf{B}_-) + \chi\mathbf{E}_-, \\ 0 &= M_1(\mathbf{n}'\times\mathbf{E}_+, \mathbf{n}'\cdot\mathbf{E}_+, \mathbf{n}'\times\mathbf{B}_+) - \chi\mathbf{E}_+, \end{aligned} \tag{2.17}$$

where $\mathbf{E}_+$ is the limit of $\mathbf{E_1}$ with $\mathbf{x}$ approaching the surface from the inside of the object while $\mathbf{E}_-$ is the limit of $\mathbf{E_0}$ with $\mathbf{x}$ approaching the surface from the outside of the object. These equations, because of the limits taken, contains singular integrals that must be interpreted as Cauchy principal integrals. Adding the first two equations of (2.17) gives us

$$\begin{aligned} \mathbf{E}_+ = {} & M_1(\mathbf{n}'\times\mathbf{E}_+, \mathbf{n}'\cdot\mathbf{E}_+, \mathbf{n}'\times\mathbf{B}_+) + M_0(\mathbf{n}'\times\mathbf{E}_-, \mathbf{n}'\cdot\mathbf{E}_-, \mathbf{n}'\times\mathbf{B}_-) \\ & + \chi\mathbf{E}_+ - \chi\mathbf{E}_-, \end{aligned} \tag{2.18}$$

and adding the last two equations of (2.17) gives us

$$\begin{aligned} \mathbf{E}_- = {} & M_0(\mathbf{n}'\times\mathbf{E}_-, \mathbf{n}'\cdot\mathbf{E}_-, \mathbf{n}'\times\mathbf{B}_-) + M_1(\mathbf{n}'\times\mathbf{E}_+, \mathbf{n}'\cdot\mathbf{E}_+, \mathbf{n}'\times\mathbf{B}_+) \\ & + \chi\mathbf{E}_- - \chi\mathbf{E}_+. \end{aligned} \tag{2.19}$$

Repeating the derivations we just did for the electric field, give us, in a similar way, the following set of equations for the magnetic field

$$\begin{aligned} \mathbf{B}_+ = {} & N_1(\mathbf{n}'\times\mathbf{B}_+, \mathbf{n}'\cdot\mathbf{B}_+, \mathbf{n}'\times\mathbf{E}_+) + N_0(\mathbf{n}'\times\mathbf{B}_-, \mathbf{n}'\cdot\mathbf{B}_-, \mathbf{n}'\times\mathbf{E}_-) \\ & + \chi\mathbf{B}_+ - \chi\mathbf{B}_-, \end{aligned} \tag{2.20}$$

$$\begin{aligned} \mathbf{B}_- = {} & N_0(\mathbf{n}'\times\mathbf{B}_-, \mathbf{n}'\cdot\mathbf{B}_-, \mathbf{n}'\times\mathbf{E}_-) + N_1(\mathbf{n}'\times\mathbf{B}_+, \mathbf{n}'\cdot\mathbf{B}_+, \mathbf{n}'\times\mathbf{E}_+) \\ & + \chi\mathbf{B}_- - \chi\mathbf{B}_+, \end{aligned} \tag{2.21}$$

where $\mathbf{B}_+$ is the limit of $\mathbf{B_1}$ with $\mathbf{x}$ approaching the surface from the inside of the object while $\mathbf{B}_-$ is the limit of $\mathbf{B_0}$ with $\mathbf{x}$ approaching the surface from the outside of the object. Also in these equations the singular integrals that occur must be interpreted as Cauchy principal value integrals. So far, we have two outer equations for the outer limit fields $\mathbf{E}_-$, $\mathbf{B}_-$ and two inner equations for the inner limit fields $\mathbf{E}_+$, $\mathbf{B}_+$. We also have the usual electromagnetic boundary conditions at the surface S which separate regions with different susceptibilities

and permittivities

$$\begin{aligned}
\mathbf{n}' \times \mathbf{E}_+ &= \mathbf{n}' \times \mathbf{E}_-, \\
\mathbf{n}' \times \mathbf{B}_+ &= \frac{u_1}{u_0} \mathbf{n}' \times \mathbf{B}_-, \\
\mathbf{n}' \cdot \mathbf{B}_+ &= \mathbf{n}' \cdot \mathbf{B}_-, \\
\mathbf{n}' \cdot \mathbf{E}_+ &= \frac{\varepsilon_0}{\varepsilon_1} \mathbf{n}' \cdot \mathbf{E}_-.
\end{aligned}$$

It might appear that we have more equations than we need here. The very same problem was encountered earlier while deriving the EOS formulation for two 1D toy models [15]. It appears as if we can use the two outer equations to solve for $\mathbf{E}_-$ and $\mathbf{B}_-$ and then use the boundary conditions to find $\mathbf{E}_+$ and $\mathbf{B}_+$. But these field values inside the scattering object cannot in general be consistent with the field values derived directly from the two inner equations for $\mathbf{E}_+$ and $\mathbf{B}_+$. For example, if there is a source inside of V_1 and no source outside of V_1, the first approach would give vanishing electric and magnetic field whereas the second approach certainly would not. On the other hand, for a given source, the Maxwell equations has a unique solution, which by construction also satisfy all the integral identities.

In order to understand what the problem is, and how to fix it, we must just realize that, from an abstract point of view, we have the following formal situation

$$\begin{aligned}
A\mathbf{X} &= \mathbf{b}, \\
B\mathbf{X} &= \mathbf{c},
\end{aligned} \tag{2.22}$$

where A and B are singular but where we know that (2.22) has a unique solution.

In this situation, let us assume that $\alpha A + B$ is nonsingular for some choice of α. Any solution of (2.22) is a solution of

$$(\alpha A + B)\mathbf{X} = \alpha \mathbf{b} + \mathbf{c}, \tag{2.23}$$

and since $\alpha A + B$ is nonsingular the unique solution of the singular system (2.22) must in fact be the unique solution of the nonsingular system (2.23). We know that the solution of Maxwell is unique for a given source, so since the integral equations are equivalent to Maxwell, our four integral equations for the two unknown fields on S must have a unique solution. This happens only if they are singular. Thus in our situation, we can simply add (2.18) and (2.19), which gives

$$\begin{aligned}
\mathbf{E}_+ + \mathbf{E}_- = 2(&M_1(\mathbf{n}' \times \mathbf{E}_+, \mathbf{n}' \cdot \mathbf{E}_+, \mathbf{n}' \times \mathbf{B}_+) \\
&+ M_0(\mathbf{n}' \times \mathbf{E}_-, \mathbf{n}' \cdot \mathbf{E}_-, \mathbf{n}' \times \mathbf{B}_-)),
\end{aligned} \tag{2.24}$$

and add (2.20) and (2.21), which gives

$$\begin{aligned}
\mathbf{B}_+ + \mathbf{B}_- = 2(&N_1(\mathbf{n}' \times \mathbf{B}_+, \mathbf{n}' \cdot \mathbf{B}_+, \mathbf{n}' \times \mathbf{E}_+) \\
&+ N_0(\mathbf{n}' \times \mathbf{B}_-, \mathbf{n}' \cdot \mathbf{B}_-, \mathbf{n}' \times \mathbf{E}_-)).
\end{aligned} \tag{2.25}$$

Observe that for any vector $\mathbf{A}$, the following identities hold true

$$\begin{aligned}
\mathbf{n} \times (\mathbf{n} \times \mathbf{A}) &= (\mathbf{n} \cdot \mathbf{A})\mathbf{n} - (\mathbf{n} \cdot \mathbf{n})\mathbf{A}, \\
\mathbf{A} &= (\mathbf{n} \cdot \mathbf{A})\mathbf{n} - \mathbf{n} \times (\mathbf{n} \times \mathbf{A}).
\end{aligned} \tag{2.26}$$

Performing (2.26) on (2.24) and (2.25) we obtain the following final boundary integral identities

$$(I+\frac{1}{2}(\frac{\varepsilon_1}{\varepsilon_0}-1)\mathbf{n}\ \mathbf{n})\mathbf{E}_+(\mathbf{x},t)=\mathbf{I}_e+\mathbf{O}_e+\mathbf{B}_e, \tag{2.27a}$$

$$(I+\frac{1}{2}(1-\frac{\mu_0}{\mu_1})\mathbf{n}\ \mathbf{n})\mathbf{B}_+(\mathbf{x},t)=\mathbf{I}_b+\mathbf{O}_b+\mathbf{B}_b, \tag{2.27b}$$

where $\mathbf{x}\in S$, $\mathbf{n}$ is the unit normal vector pointing out of V_1 at the point $\mathbf{x}$, I is the identity matrix and

$$\mathbf{I}_e=-\partial_t\frac{\mu_1}{4\pi}\int_{V_1}\mathrm{d}V'\frac{\mathbf{J}_1(\mathbf{x}',T)}{|\mathbf{x}'-\mathbf{x}|}-\frac{1}{4\pi\varepsilon_1}\nabla\int_{V_1}\mathrm{d}V'\frac{\rho_1(\mathbf{x}',T)}{|\mathbf{x}'-\mathbf{x}|}, \tag{2.28}$$

$$\mathbf{O}_e=-\partial_t\frac{\mu_0}{4\pi}\int_{V_0}\mathrm{d}V'\frac{\mathbf{J}_0(\mathbf{x}',T)}{|\mathbf{x}'-\mathbf{x}|}-\nabla\frac{1}{4\pi\varepsilon_0}\int_{V_0}\mathrm{d}V'\frac{\rho_0(\mathbf{x}',T)}{|\mathbf{x}'-\mathbf{x}|}, \tag{2.29}$$

$$\begin{aligned}\mathbf{B}_e=&\frac{1}{4\pi}\partial_t\int_S\mathrm{d}S'\{(\frac{1}{c_1}-\frac{1}{c_0})\frac{1}{|\mathbf{x}'-\mathbf{x}|}(\mathbf{n}'\times\mathbf{E}_+(\mathbf{x}',T))\times\nabla'|\mathbf{x}'-\mathbf{x}|\\&+(\frac{1}{c_1}-\frac{\varepsilon_1}{\varepsilon_0c_0})\frac{1}{|\mathbf{x}'-\mathbf{x}|}(\mathbf{n}'\cdot\mathbf{E}_+(\mathbf{x}',T))\nabla'|\mathbf{x}'-\mathbf{x}|\\&+(1-\frac{\mu_0}{\mu_1})\frac{1}{|\mathbf{x}'-\mathbf{x}|}\mathbf{n}'\times\mathbf{B}_+(\mathbf{x}',T)\}\\&-\frac{1}{4\pi}\int_S\mathrm{d}S'((1-\frac{\varepsilon_1}{\varepsilon_0})(\mathbf{n}'\cdot\mathbf{E}_+(\mathbf{x}',T))\nabla'\frac{1}{|\mathbf{x}'-\mathbf{x}|}),\end{aligned} \tag{2.30}$$

$$\mathbf{I}_b=\nabla\times\frac{\mu_1}{4\pi}\int_{V_1}\mathrm{d}V'\frac{\mathbf{J}_1(\mathbf{x}',T)}{|\mathbf{x}'-\mathbf{x}|}, \tag{2.31}$$

$$\mathbf{O}_b=\nabla\times\frac{\mu_0}{4\pi}\int_{V_0}\mathrm{d}V'\frac{\mathbf{J}_0(\mathbf{x}',T)}{|\mathbf{x}'-\mathbf{x}|}, \tag{2.32}$$

$$\begin{aligned}\mathbf{B}_b=&\frac{1}{4\pi}\partial_t\int_S\mathrm{d}S'\{(\frac{1}{c_1}-\frac{\mu_0}{\mu_1c_0})\frac{1}{|\mathbf{x}'-\mathbf{x}|}(\mathbf{n}'\times\mathbf{B}_+(\mathbf{x}',T))\times\nabla'|\mathbf{x}'-\mathbf{x}|\\&+(\frac{1}{c_1}-\frac{1}{c_0})\frac{1}{|\mathbf{x}'-\mathbf{x}|}(\mathbf{n}'\cdot\mathbf{B}_+(\mathbf{x}',T))\nabla'|\mathbf{x}'-\mathbf{x}|\\&+(\frac{1}{c_0^2}-\frac{1}{c_1^2})\frac{1}{|\mathbf{x}'-\mathbf{x}|}\mathbf{n}'\times\mathbf{E}_+(\mathbf{x}',T)\}\\&-\frac{1}{4\pi}\int_S\mathrm{d}S'\{(1-\frac{u_0}{u_1})(\mathbf{n}'\times\mathbf{B}_+(\mathbf{x}',T))\times\nabla'\frac{1}{|\mathbf{x}'-\mathbf{x}|}\}.\end{aligned} \tag{2.33}$$

Note that $\mathbf{O}_e$ and $\mathbf{O}_b$ are fields on the surfaces generated by the source in the absence of the scattering objects. Equations (2.4) and (2.5) together with the boundary integral identities (2.27a) and (2.27b) compose the EOS formulations of our model.

3 Artificial source test and numerical implementation

The motivation, for introducing the EOS formulation for Maxwell's equations, is a numerical one. The technical issues occuring for the numerical implementation discussed in this paper, will be part of any numerical implementation of

our scheme, which in general will involve multiple, arbitrarily shaped, scattering objects, that include linear and nonlinear optical response. We expect however, that the general nature of these issues will reveal themselves already in the simplest possible setting, where we have one scattering object of rectangular shape. The numerical implementation consists of a domain method for the model (2.4) and (2.5), determining the evolution of the fields inside the scattering object, and a scheme for updating the boundary values of the fields using the integral identities (2.27a) and (2.27b). For the internal domain method we choose to use a combination of Lax-Wendroff on (2.4) and modified Euler's method on (2.5), this is similar to what we did for the simple 1D case [15], previously. For the boundary part of the scheme we use the mid-point rule to the nonsingular integrals appearing in (2.27). The treatment of the singular integrals is technical and rather lengthy and will therefore be reported elsewhere [17]. Here it is enough to note that we calculate the singular integrals by reducing them to a singular core, which we calculate exactly, and nonsingular surface and line integrals, that we calculate numerically. The reductions proceed through a nontrivial use of well known integral identities.

For the inside of the scattering object we will use a rectangular grid. This grid is however not uniform close to the boundary. This is because the grid has to support both the discrete approximations to the partial derivatives and discrete approximations to the integrals, used to update the boundary values based on the current and previous internal values of the fields. The fact that in our scheme the boundary values are dynamical variables, enforce some special difference rules that applies close to the boundary. This is an extra complication for our scheme, but they are manageable, and will be part of any scheme that implements the EOS formulation introduced in this paper. Details are given in [17].

What we do in this section is to report on some tests that we have run on our scheme. A usual approach to testing of numerical implementations involve finding exact special solutions corresponding to special source functions. In this section we do not use this approach, but rather use an artificial source test to verify the correctness of our EOS formulations. The basic idea behind the artificial source test, of some numerical scheme designed for a system of PDEs, $\mathscr{L}\psi = 0$, is to slightly modify the system by adding an arbitrary source to all the equations in the system, creating a new modified system $\mathscr{L}\psi = g$. This modification typically lead to minimal modifications to the numerical scheme, where most of the effort and complexity are usually spent on the derivatives and nonlinear terms. For the equations, however, the presence of the sources change the situation completely. This is because the presence of the added sources implies that *any* function is a solution to the equations for *some* choice of sources. Thus we can pick a function ψ_0 and insert it into the model and calculate the source function $g_0 = \mathscr{L}\psi_0$ so that our chosen function is a solution to the extended equation. Finally we run the numerical scheme with the calculated source function and compare the numerical solution with the exact solution ψ_0.

A modified model of (2.4) and (2.5) with artificial sources is generally con-

structed by

$$\begin{aligned}
&\partial_t \mathbf{B} + \nabla \times \mathbf{E} = \boldsymbol{\varphi}_1, \\
&\frac{1}{c_1^2}\partial_t \mathbf{E} - \nabla \times \mathbf{B} = -\mu_1 \mathbf{J} + \boldsymbol{\varphi}_2, \\
&\nabla \cdot \mathbf{E} = \frac{1}{\varepsilon_1}\rho + \varphi_3, \\
&\nabla \cdot \mathbf{B} = \boldsymbol{\varphi}_4, \\
&\partial_t \mathbf{J} = (\alpha - \beta\rho)\mathbf{E} - \gamma \mathbf{J} + \boldsymbol{\varphi}_5,
\end{aligned}$$

where $\boldsymbol{\varphi}_1, \boldsymbol{\varphi}_2, \boldsymbol{\varphi}_4$ and $\boldsymbol{\varphi}_5$ are a set of vector functions and φ_3 is a scale function. Observe that

$$\nabla \cdot (\nabla \times \mathbf{E}) + \nabla \cdot \partial_t \mathbf{B} = \nabla \cdot \boldsymbol{\varphi}_1,$$

and this yields

$$\partial_t \boldsymbol{\varphi}_4 = \nabla \cdot \boldsymbol{\varphi}_1.$$

Based on this we suppose $\boldsymbol{\varphi}_1 = 0$ and $\boldsymbol{\varphi}_4 = 0$ which can simplify the choice of the exact solutions. We also observe that if φ_2 and φ_3 are set to be both 0, then the continuity equation

$$\partial_t \rho + \nabla \cdot \mathbf{J} = 0$$

is automatically satisfied. So in the end, the source extended model is given by

$$\partial_t \mathbf{B} + \nabla \times \mathbf{E} = 0, \tag{3.1a}$$

$$\frac{1}{c_1^2}\partial_t \mathbf{E} - \nabla \times \mathbf{B} = -\mu_1 \mathbf{J}, \tag{3.1b}$$

$$\nabla \cdot \mathbf{E} = \frac{1}{\varepsilon_1}\rho, \tag{3.1c}$$

$$\partial_t \mathbf{J} = (\alpha - \beta\rho)\mathbf{E} - \gamma \mathbf{J} + \boldsymbol{\varphi}. \tag{3.1d}$$

For model (3.1), any choice of $\tilde{\mathbf{E}}, \tilde{\mathbf{B}}$ can be a solution if the artificial source is given by

$$\boldsymbol{\varphi} = \partial_t \tilde{\mathbf{J}} - (\alpha - \beta\tilde{\rho})\tilde{\mathbf{E}} - \gamma \tilde{\mathbf{J}},$$

where $\tilde{\mathbf{J}}$ and $\tilde{\rho}$ are given respectively by

$$\begin{aligned}
&\tilde{\mathbf{J}} = \frac{1}{\mu_1}(\nabla \times \tilde{\mathbf{B}} - \frac{1}{c_1^2}\partial_t \tilde{\mathbf{E}}), \\
&\tilde{\rho} = \varepsilon_1 \nabla \cdot \tilde{\mathbf{E}}.
\end{aligned}$$

Due to (3.1a), we can simply choose a vector function $\boldsymbol{\phi}$, such that

$$\begin{aligned}
&\tilde{\mathbf{E}} = -\partial_t \boldsymbol{\phi}, \\
&\tilde{\mathbf{B}} = \nabla \times \boldsymbol{\phi}.
\end{aligned} \tag{3.2}$$

Figure 3.1 shows the comparison between the numerical implementations and the exact solutions where we have used

$$\boldsymbol{\phi} = (\arctan(b^2 t^2) e^{-\alpha_1 (x - x_o + y - y_o + z - z_o + \beta_1 (t - t_a))^2}, 0, 0).$$

Values of the parameters are listed below the figure. From figure it is evident that the agreement between the exact solution and the numerical solution is excellent.

For a general case where the electromagnetic fields inside the object are produced by the outside source, we set up the outside source $\mathbf{J}_0$ and ρ_0 to be a combination of a bump function in time and a delta function in space which is easily integrated in space. In order to satisfy the continuity equation

$$\partial_t \rho_0 + \nabla \cdot \mathbf{J}_0 = 0,$$

we can choose a vector function $\boldsymbol{\varphi}$ such that

$$\begin{aligned} \mathbf{J}_0 &= -\partial_t \boldsymbol{\varphi}, \\ \rho_0 &= \nabla \cdot \boldsymbol{\varphi}. \end{aligned} \tag{3.3}$$

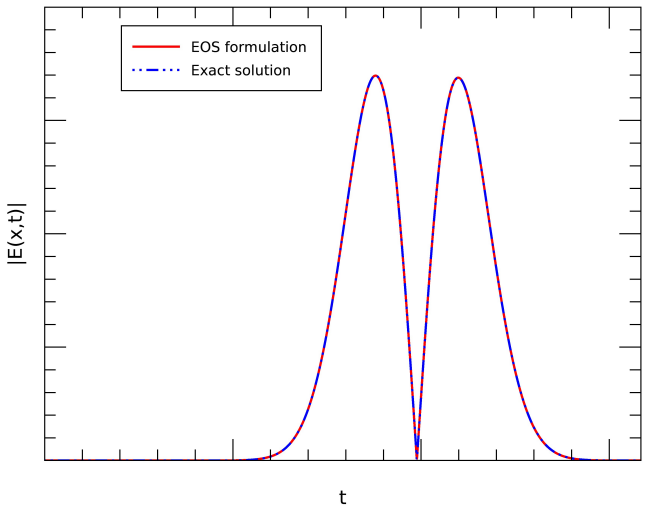

Figure 3.1: Artificial source test: $|\mathbf{E}(\mathbf{x}, t)|$. Intensity of electric field at a specific point at different times. $b = 1.0, \alpha_1 = 40, \beta_1 = 1.0, x_o = 0.0, y_o = 0.0, z_o = 0.0, t_a = 1.0, c_0 = 1.0, \mu_0 = 1.0, \varepsilon_0 = 1.0, c_1 = 0.82, \mu_1 = 1.0, \varepsilon_1 = 1.5, \tau = 0.45, \alpha = 1.0, \beta = 0.01, \gamma = 0.01$.

Figure 3.2 shows the intensity of the electric field on a surface in yz plane at different times. Values of parameters used are shown below the figure. The figure shows a pulse of light passing through the plane, which is what we would expect from the nature of our chosen source. For figure 3.2 , we have chosen

$$\boldsymbol{\varphi} = (\varphi, 0, 0),$$

where

$$\varphi(\mathbf{x}, t) = \begin{cases} \delta(\mathbf{x} - \mathbf{x}_0) e^{\frac{1}{(t-t_0)^2 - 1}} & t \in [t_0 - 1, t_0 + 1], \\ 0 & t \notin [t_0 - 1, t_0 + 1], \end{cases}$$

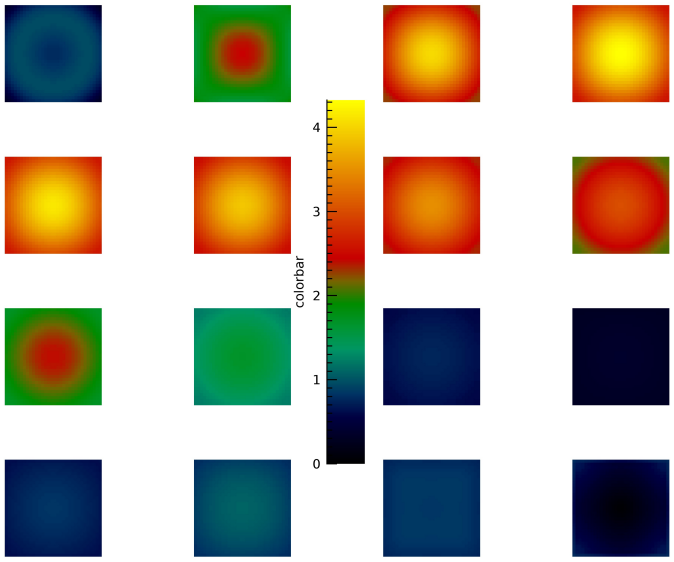

Figure 3.2: The intensity of the electric field on a specific surface in yz plane at different times. $t_0 = 1.5, x_0 = -0.3, y_0 = 0.0, z_0 = 0.0, c_0 = 1.0, \mu_0 = 1.0, \varepsilon_0 = 1.0, c_1 = 0.82, \mu_1 = 1.0, \varepsilon_1 = 1.5, \tau = 0.45, \alpha = 0.1, \beta = 0.01, \gamma = 2$.

with $\mathbf{x}_0 = (x_0, y_0, z_0)$.

Our numerical scheme, being explicit, is not unconditionally stable. There is however a stable range, $\tau_1 < \tau < \tau_2$, for the time step Δt

$$\Delta t = \frac{\tau}{c_1} Min\{\Delta x, \Delta y, \Delta z\},$$

where τ_1 and τ_2 determine the lower and upper boundaries of the stability range for the sceheme. We have carefully investigated the source of the upper and lower bound of the range and how the width of the stability range depends on material parameters. It is not appropriate to include these fairly techincal numerical investigations here, a full discussion will be presented elsewhere in [17]. Here it is enough to note that the source of the lower stability bound is the numerical implementation of the boundary part of the algoritm, and the source of the upper bound is the numerical implementation of the domain part of the algorithm, for our case this is a combination of Lax-Wendroff for the electromagnetic fields, and modified Euler for the current .

4 Conclusions

In this paper we have showed that our EOS formulation of electromagnetic scattering can be accurately and stably implemented using one particular choice of numerical scheme for the inside of the objects and for the integral representation of the boundary values required by the inside scheme. For a stable numerical solution, the time step needs to be confined in some range, where we have found that this range is not only determined by the internal domain-base method due

to the non-uniform grids but also determined by the boundary integral representations. Discussions on how the internal non-uniform grids and the boundary integral representation effect the time stable range is reported in [15] which will be published elsewhere. It is worth stressing that the existence of the stability range and its width depends not only on the material parameters but certainly on choices made for the numerical implementation of the boundary part and domain part of the algorithm. In principle, any numerical scheme can be used for the domain part of the algorithm, also the extremely well established FDTD method. It would be interesting to see how this method would perform with respect to stability. There is also the question of going fully implicit, both for the boundary part and the domain part of the algorithm. One would think that this would have a chance of producing an unconditionally stable algorithm for our EOS formulation for Maxwell's equations.

Appendices

A The integral identity for a 3D wave equation

We will start by considering a wave equation in 3D

$$\frac{1}{c^2}\partial_{tt}\varphi(\mathbf{x},t) - \nabla^2\varphi(\mathbf{x},t) = \rho(\mathbf{x},t), \tag{A.1}$$

where $\mathbf{x} = (x, y, z)$, c is the propagation speed and

$$\nabla^2 = \partial_x^2 + \partial_y^2 + \partial_z^2.$$

Let $D \times T$ be a given space-time domain. We will assume that the source $\rho(\mathbf{x}, t)$ is entirely contained in $D \times T$. The operator

$$\mathcal{L} = \frac{1}{c^2}\partial_{tt} - \nabla^2$$

is formally self adjoint. Observe that for any pair of functions defined in $D \times T$ we have

$$\begin{aligned}
&\mathcal{L}\varphi(\mathbf{x},t)\psi(\mathbf{x},t) - \varphi(\mathbf{x},t)\mathcal{L}\psi(\mathbf{x},t)\\
&= \frac{1}{c^2}\partial_t(\partial_t\varphi(\mathbf{x},t)\psi(\mathbf{x},t) - \varphi(\mathbf{x},t)\partial_t\psi(\mathbf{x},t))\\
&- \nabla\cdot(\nabla\varphi(\mathbf{x},t)\psi(\mathbf{x},t) - \varphi(\mathbf{x},t)\nabla\psi(\mathbf{x},t)),
\end{aligned}$$

so

$$\begin{aligned}
&\int_{D\times T}\{\mathcal{L}\varphi(\mathbf{x},t)\psi(\mathbf{x},t) - \varphi(\mathbf{x},t)\mathcal{L}\psi(\mathbf{x},t)\}\,\mathrm{d}V\,\mathrm{d}t\\
&= \frac{1}{c^2}\int_{D_2}\{\partial_t\varphi(\mathbf{x},t)\psi(\mathbf{x},t) - \varphi(\mathbf{x},t)\partial_t\psi(\mathbf{x},t)\}\,\mathrm{d}V\\
&- \frac{1}{c^2}\int_{D_1}\{\partial_t\varphi(\mathbf{x},t)\psi(\mathbf{x},t) - \varphi(\mathbf{x},t)\partial_t\psi(\mathbf{x},t)\}\,\mathrm{d}V\\
&- \int_{S\times T}\{\partial_{\mathbf{n}}\varphi(\mathbf{x},t)\psi(\mathbf{x},t) - \varphi(\mathbf{x},t)\partial_{\mathbf{n}}\psi(\mathbf{x},t)\}\,\mathrm{d}S\,\mathrm{d}t.
\end{aligned} \tag{A.2}$$

This is the fundamental integral identity for the wave equation in 3D. Next we will need the advanced Green's function for $\mathcal{L}$ which is given by

$$G(\mathbf{x}, t, \mathbf{x}', t') = Q(\mathbf{x} - \mathbf{x}', t - t'),$$

where $Q(\mathbf{y}, s)$ satisfies

$$\frac{1}{c^2}\partial_{ss}Q(\mathbf{y}, s) - \nabla^2 Q(\mathbf{y}, s) = \delta(\mathbf{y})\delta(s), \qquad s < 0, \tag{A.3}$$

and

$$Q(\mathbf{y}, s) = 0, \qquad s > 0.$$

Because of translational invariance, we can take the Fourier transform of (A.3) and get

$$[-(\frac{\omega}{c})^2 + \zeta^2]\hat{Q}(\xi, \omega) = 1, \qquad \zeta = |\xi|,$$

$$\hat{Q}(\xi, \omega) = \frac{1}{D(\xi, \omega)}, \tag{A.4}$$

where

$$D(\xi, \omega) = -(\frac{\omega}{c})^2 + \zeta^2.$$

Applying the inverse Fourier transform on (A.4) gives

$$Q(\mathbf{y}, s) = \frac{1}{16\pi^4}\int q(\xi, s)e^{i\xi\cdot\mathbf{y}}\,\mathrm{d}\xi,$$

where

$$q(\xi, s) = \int_{C_\varepsilon} \frac{e^{-izs}}{D(\xi, z)}\,\mathrm{d}z,$$

and C_ε is a contour slightly below the real axis. Observe that the integrand has simple poles at $z = \pm c\zeta$, so if $s > 0$, we must close the contour in the lower half-plane. By Cauchy,

$$q(\xi, s) = 0.$$

If $s < 0$, we must now close the contour in the upper half plane and Cauchy's theorem gives

$$q(\xi, s) = \frac{c\pi i}{\zeta}[e^{isc\zeta} - e^{-isc\zeta}],$$

and

$$\frac{1}{16\pi^4}\int \mathrm{d}\xi\ \frac{c\pi i}{\zeta}e^{isc\zeta}e^{i\xi\cdot\mathbf{y}} = \frac{c}{8\pi^2 r}[\int_0^\infty \mathrm{d}\zeta\ e^{i(r+sc)\zeta} - \int_0^\infty \mathrm{d}\zeta\ e^{-i(r-sc)\zeta}],$$

where $r = |\mathbf{y}|$. Similarly,

$$-\frac{1}{16\pi^4}\int \mathrm{d}\xi\frac{c\pi i}{\zeta}e^{-isc\zeta}e^{i\xi\cdot\mathbf{y}} = \frac{-c}{8\pi^2 r}[\int_0^\infty \mathrm{d}\zeta\ e^{i(r-sc)\zeta} - \int_0^\infty \mathrm{d}\zeta\ e^{-i(r+sc)\zeta}].$$

In the end,

$$Q(\mathbf{y}, s) = \frac{c}{4\pi r}[\delta(r + sc) - \delta(r - sc)].$$

Since if $s < 0$, $\delta(r - sc) = 0$, finally

$$Q(\mathbf{y}, s) = \frac{1}{4\pi r}\delta(s + \frac{r}{c}).$$

Thus our advanced Green's function is

$$G(\mathbf{x}, t, \mathbf{x}', t') = \begin{cases} 0 & \text{if } t > t' \\ \frac{1}{4\pi|\mathbf{x}-\mathbf{x}'|}\delta(t - t' + \frac{|\mathbf{x}-\mathbf{x}'|}{c}), & \text{if } t < t'. \end{cases} \tag{A.5}$$

We now apply (A.5) to the fundamental integral identity (A.2). Let $\varphi(\mathbf{x}, t)$ be a solution to the wave equation (A.1)

$$\mathcal{L}\varphi(\mathbf{x}, t) = \rho(\mathbf{x}, t),$$

then for any $(\mathbf{x}, t) \in D \times T$, we have

$$\begin{aligned}
&\int_{D\times T} \mathrm{d}V'\,\mathrm{d}t'\{\mathcal{L}\varphi(\mathbf{x}', t')G(\mathbf{x}', t', \mathbf{x}, t) - \varphi(\mathbf{x}', t')\mathcal{L}G(\mathbf{x}', t', \mathbf{x}, t)\} \\
&= \frac{1}{c^2}\int_{D_2} \mathrm{d}V'\{\partial_{t'}\varphi(\mathbf{x}', t')G(\mathbf{x}', t', \mathbf{x}, t) - \varphi(\mathbf{x}', t')\partial_{t'}G(\mathbf{x}', t', \mathbf{x}, t)\}|_{t'=t_2} \\
&- \frac{1}{c^2}\int_{D_1} \mathrm{d}V'\{\partial_{t'}\varphi(\mathbf{x}', t')G(\mathbf{x}', t', \mathbf{x}, t) - \varphi(\mathbf{x}', t')\partial_{t'}G(\mathbf{x}', t', \mathbf{x}, t)\}|_{t'=t_1} \\
&- \int_{S\times T} \mathrm{d}S'\,\mathrm{d}t'\{\partial_{\mathbf{n}'}\varphi(\mathbf{x}', t')G(\mathbf{x}', t', \mathbf{x}, t) - \varphi(\mathbf{x}', t')\partial_{\mathbf{n}'}G(\mathbf{x}', t', \mathbf{x}, t)\}.
\end{aligned}$$

Since $t_2 > t$, for the advance Green's function

$$G(\mathbf{x}', t', \mathbf{x}, t)|_{t'=t_2} = 0.$$

And since the field is entirely driven by the source

$$\varphi(\mathbf{x}, t_1) = 0,$$

we get

$$\begin{aligned}
\varphi(\mathbf{x}, t) = &\int_{D\times T} \mathrm{d}V'\,\mathrm{d}t'\rho(\mathbf{x}', t')G(\mathbf{x}', t', \mathbf{x}, t) \\
&+ \int_{S\times T} \mathrm{d}S'\,\mathrm{d}t'\{\partial_{\mathbf{n}'}\varphi(\mathbf{x}', t')G(\mathbf{x}', t', \mathbf{x}, t) - \varphi(\mathbf{x}', t')\partial_{\mathbf{n}'}G(\mathbf{x}', t', \mathbf{x}, t)\}.
\end{aligned}$$

and

$$G(\mathbf{x}', t', \mathbf{x}, t) = h(\mathbf{x}', \mathbf{x})\theta(t - t')\delta(|\mathbf{x}' - \mathbf{x}| + c(t' - t)),$$

where

$$h(\mathbf{x}', \mathbf{x}) = \frac{c}{4\pi|\mathbf{x}' - \mathbf{x}|}.$$

Since

$$\begin{aligned}
\partial_{\mathbf{n}'}G(\mathbf{x}', t', \mathbf{x}, t) = &\theta(t - t')\partial_{\mathbf{n}'}h(\mathbf{x}', \mathbf{x})\delta(|\mathbf{x}' - \mathbf{x}| + c(t' - t)) \\
&+ \theta(t - t')h(\mathbf{x}', \mathbf{x})\partial_{\mathbf{n}'}\delta(|\mathbf{x}' - \mathbf{x}| + c(t' - t)),
\end{aligned}$$

and

$$\partial_{\mathbf{n}'}\delta(|\mathbf{x}'-\mathbf{x}|+c(t'-t)) = \frac{1}{c}\partial_{\mathbf{n}'}|\mathbf{x}'-\mathbf{x}|\partial_{t'}\delta(|\mathbf{x}'-\mathbf{x}|+c(t'-t)),$$

we thus have

$$\int_{D\times T} \mathrm{d}V'\,\mathrm{d}t'\rho(\mathbf{x}',t')G(\mathbf{x}',t',\mathbf{x},t) = \int_D \mathrm{d}V' h(\mathbf{x}',\mathbf{x})\rho(\mathbf{x}',T),$$

where

$$T = T(t,\mathbf{x}',\mathbf{x}) = t - \frac{1}{c}|\mathbf{x}'-\mathbf{x}|.$$

From

$$\int_{S\times T} \mathrm{d}S'\,\mathrm{d}t'\partial_{\mathbf{n}'}\varphi(\mathbf{x}',t')G(\mathbf{x}',t',\mathbf{x},t) = \int_S \mathrm{d}S' h(\mathbf{x}',\mathbf{x})(\partial_{\mathbf{n}'}\varphi)(\mathbf{x}',T),$$

and

$$\begin{aligned}
&-\int_{S\times T} \mathrm{d}S'\,\mathrm{d}t'\varphi(\mathbf{x}',t')\partial_{\mathbf{n}'}G(\mathbf{x}',t',\mathbf{x},t)\\
&= -\int_S \mathrm{d}S'\partial_{\mathbf{n}'}h(\mathbf{x}',\mathbf{x})\varphi(\mathbf{x}',T) + \int_S \mathrm{d}S'\frac{1}{c}h(\mathbf{x}',\mathbf{x})\partial_{\mathbf{n}'}|\mathbf{x}'-\mathbf{x}|(\partial_{t'}\varphi)(\mathbf{x}',T).
\end{aligned}$$

finally we get

$$\begin{aligned}
\varphi(\mathbf{x},t) = &\int_D \mathrm{d}V' h(\mathbf{x}',\mathbf{x})\rho(\mathbf{x}',T) + \int_S \mathrm{d}S'\{h(\mathbf{x}',\mathbf{x})(\partial_{\mathbf{n}'}\varphi)(\mathbf{x}',T)\\
&- \partial_{\mathbf{n}'}h(\mathbf{x}',\mathbf{x})\varphi(\mathbf{x}',T) + \frac{h(\mathbf{x}',\mathbf{x})}{c}\partial_{\mathbf{n}'}|\mathbf{x}'-\mathbf{x}|(\partial_{t'}\varphi)(\mathbf{x}',T)\}.
\end{aligned} \tag{A.6}$$

This is the integral identity for an operator defining a 3D wave equation and it holds for any solution of the scalar 3D wave equation.

B The integral identity of the electric wave equation

Here we do some calculations to derive (2.8) from (2.7). For the writing in simplicity, we write $\mathbf{E},\mathbf{J},\rho,c,\mu,\epsilon$ instead of $\mathbf{E}_j,\mathbf{J}_j,\rho_j,c_j,\mu_j,\epsilon_j$, $j=0,1$ respectively here. Observe first that

$$\begin{aligned}
\partial_{\mathbf{n}'}(\mathbf{E}(\mathbf{x}',T)) = (\mathbf{n}'\cdot\nabla')(\mathbf{E}(\mathbf{x}',T)) = ((\mathbf{n}'\cdot\nabla')\mathbf{E})(\mathbf{x}',T)\\
+ (\partial_{t'}E)(\mathbf{x}',T)(-\frac{1}{c}(\mathbf{n}'\cdot\nabla')|\mathbf{x}'-\mathbf{x}|),
\end{aligned}$$

so,

$$\begin{aligned}\mathbf{E}(\mathbf{x},t) = &-\int_D \mathrm{d}V' h(\mathbf{x}',\mathbf{x})\{\mu\partial_{t'}\mathbf{J} + \frac{1}{\varepsilon}\nabla'\rho\}(\mathbf{x}',T)\\ &+\int_S \mathrm{d}S'\{h(\mathbf{x}',\mathbf{x})\partial_{\mathbf{n}'}(\mathbf{E}(\mathbf{x}',T)) + \frac{1}{c}h(\mathbf{x}',\mathbf{x})(\partial_{t'}\mathbf{E})(\mathbf{x}',T)\partial_{\mathbf{n}'}|\mathbf{x}'-\mathbf{x}|\\ &-\partial_{\mathbf{n}'}h(\mathbf{x}',\mathbf{x})\mathbf{E}(\mathbf{x}',T) + \frac{1}{c}h(\mathbf{x}',\mathbf{x})(\partial_{t'}\mathbf{E})(\mathbf{x}',T)\partial_{\mathbf{n}'}|\mathbf{x}'-\mathbf{x}|\}\\ &+\int_S \mathrm{d}S'\{h(\mathbf{x}',\mathbf{x})\partial_{\mathbf{n}'}(\mathbf{E}(\mathbf{x}',T)) - \partial_{\mathbf{n}'}h(\mathbf{x}',\mathbf{x})\mathbf{E}(\mathbf{x}',T)\\ &+\frac{2}{c}h(\mathbf{x}',\mathbf{x})(\partial_{t'}\mathbf{E})(\mathbf{x}',T)\partial_{\mathbf{n}'}|\mathbf{x}'-\mathbf{x}|\}.\end{aligned} \tag{B.1}$$

We are going to rework the first term in the integral (B.1). Observe that for a vector field $\mathbf{a}$ and a scalar f we have,

$$\begin{aligned}(\mathbf{n}\cdot\nabla)(f\mathbf{a}) &= (\mathbf{n}\cdot\nabla f)\mathbf{a} + f(\mathbf{n}\cdot\nabla)\mathbf{a},\\ \nabla\cdot(f\mathbf{a}) &= \nabla f\cdot\mathbf{a} + f\nabla\cdot\mathbf{a},\\ \nabla\times(f\mathbf{a}) &= \nabla f\times\mathbf{a} + f\nabla\times\mathbf{a},\end{aligned}$$

so,

$$\mathbf{n}\times(\nabla\times(f\mathbf{a})) = \nabla f(\mathbf{n}\cdot\mathbf{a}) - \mathbf{a}(\mathbf{n}\cdot\nabla f) + f\mathbf{n}\times(\nabla\times\mathbf{a}).$$

Further,

$$\begin{aligned}&(\mathbf{n}\cdot\nabla)(f\mathbf{a}) + \mathbf{n}\times(\nabla\times(f\mathbf{a})) - n\nabla\cdot(f\mathbf{a})\\ &= f(\mathbf{n}\cdot\nabla)\mathbf{a} + (\mathbf{n}\times\nabla f)\times\mathbf{a} + f\mathbf{n}\times(\nabla\times\mathbf{a}) - f\mathbf{n}\nabla\cdot\mathbf{a}.\end{aligned}$$

so if we let $f = h(\mathbf{x}',\mathbf{x})$ and $\mathbf{a} = \mathbf{E}(\mathbf{x}',T)$, we thus have

$$\begin{aligned}&\int_S \mathrm{d}S' h(\mathbf{x}',\mathbf{x})\partial_{\mathbf{n}'}(\mathbf{E}(\mathbf{x}',T))\\ &= \int_S \mathrm{d}S'\{-(\mathbf{n}'\times\nabla' h(\mathbf{x}',\mathbf{x}))\times\mathbf{E}(\mathbf{x}',T)\\ &- h(\mathbf{x}',\mathbf{x})\mathbf{n}'\times(\nabla'\times(\mathbf{E}(\mathbf{x}',T)))\\ &+ h(\mathbf{x}',\mathbf{x})\mathbf{n}'\nabla'\cdot(\mathbf{E}(\mathbf{x}',T))\}.\end{aligned} \tag{B.2}$$

Inserting (B.2) into (B.1) leads to

$$\begin{aligned}\mathbf{E}(\mathbf{x},t) = &-\int_D \mathrm{d}V' h(\mathbf{x}',\mathbf{x})\{\mu\partial_{t'}J + \frac{1}{\varepsilon}\nabla'\rho\}(\mathbf{x},T)\\ &+\int_S \mathrm{d}S'\{h(\mathbf{x}',\mathbf{x})\mathbf{n}'\nabla'\cdot(\mathbf{E}(\mathbf{x}',T)) - (\mathbf{n}'\times\nabla' h(\mathbf{x}',\mathbf{x}))\times\mathbf{E}(\mathbf{x}',T)\\ &-h(\mathbf{x}',\mathbf{x})\mathbf{n}'\times(\nabla'\times(\mathbf{E}(\mathbf{x}',T))) - \partial_{\mathbf{n}'}h(\mathbf{x}',\mathbf{x})\mathbf{E}(\mathbf{x}',T)\\ &+\frac{2}{c}h(\mathbf{x}',\mathbf{x})(\partial_{t'}\mathbf{E})(\mathbf{x},T)\partial_{\mathbf{n}'}|\mathbf{x}'-\mathbf{x}|\}.\end{aligned}$$

Since

$$\begin{aligned}\nabla'(\mathbf{E}(\mathbf{x}',T)) &= (\nabla'\cdot\mathbf{E})(\mathbf{x}',T) - \frac{1}{c}(\partial_{t'}\mathbf{E})(\mathbf{x}',T)\cdot\nabla'|\mathbf{x}'-\mathbf{x}|,\\ \nabla'\times(\mathbf{E}(\mathbf{x}',T)) &= (\nabla'\times\mathbf{E})(\mathbf{x}',T) + \frac{1}{c}(\partial_{t'}\mathbf{E})(\mathbf{x}',T)\times\nabla'|\mathbf{x}'-\mathbf{x}|,\end{aligned}$$

in the end, (B.1) can be written in the following form

$$\begin{aligned}\mathbf{E}(\mathbf{x},t) = &-\int_D \mathrm{d}V' h(\mathbf{x}',\mathbf{x})\{\mu\partial_{t'}\mathbf{J} + \frac{1}{\varepsilon}\nabla'\rho\}(\mathbf{x}',T)\\ &+\int_S \mathrm{d}S'\{h(\mathbf{x}',\mathbf{x})\mathbf{n}'(\nabla'\cdot\mathbf{E})(\mathbf{x}',T)\\ &-\frac{1}{c}h(\mathbf{x}',\mathbf{x})\mathbf{n}'(\partial_{\mathbf{t}'}\mathbf{E})(\mathbf{x}',\mathbf{T})\cdot\nabla'|\mathbf{x}'-\mathbf{x}|)\\ &-(\mathbf{n}'\times\nabla' h(\mathbf{x}',\mathbf{x}))\times\mathbf{E}(\mathbf{x}',T) - h(\mathbf{x}',\mathbf{x})\mathbf{n}'\times(\nabla'\times\mathbf{E})(\mathbf{x}',T)\\ &-\frac{1}{c}h(\mathbf{x}',\mathbf{x})\mathbf{n}'\times((\partial_{t'}\mathbf{E})(\mathbf{x}',T)\times\nabla'|\mathbf{x}'-\mathbf{x}|)\\ &-\partial_{\mathbf{n}'}h(\mathbf{x}',\mathbf{x})\mathbf{E}(\mathbf{x}',T) + \frac{2}{c}h(\mathbf{x}',\mathbf{x})(\partial_{t'}\mathbf{E})(\mathbf{x}',T)\partial_{\mathbf{n}'}|\mathbf{x}'-\mathbf{x}|\}.\end{aligned}$$

Notice that

$$(\mathbf{n}\times\mathbf{a})\times\nabla f - (\mathbf{n}\times\nabla f)\times\mathbf{a} = (\mathbf{n}\cdot\nabla f)\mathbf{a} - (\mathbf{n}\cdot\mathbf{a})\nabla f,$$

and

$$-(\mathbf{n}\times\nabla f)\times\mathbf{a} - (\mathbf{n}\cdot\nabla f)\mathbf{a} = -(\mathbf{n}\times\mathbf{a})\times\nabla f - (\mathbf{n}\cdot\mathbf{a})\nabla f,$$

and performing them on h and $\mathbf{E}$ gives

$$\begin{aligned}&-(\mathbf{n}'\times\nabla' h(\mathbf{x}',\mathbf{x}))\times\mathbf{E}(\mathbf{x}',T) - \partial_{\mathbf{n}'}h(\mathbf{x}',\mathbf{x})\mathbf{E}(\mathbf{x}',T)\\ &=-(\mathbf{n}'\times\mathbf{E}(\mathbf{x}',T))\times\nabla' h(\mathbf{x}',\mathbf{x}) - (\mathbf{n}'\cdot\mathbf{E}(\mathbf{x}',T))\nabla' h(\mathbf{x}',\mathbf{x}).\end{aligned}$$

In addition

$$\begin{aligned}&(\mathbf{n}\times\mathbf{a})\times\nabla f + \mathbf{n}\times(\mathbf{a}\times\nabla f)\\ &= 2(\mathbf{n}\cdot\nabla f)\mathbf{a} - (\mathbf{a}\cdot\nabla f)\mathbf{n} - (\mathbf{n}\cdot\mathbf{a})\nabla f,\end{aligned}$$

and

$$\begin{aligned}&-(\mathbf{a}\cdot\nabla f)\mathbf{n} - \mathbf{n}\times(\mathbf{a}\times\nabla f) + 2(\mathbf{n}\cdot\nabla f)\mathbf{a}\\ &=(\mathbf{n}\times\mathbf{a})\times\nabla f + (\mathbf{n}\cdot\mathbf{a})\nabla f,\end{aligned}$$

give

$$\begin{aligned}&-\mathbf{n}'((\partial_{t'}\mathbf{E})(\mathbf{x}',T)\cdot\nabla'|\mathbf{x}'-\mathbf{x}|) - \mathbf{n}'\times((\partial_{t'}\mathbf{E})(\mathbf{x},T)\times\nabla'|\mathbf{x}'-\mathbf{x}|)\\ &+2\partial_{\mathbf{n}'}|\mathbf{x}'-\mathbf{x}|(\partial_{t'}\mathbf{E})(\mathbf{x}',T)\\ &=(\mathbf{n}'\times(\partial_{t'}\mathbf{E})(\mathbf{x}',T))\times\nabla'|\mathbf{x}'-\mathbf{x}| + (\mathbf{n}'\cdot(\partial_{t'}\mathbf{E})(\mathbf{x}',T))\nabla'|\mathbf{x}'-\mathbf{x}|.\end{aligned}$$

Thus

$$\begin{aligned}\mathbf{E}(\mathbf{x},t) = &-\int_D \mathrm{d}V' h(\mathbf{x}',\mathbf{x})\{\mu\partial_{t'}\mathbf{J} + \frac{1}{\varepsilon}\nabla'\rho\}(\mathbf{x}',T)\\ &+\int_S \mathrm{d}S'\{h(\mathbf{x}',\mathbf{x})\mathbf{n}'(\nabla'\cdot\mathbf{E})(\mathbf{x}',T) - (\mathbf{n}'\times E(\mathbf{x}',T))\times\nabla' h(\mathbf{x}',\mathbf{x})\\ &-(\mathbf{n}'\cdot E(\mathbf{x}',T))\nabla' h(\mathbf{x}',\mathbf{x}) + \frac{1}{c}h(\mathbf{x}',\mathbf{x})(\mathbf{n}'\times(\partial_{t'}\mathbf{E})(\mathbf{x}',T))\times\nabla'|\mathbf{x}'-\mathbf{x}|\\ &+\frac{1}{c}h(\mathbf{x}',\mathbf{x})(\mathbf{n}'\cdot(\partial_{t'}\mathbf{E})(\mathbf{x}',T))\nabla'|\mathbf{x}'-\mathbf{x}| - h(\mathbf{x}',\mathbf{x})\mathbf{n}'\times(\nabla'\times\mathbf{E})(\mathbf{x}',T)\}.\end{aligned}$$

Using the special form of the divergence theorem, we have

$$\begin{aligned}
&\int_S \mathrm{d}S' h(\mathbf{x}', \mathbf{x}) \mathbf{n}' (\nabla' \cdot \mathbf{E})(\mathbf{x}', T) \\
&= \int_D \mathrm{d}V' h(\mathbf{x}', \mathbf{x}) \frac{1}{\varepsilon} (\nabla' \rho)(\mathbf{x}', T) - \int_D , \mathrm{d}V' h(\mathbf{x}', \mathbf{x}) \frac{1}{\varepsilon} \nabla \rho(\mathbf{x}', T) \\
&+ \int_D \mathrm{d}V' \frac{1}{\varepsilon} \rho(\mathbf{x}', T) \nabla' h(\mathbf{x}', \mathbf{x}),
\end{aligned}$$

where

$$\nabla' h(\mathbf{x}', \mathbf{x}) = \frac{1}{4\pi} \nabla' \frac{1}{|\mathbf{x}' - \mathbf{x}|} = -\nabla h(\mathbf{x}', \mathbf{x}).$$

Together with

$$(\partial_{t'} \mathbf{J})(\mathbf{x}', T) = \partial_t (\mathbf{J}(\mathbf{x}', T)),$$

we finally get

$$\begin{aligned}
\mathbf{E}(\mathbf{x}, t) &= -\partial_t \frac{\mu}{4\pi} \int_D \mathrm{d}V' \frac{\mathbf{J}(\mathbf{x}', T)}{|\mathbf{x}' - \mathbf{x}|} - \nabla \frac{1}{4\pi\varepsilon} \int_D \mathrm{d}V' \frac{\rho(\mathbf{x}', T)}{|\mathbf{x}' - \mathbf{x}|} \\
&+ \partial_t [\frac{1}{4\pi} \int_S \mathrm{d}S' \{ \frac{1}{c|\mathbf{x}' - \mathbf{x}|} (\mathbf{n}' \times \mathbf{E}(\mathbf{x}', T)) \times \nabla' |\mathbf{x}' - \mathbf{x}| \\
&+ \frac{1}{c|\mathbf{x}' - \mathbf{x}|} (\mathbf{n}' \cdot \mathbf{E}(\mathbf{x}', T)) \nabla' |\mathbf{x}' - \mathbf{x}| + \frac{1}{|\mathbf{x}' - \mathbf{x}|} \mathbf{n}' \times \mathbf{B}(\mathbf{x}', T) \}] \\
&- \frac{1}{4\pi} \int_S \mathrm{d}S' \{ (\mathbf{n}' \times \mathbf{E}(\mathbf{x}', T)) \times \nabla' \frac{1}{|\mathbf{x}' - \mathbf{x}|} \\
&+ (\mathbf{n}' \cdot \mathbf{E}(\mathbf{x}', T)) \nabla' \frac{1}{|\mathbf{x}' - \mathbf{x}|} \}.
\end{aligned}$$

This is the integral identity of the electric wave equation (2.6).

C The first order, the second order and the mixed space derivatives

Here we illustrate a general rule. Suppose we have a three variable function $f(x, y, z)$ defined on grids (D.1). In order to get a second order accuracy, we apply the polynomials in two variables of degree 3 which is expressed by

$$\begin{aligned}
f(x, y, z) = f(x_i, y_i, z_k) &+ \zeta_1 \delta x + \zeta_2 \delta x^2 + \zeta_3 \delta x^3 + \zeta_4 \delta x \delta y + \zeta_5 \delta x^2 \delta y \\
&+ \zeta_6 \delta x \delta y^2 + \zeta_7 \delta y + \zeta_8 \delta y^2 + \zeta_9 \delta y^3,
\end{aligned}$$

where $\delta x = x - x_i$, $\delta y = y - y_i$ and

$$\begin{aligned}
\zeta_1 &= \frac{\partial f(x_i, y_j, z_k)}{\partial x}, \qquad \zeta_2 = \frac{\partial^2 f(x_i, y_j, z_k)}{\partial x^2}, \qquad \zeta_3 = \frac{\partial^3 f(x_i, y_j, z_k)}{\partial x^3}, \\
\zeta_4 &= \frac{\partial^2 f(x_i, y_j, z_k)}{\partial x \partial y}, \qquad \zeta_5 = \frac{\partial^3 f(x_i, y_j, z_k)}{\partial x^2 \partial y}, \qquad \zeta_6 = \frac{\partial^3 f(x_i, y_j, z_k)}{\partial x \partial y^2}, \\
\zeta_7 &= \frac{\partial f(x_i, y_j, z_k)}{\partial y}, \qquad \zeta_8 = \frac{\partial^2 f(x_i, y_j, z_k)}{\partial y^2}, \qquad \zeta_9 = \frac{\partial^3 f(x_i, y_j, z_k)}{\partial y^3}.
\end{aligned}$$

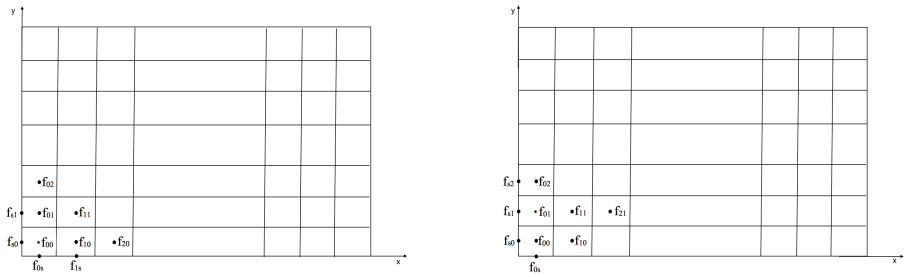

(a) $i = 0, j = 0$ (b) $i = 0, j = 1$

Figure C.1: Two examples of the involved grid points for calculating the space derivatives of e_p and b_p, $p = 1, 2, 3$.

Except for $f(x_i, y_j, z_k)$, we always need 9 extra grid points that are closest to (x_i, y_j, z_k) in order to get the expressions of $\zeta_1, \zeta_2, \cdots, \zeta_9$. We'll see that these expressions vary depending on the locations of i and j. For example, if $i = 0, j = 0$, the involved grid points are $f_{s,0}$, $f_{0,0}$, $f_{1,0}$, $f_{2,0}$, $f_{0,s}$, $f_{1,s}$, $f_{s,1}$, $f_{0,1}$, $f_{1,1}$ and $f_{0,2}$ while if $i = 0, j = 1$, the involved grid points are $f_{s,0}$, $f_{0,0}$, $f_{1,0}$, $f_{0,s}$, $f_{s,1}$, $f_{0,1}$, $f_{1,1}$, $f_{2,1}$, $f_{s,2}$ and $f_{0,2}$ where

$$f_{s,j} = \begin{cases} f(x_a, y_j, z_k) & i = 0 \\ f(x_b, y_j, z_k) & i = N_x - 1 \end{cases}$$

$$f_{i,s} = \begin{cases} f(x_i, y_a, z_k) & j = 0 \\ f(x_i, y_b, z_k) & j = N_y - 1 \end{cases}$$

$$f_{i,j} = f(x_i, y_j, z_k),$$

and so on. Figure C.1 illustrates two examples of the involved grid points. Finally if $i = 0$ or $i = N_x - 1$ we have

$$\frac{\partial f(x_i, y_j, z_k)}{\partial x} = \pm(f_{s,j},\ f_{i,j},\ f_{i\pm1,j},\ f_{i\pm2,j}\ ) \cdot W_1,$$

$$\frac{\partial^2 f(x_i, y_j, z_k)}{\partial x^2} = (f_{s,j},\ f_{i,j},\ f_{i\pm1,j},\ f_{i\pm2,j}\ ) \cdot W_2,$$

$$\frac{\partial^2 f(x_i, y_j, z_k)}{\partial x \partial y} =$$

$$\begin{cases} \pm(\ f_{s,j},\ f_{s,j+1},\ f_{i,s},\ f_{i,j},\ f_{i,j+1},\ f_{i\pm1,s},\ f_{i\pm1,j},\ f_{i\pm1,j+1}\ ) \cdot W_3 & j = 0 \\ \mp(\ f_{s,j},\ f_{s,j-1},\ f_{i,s},\ f_{i,j},\ f_{i,j-1},\ f_{i\pm1,s},\ f_{i\pm1,j},\ f_{i\pm1,j-1}\ ) \cdot W_3 & j = N_y - 1 \\ \pm(\ f_{s,j-1}, f_{s,j}, f_{s,j+1}, f_{i,j}, f_{i,j+1}, f_{i\pm1,j-1}, f_{i\pm1,j}\ ) \cdot W_4 & 0 < j < \frac{N_y}{2} \\ \mp(\ f_{s,j+1}, f_{s,j}, f_{s,j-1}, f_{i,j}, f_{i,j-1}, f_{i\pm1,j+1}, f_{i\pm1,j}\ ) \cdot W_4 & \frac{N_y}{2} <= j < N_y - 1 \end{cases}$$

It takes the upper sign for $i = 0$ and the nether sign for $i = N_x - 1$.
If $0 < i < N_x - 1$, we have

$$\frac{\partial f(x_i, y_j, z_k)}{\partial x} = \ (f_{i-1,j},\ f_{i+1,j}\ ) \cdot W_5,$$
$$\frac{\partial^2 f(x_i, y_j, z_k)}{\partial x^2} = \ (f_{i-1,j},\ f_{i,j},\ f_{i+1,j}\ ) \cdot W_6,$$
$$\frac{\partial^2 f(x_i, y_j, z_k)}{\partial x \partial y} =$$
$$\begin{cases} \pm(\ f_{i\mp1,s},\ f_{i,s},\ f_{i,j},\ f_{i\pm1,s},\ f_{i\pm1,j},\ f_{i\mp1,j+1},\ f_{i,j+1}\ ) \cdot W_4 & j = 0 \\ \mp(\ f_{i\mp1,s},\ f_{i,s},\ f_{i,j},\ f_{i\pm1,s},\ f_{i\pm1,j},\ f_{i\mp1,j-1},\ f_{i,j-1}\ ) \cdot W_4 & j = N_y - 1 \\ (\ f_{i+1,j+1},\ f_{i+1,j-1},\ f_{i-1,j+1},\ f_{i-1,j-1}\ ) \cdot W_7 & 0 < j < N_y - 1 \end{cases}$$

It takes the upper sign for $0 < i < N_x - 2$ and the nether sign for $i = N_x - 2$.
In the above expressions, $W_i, W_2, \cdots, W_7$ are vectors expressed by

$$W_1 = \frac{1}{30\ \Delta x} \begin{pmatrix} -32 \\ 15 \\ 20 \\ -3 \end{pmatrix}, \qquad W_2 = \frac{1}{(\Delta x)^2} \begin{pmatrix} 3.2 \\ -5 \\ 2 \\ -0.2 \end{pmatrix},$$
$$W_3 = \frac{1}{3\ \Delta x \Delta y} \begin{pmatrix} 4 \\ -4 \\ 4 \\ -9 \\ 5 \\ -4 \\ 5 \\ -1 \end{pmatrix}, \qquad W_4 = \frac{1}{3\ \Delta x \Delta y} \begin{pmatrix} 1 \\ 2 \\ -3 \\ -3 \\ 3 \\ -1 \\ 1 \end{pmatrix},$$
$$W_5 = \frac{1}{2\ \Delta x} \begin{pmatrix} -1 \\ 1 \end{pmatrix}, \qquad W_6 = \frac{1}{(\Delta x)^2} \begin{pmatrix} 1 \\ -2 \\ 1 \end{pmatrix},$$
$$W_7 = \frac{1}{4\,\Delta x \Delta y} \begin{pmatrix} 1 \\ -1 \\ -1 \\ 1 \end{pmatrix}.$$

These rules apply to all space derivatives of $e_1, e_2, e_3, b_1, b_2, b_3$.

D Numerical discretizations of the EOS formulations

In this section, we present the numerical discretizations of the EOS formulations of the model described by the 3D maxwell equations where the scattering object is confined in $V_1 = [x_a, x_b] \times [y_a, y_b] \times [z_a, z_b]$. Similarly as in the 1D toy models [15], for a second order accuracy solutions, we perform the Lax-Wendroff method on (2.4) and the modified Euler's method on (2.5) and we use the mid-point

rules to the integrals in (2.27). Based on this, we discretize the space domain by the following non-uniform grids in V_1,

$$\begin{aligned} x_i &= x_a + (i+0.5)\Delta x, \qquad i = 0, 1, 2, \cdots N_x - 1, \\ y_j &= y_a + (j+0.5)\Delta y, \qquad j = 0, 1, 2, \cdots N_y - 1, \\ z_k &= z_a + (k+0.5)\Delta z, \qquad k = 0, 1, 2, \cdots N_z - 1, \end{aligned} \tag{D.1}$$

with

$$\begin{aligned} \Delta x &= \frac{x_b - x_a}{N_x}, \\ \Delta y &= \frac{y_b - y_a}{N_y}, \\ \Delta z &= \frac{z_b - z_a}{N_z}, \end{aligned}$$

where N_x, N_y and N_z are positive integer numbers. The time step is designated to be

$$t_n = n\Delta t, \ n = 0, 1, 2 \cdots,$$

where

$$\Delta t = \frac{\tau}{c_1} Min\{\Delta x, \Delta y, \Delta z\}$$

and $0 < \tau < 1$ for an explicit numerical method. If we write the vector fields using notations

$$\begin{aligned} \mathbf{E}_1 &= (e_1, e_2, e_3), \\ \mathbf{B}_1 &= (b_1, b_2, b_3), \\ \mathbf{J}_1 &= (j_1, j_2, j_3), \\ F_1 &= F(e_1, j_1), \\ F_2 &= F(e_2, j_2), \\ F_3 &= F(e_3, j_3), \end{aligned}$$

then (2.4) and (2.5) can be expanded into the following formulas

$$\partial_t e_1 = c_1^2 (\frac{\partial b_3}{\partial y} - \frac{\partial b_2}{\partial z} - \mu_1 j_1), \tag{D.2}$$

$$\partial_t e_2 = c_1^2 (\frac{\partial b_1}{\partial z} - \frac{\partial b_3}{\partial x} - \mu_1 j_2), \tag{D.3}$$

$$\partial_t e_3 = c_1^2 (\frac{\partial b_2}{\partial x} - \frac{\partial b_1}{\partial y} - \mu j_3), \tag{D.4}$$

$$\partial_t b_1 = \frac{\partial e_2}{\partial z} - \frac{\partial e_3}{\partial y}, \tag{D.5}$$

$$\partial_t b_2 = \frac{\partial e_3}{\partial x} - \frac{\partial e_1}{\partial z}, \tag{D.6}$$

$$\partial_t b_3 = \frac{\partial e_1}{\partial y} - \frac{\partial e_2}{\partial x}, \tag{D.7}$$

$$\partial_t \rho_1 = -(\frac{\partial j_1}{\partial x} + \frac{\partial j_2}{\partial y} + \frac{\partial j_3}{\partial z}), \tag{D.8}$$

$$\partial_t j_1 = (\alpha - \beta\rho_1)e_1 - \gamma j_1 = F_1, \tag{D.9}$$

$$\partial_t j_2 = (\alpha - \beta\rho_1)e_2 - \gamma j_2 = F_2, \tag{D.10}$$

$$\partial_t j_3 = (\alpha - \beta\rho_1)e_3 - \gamma j_3 = F_3. \tag{D.11}$$

Now we take a look at the solutions at the grid point (x_i, y_j, z_k) at time t_n. From Taylor series we have the following solutions to (D.2) - (D.8),

$$\phi^{n+1}_{i,j,k} = \phi^n_{i,j,k} + \Delta t(\frac{\partial\phi}{\partial t})^n_{i,j,k} + \frac{1}{2}(\Delta t)^2(\frac{\partial^2\phi}{\partial t^2})^n_{i,j,k}, \tag{D.12}$$

where ϕ represents $e_1, e_2, e_3, b_1, b_2, b_3, \rho_1$ and

$$(\frac{\partial e_1}{\partial t})^n_{i,j,k} = c_1^2[\frac{\partial b_3}{\partial y} - \frac{\partial b_2}{\partial z} - \mu_1 j_1]^n_{i,j,k}$$

$$(\frac{\partial e_2}{\partial t})^n_{i,j,k} = c_1^2[\frac{\partial b_1}{\partial z} - \frac{\partial b_3}{\partial x} - \mu_1 j_2]^n_{i,j,k}$$

$$(\frac{\partial e_3}{\partial t})^n_{i,j,k} = c_1^2[\frac{\partial b_2}{\partial x} - \frac{\partial b_1}{\partial y} - \mu_1 j_3]^n_{i,j,k}$$

$$(\frac{\partial b_1}{\partial t})^n_{i,j,k} = (\frac{\partial e_2}{\partial z} - \frac{\partial e_3}{\partial y})^n_{i,j,k},$$

$$(\frac{\partial b_2}{\partial t})^n_{i,j,k} = (\frac{\partial e_3}{\partial x} - \frac{\partial e_1}{\partial z})^n_{i,j,k},$$

$$(\frac{\partial b_3}{\partial t})^n_{i,j,k} = (\frac{\partial e_1}{\partial y} - \frac{\partial e_2}{\partial x})^n_{i,j,k},$$

$$(\frac{\partial \rho_1}{\partial t})^n_{i,j,k} = -(\frac{\partial j_1}{\partial x} + \frac{\partial j_2}{\partial y} + \frac{\partial j_3}{\partial z})^n_{i,j,k}$$

and

$$(\frac{\partial^2 e_1}{\partial t^2})^n_{i,j,k} = c_1^2[\frac{\partial^2 e_1}{\partial y^2} - \frac{\partial}{\partial y}\frac{\partial e_2}{\partial x} - \frac{\partial}{\partial z}\frac{\partial e_3}{\partial x} + \frac{\partial^2 e_1}{\partial z^2} - \mu_1 F_1]^n_{i,j,k},$$

$$(\frac{\partial^2 e_2}{\partial t^2})^n_{i,j,k} = c_1^2[\frac{\partial^2 e_2}{\partial z^2} - \frac{\partial}{\partial z}\frac{\partial e_3}{\partial y} - \frac{\partial}{\partial x}\frac{\partial e_1}{\partial y} + \frac{\partial^2 e_2}{\partial x^2} - \mu_1 F_2]^n_{i,j,k},$$

$$(\frac{\partial^2 e_3}{\partial t^2})^n_{i,j,k} = c_1^2[\frac{\partial^2 e_3}{\partial x^2} - \frac{\partial}{\partial x}\frac{\partial e_1}{\partial z} - \frac{\partial}{\partial y}\frac{\partial e_2}{\partial z} + \frac{\partial^2 e_3}{\partial y^2} - \mu_1 F_3]^n_{i,j,k},$$

$$(\frac{\partial^2 b_1}{\partial t^2})^n_{i,j,k} = c_1^2[\frac{\partial^2 b_1}{\partial y^2} - \frac{\partial}{\partial y}\frac{\partial b_2}{\partial x} - \frac{\partial}{\partial z}\frac{\partial b_3}{\partial x} + \frac{\partial^2 b_1}{\partial z^2} + \mu_1(\frac{\partial j_3}{\partial y} - \frac{\partial j_2}{\partial z})]^n_{i,j,k},$$

$$(\frac{\partial^2 b_2}{\partial t^2})^n_{i,j,k} = c_1^2[\frac{\partial^2 b_2}{\partial z^2} - \frac{\partial}{\partial z}\frac{\partial b_3}{\partial y} - \frac{\partial}{\partial x}\frac{\partial b_1}{\partial y} + \frac{\partial^2 b_2}{\partial x^2} + \mu_1(\frac{\partial j_1}{\partial z} - \frac{\partial j_3}{\partial x})]^n_{i,j,k},$$

$$(\frac{\partial^2 b_3}{\partial t^2})^n_{i,j,k} = c_1^2[\frac{\partial^2 b_3}{\partial x^2} - \frac{\partial}{\partial x}\frac{\partial b_1}{\partial z} - \frac{\partial}{\partial y}\frac{\partial b_2}{\partial z} + \frac{\partial^2 b_3}{\partial y^2} + \mu_1(\frac{\partial j_2}{\partial x} - \frac{\partial j_1}{\partial y})]^n_{i,j,k},$$

$$(\frac{\partial^2 \rho_1}{\partial t^2})^n_{i,j,k} = -[\frac{\partial F_1}{\partial x} + \frac{\partial F_2}{\partial y} + \frac{\partial F_3}{\partial z}]^n_{i,j,k}.$$

For equations (D.9)-(D.11), the modified Euler's method is performed which gives

$$\begin{aligned}(\bar{j_p})_{i,j,k}^{n+1} &= (j_p)_{i,j,k}^n + \Delta t \cdot F((e_p)_{i,j,k}^n, (j_p)_{i,j,k}^n),\\ (j_p)_{i,j,k}^{n+1} &= \frac{1}{2}((j_p)_{i,j,k}^n + (\bar{j_p})_{i,j,k}^{n+1} + \Delta t \cdot F((e_p)_{i,j,k}^{n+1}, (\bar{j_p})_{i,j,k}^{n+1})),\end{aligned} \tag{D.13}$$

where $p = 1, 2, 3$. The electric field and the magnetic field inside the object are aroused by the light sources located outside the scattering object so that the values of them will be effected by the values on the boundary. While the charge density and the current density are entirely induced by the changing electric field and the changing magnetic field inside the object and this generally produces discontinuity of J_1 and ρ_1 on the surface of the object. Due to this, the space derivatives of $\mathbf{E}_1$ and $\mathbf{B}_1$ near the boundary will involve the inside values and also the surface value while the space derivatives of ρ_1, j_p and $F_p, p = 1, 2, 3$ near the boundary will only involve the inside values. Here we only write down the space derivatives with respect to x of them and the same rules are applied to the space derivatives with respect to y and z. Except the internal nodes closest to the surface, the space derivatives are approximated to second order accuracy by the following standard finite difference formulas

$$\begin{aligned}(\frac{\partial \phi}{\partial x})_{i,j,k}^n &= \frac{\phi_{i+1,j,k}^n - \phi_{i-1,j,k}^n}{2\,\Delta x},\\ (\frac{\partial^2 \phi}{\partial x^2})_{i,j,k}^n &= \frac{\phi_{i+1,j,k}^n - 2\phi_{i,j,k}^n + \phi_{i-1,j,k}^n}{(\Delta x)^2}, \qquad 0 < i < N_x - 1.\end{aligned}$$

For the internal nodes closest to the surface, the following second order accuracy difference rules are applied

$$\begin{aligned}(\frac{\partial \phi}{\partial x})_{0,j,k}^n &= \frac{1}{2 \cdot \Delta x}(4\phi_{1,j,k}^n - 3\phi_{0,j,k}^n - \phi_{2,j,k}^n),\\ (\frac{\partial \phi}{\partial x})_{N_x-1,j,k}^n &= -\frac{1}{2 \cdot \Delta x}(4\phi_{N_x-2,j,k}^n - 3\phi_{N_x-1,j,k}^n - \phi_{N_x-3,j,k}^n)\end{aligned}$$

where $\phi = \rho_1, j_p, F_p$, $p = 1, 2, 3$. For the electric fields $\mathbf{E}_1$ and the magnetic field $\mathbf{B}_1$, we need the space derivatives of both the first order and the second order including the mixed derivatives.

Next step, we need to discretize the boundary integral identities (2.27a) and (2.27b). We take a look at the field values at grid point $\mathbf{x}_p$, $p = 0, 1, 2, \cdots, N_s$ where

$$N_s = 2(N_x N_y + N_x N_z + N_y N_z).$$

The discretized form of (2.28) can be written as

$$\begin{aligned}(\mathbf{I}_e)_p^n = -\frac{1}{4\pi} \sum_{i=0}^{N_x} \sum_{j=0}^{N_y} \sum_{k=0}^{N_z} (&\mu_1 f_1 \partial_t \mathbf{J}_1(\mathbf{x}_{i,j,k}, T_1) + \frac{1}{\varepsilon_1} \mathbf{f}_3 \rho_1(\mathbf{x}_{i,j,k}, T_1)\\ &+ \frac{1}{\varepsilon_1 c_1} \mathbf{f}_2 \partial_t \rho_1(\mathbf{x}_{i,j,k}, T_1)),\end{aligned}$$

where

$$T_1 = t_n - \frac{|\mathbf{x}_{i,j,k} - \mathbf{x}_p|}{c_1},$$

and

$$
\begin{aligned}
f_1 &= \iiint_{V_{i,j,k}} \frac{1}{|\mathbf{x}' - \mathbf{x}_p|}\,\mathrm{d}V, \\
\mathbf{f}_2 &= \iiint_{V_{i,j,k}} \frac{\mathbf{x}' - \mathbf{x}}{|\mathbf{x}' - \mathbf{x}_p|^2}\,\mathrm{d}V, \\
\mathbf{f}_3 &= \iiint_{V_{i,j,k}} \frac{\mathbf{x}' - \mathbf{x}}{|\mathbf{x}' - \mathbf{x}_p|^3}\,\mathrm{d}V,
\end{aligned}
\tag{D.14}
$$

with

$$
V_{i,j,k} = [x_i - \frac{\Delta x}{2}, x_i + \frac{\Delta x}{2}] \times [y_j - \frac{\Delta y}{2}, y_j + \frac{\Delta y}{2}] \times [z_k - \frac{\Delta z}{2}, z_k + \frac{\Delta z}{2}].
$$

Notice that expressions $(D.14)$ are singular when $\mathbf{x_p}$ is located on one of the surfaces of $V_{i,j,k}$. All calculations of the singular integrals, both the singular volume integrals and the singular surface integrals in this paper will be discussed in [16]. It is observed that for vectors $\mathbf{A}$ and $\mathbf{C}$, we have the following identity

$$
\mathbf{A} \times \boldsymbol{\varphi} \times \mathbf{C} = (\mathbf{C} \cdot \mathbf{A})\boldsymbol{\varphi} - (\mathbf{AC}) \cdot \boldsymbol{\varphi},
$$

and due to

$$
\begin{aligned}
\nabla' |\mathbf{x}' - \mathbf{x}| &= \frac{\mathbf{x}' - \mathbf{x}}{|\mathbf{x}' - \mathbf{x}|}, \\
\nabla' \frac{1}{|\mathbf{x}' - \mathbf{x}|} &= -\frac{\mathbf{x}' - \mathbf{x}}{|\mathbf{x}' - \mathbf{x}|^3},
\end{aligned}
$$

we get the following relationships

$$
\begin{aligned}
&\frac{1}{|\mathbf{x}' - \mathbf{x}|}(\mathbf{n}' \times \mathbf{E}_+(\mathbf{x}', T)) \times \nabla' |\mathbf{x}' - \mathbf{x}| \\
&= (\frac{\mathbf{x}' - \mathbf{x}}{|\mathbf{x}' - \mathbf{x}|^2} \cdot \mathbf{n}')\mathbf{E}_+(\mathbf{x}', T) - (\mathbf{n}' \frac{\mathbf{x}' - \mathbf{x}}{|\mathbf{x}' - \mathbf{x}|^2}) \cdot \mathbf{E}_+(\mathbf{x}', T), \\
&(\mathbf{n}' \cdot \mathbf{E}_+(\mathbf{x}', T)) \nabla' |\mathbf{x}' - \mathbf{x}| = (\frac{\mathbf{x}' - \mathbf{x}}{|\mathbf{x}' - \mathbf{x}|} \mathbf{n}') \cdot \mathbf{E}_+(\mathbf{x}', T), \\
&(\mathbf{n}' \times \mathbf{E}_+(\mathbf{x}', T)) \times \nabla' \frac{1}{|\mathbf{x}' - \mathbf{x}|} \\
&= (\mathbf{n}' \frac{\mathbf{x}' - \mathbf{x}}{|\mathbf{x}' - \mathbf{x}|^3}) \cdot \mathbf{E}_+(\mathbf{x}', T) - (\frac{\mathbf{x}' - \mathbf{x}}{|\mathbf{x}' - \mathbf{x}|^3} \cdot \mathbf{n}')\mathbf{E}_+(\mathbf{x}', T), \\
&(\mathbf{n}' \cdot \mathbf{E}_+(\mathbf{x}', T)) \nabla' \frac{1}{|\mathbf{x}' - \mathbf{x}|} = -(\frac{\mathbf{x}' - \mathbf{x}}{|\mathbf{x}' - \mathbf{x}|^3} \mathbf{n}') \cdot \mathbf{E}_+(\mathbf{x}', T).
\end{aligned}
$$

Inserting the above relationships in (2.30), we obtain

$$
\begin{aligned}
(\mathbf{B}_e)_p^n = \frac{1}{4\pi} \sum_{q=0}^{N_s} &(K_1(\mathbf{n}_q \cdot \mathbf{E}_+(\mathbf{x}_q, T_2))\mathbf{g}_3 + K_2(\mathbf{n}_q \times \partial_t \mathbf{E}_+(\mathbf{x}_q, T_2)) \times \mathbf{g}_2 \\
&+ K_3(\mathbf{n}_q \cdot \partial_t \mathbf{E}_+(\mathbf{x}_q, T_2))\mathbf{g}_2 + K_4(\mathbf{n}_q \times \partial_t \mathbf{B}_+(\mathbf{x}_q, T_2))),
\end{aligned}
\tag{D.15}
$$

where

$$
T_2 = t_n - \frac{|\mathbf{x}_q - \mathbf{x}_p|}{c_1},
$$

and

$$
\begin{aligned}
K_1 &= 1 - \frac{\varepsilon_1}{\varepsilon_0}, \\
K_2 &= \frac{1}{c_1} - \frac{1}{c_0}, \\
K_3 &= \frac{1}{c_1} - \frac{\varepsilon_1}{c_0\varepsilon_0}, \\
K_4 &= (1 - \frac{\mu_0}{\mu_1})g_1,
\end{aligned}
$$

with

$$
\begin{aligned}
g_1 &= \int_{S_q} \frac{1}{|\mathbf{x}' - \mathbf{x}_p|}\,\mathrm{d}S', \\
\mathbf{g}_2 &= \int_{S_q} \frac{\mathbf{x}' - \mathbf{x}_p}{|\mathbf{x}' - \mathbf{x}_p|^2}\,\mathrm{d}S', \\
\mathbf{g}_3 &= \int_{S_q} \frac{\mathbf{x}' - \mathbf{x}_p}{|\mathbf{x}' - \mathbf{x}_p|^3}\,\mathrm{d}S'.
\end{aligned}
\tag{D.16}
$$

Similarly, in (2.27b) we obtain

$$
(\mathbf{I}_b)_p^n = \frac{u_1}{4\pi}\sum_{i=0}^{N_x}\sum_{j=0}^{N_y}\sum_{k=0}^{N_z}(\frac{1}{c_1}\mathbf{f}_2 \times \partial_t\mathbf{J}_1(\mathbf{x}_{i,j,k}, T_1) - \mathbf{J}_1(\mathbf{x}_{i,j,k}, T_1) \times \mathbf{f}_3)),
$$

and

$$
\begin{aligned}
(\mathbf{B}_b)_p^n = \frac{1}{4\pi}\sum_{q=0}^{N_s}(&K_5(\mathbf{n}_q \times \mathbf{B}_+(\mathbf{x}_q, T_2)) \times \mathbf{g}_3 + K_5(\mathbf{n}_q \times \partial_t\mathbf{B}_+(\mathbf{x}_q, T_2)) \times \mathbf{g}_2 \\
&+ K_2(\mathbf{n}_q \cdot \partial_t\mathbf{B}_+(\mathbf{x}_q, T_2))\mathbf{g}_2 + K_6(\mathbf{n}_q \times \partial_t\mathbf{E}_+(\mathbf{x}_q, T_2))),
\end{aligned}
\tag{D.17}
$$

with

$$
\begin{aligned}
K_5 &= \frac{1}{c_1} - \frac{\mu_0}{c_0\mu_1}, \\
K_6 &= (\frac{1}{c_0^2} - \frac{1}{c_1^2})g_1.
\end{aligned}
$$

It is clear that when the integrating point $\mathbf{x}'$ and the observing point $\mathbf{x}$ are in the same integral grid S_q, which indicates $q = p$, expressions in (D.16) are singular. The calculations of this type of sigular integrals can also be found in [16]. There are so far unknown terms on the right side of the equations of (D.15) and (D.17) due to the time derivatives $\partial_t\mathbf{E}(\mathbf{x}_q, T_2)$ and $\partial_t\mathbf{B}(\mathbf{x}_q, T_2)$ when $p = q$. Moving these unknown terms out of the summation, (D.15) and (D.17) can be compactly written as

$$
\begin{aligned}
(\mathbf{B}_e)_p^n &= \sum_{q\neq p}(\mathbf{E}_r)_q + (\mathbf{E}_r)_p, \\
(\mathbf{B}_b)_p^n &= \sum_{q\neq p}(\mathbf{B}_r)_q + (\mathbf{B}_r)_p
\end{aligned}
$$

where $\mathbf{E}_r$ and $\mathbf{B}_r$ are respectively the short notations of the right terms of (D.15) and (D.17) that are going to be summed up. For $p = q$, due to symmetric of $\mathbf{x}' - \mathbf{x}$ on S_q, there are

$$\mathbf{g}_2 = 0,$$

and

$$\mathbf{g}_3 = 0.$$

And this yields

$$\begin{aligned}
(\mathbf{E}_r)_p &= \frac{1}{4\pi} K_4 \ \mathbf{n}_p \times \partial_t \mathbf{B}_p^n \\
&= \frac{1}{4\pi} K_4 \ \mathbf{n}_p \times \frac{1}{\Delta t}(\frac{3}{2}\mathbf{B}_p^n - 2\mathbf{B}_p^{n-1} + \frac{1}{2}\mathbf{B}_p^{n-2}). \\
(\mathbf{B}_r)_p &= \frac{1}{4\pi} K_6 \ \mathbf{n}_p \times \partial_t \mathbf{E}_p^n \\
&= \frac{1}{4\pi} K_6 \ \mathbf{n}_p \times \frac{1}{\Delta t}(\frac{3}{2}\mathbf{E}_p^n - 2\mathbf{E}_p^{n-1} + \frac{1}{2}\mathbf{E}_p^{n-2}),
\end{aligned}$$

where we have used the second order polynomial approximation on the time derivatives. After moving unknowns $\mathbf{E}_p^n$ and $\mathbf{B}_p^n$ from the right of the equation to the left, we finally get a solving system

$$\begin{pmatrix} M_{11} & M_{12} \\ M_{21} & M_{22} \end{pmatrix} \begin{pmatrix} \mathbf{E}_p^n \\ \mathbf{B}_p^n \end{pmatrix} = \begin{pmatrix} \mathbf{E}_R \\ \mathbf{B}_R \end{pmatrix}, \tag{D.18}$$

where

$$\begin{aligned}
\mathbf{E}_R &= (\mathbf{I}_e)_p^n + (\mathbf{O}_e)_p^n + \sum_{q \neq p} (\mathbf{E}_r)_q + \frac{1}{4\pi} K_4 \ \mathbf{n}_p \times \frac{1}{\Delta t}(-2\mathbf{B}_p^{n-1} + \frac{1}{2}\mathbf{B}_p^{n-2}), \\
\mathbf{B}_R &= (\mathbf{I}_b)_p^n + (\mathbf{O}_b)_p^n + \sum_{q \neq p} (\mathbf{B}_r)_q + \frac{1}{4\pi} K_6 \ \mathbf{n}_p \times \frac{1}{\Delta t}(-2\mathbf{E}_p^{n-1} + \frac{1}{2}\mathbf{E}_p^{n-2}),
\end{aligned}$$

and $(\mathbf{O}_e)_p^n$ and $(\mathbf{O}_b)_p^n$ are respectively the effect on the surface point x_p at time t_n induced by the outside source which are calculated directly from the sources, and

$$\begin{aligned}
M_{11} &= I + \frac{1}{2}(\frac{\varepsilon_1}{\varepsilon_0} - 1)\mathbf{nn} \\
M_{12} &= -\frac{3}{8\pi\Delta t} K_4 m \\
M_{21} &= -\frac{3}{8\pi\Delta t} K_6 m \\
M_{22} &= I + \frac{1}{2}(1 - \frac{\mu_0}{\mu_1})\mathbf{nn}
\end{aligned}$$

with

$$m = \begin{pmatrix} 0 & -n_2 & n_1 \\ n_2 & 0 & -n_0 \\ -n_1 & n_0 & 0 \end{pmatrix},$$

where n_0, n_1 and n_2 are the three components of the normal field $\mathbf{n}$ at the surface point $\mathbf{x}_p$ and I is a 3×3 identity matrix. Equations (D.12) and (D.13) together with (D.18) are the final discretized form of the EOS formulations of model (2.4) and (2.5).

References

[1] K. Yee. Numerical solution of initial boundary value problems involving maxwell's equations in isotropic media. *IEEE Transactions on Antennas and Propagation*, 14(3):302–307, May 1966.

[2] A. Taflove. Application of the finite-difference time-domain method to sinusoidal steady state electromagnetic penetration problems. *IEEE Transactions on Electromagnetic Compatibility*, 22(3):191–202, 1980.

[3] A. Taflove et. al. *Computational Electrodynamics: the Finite-Difference Time-Domain Method, 3rd Ed.* Artech House Publishers, 2005.

[4] J. Berenger. A perfectly matched layer for the absorption of electromagnetic waves. *Journal of computational physics*, 114(2):185–200, 1994.

[5] S. Gedney. An anisotropic perfectly matched layer absorbing media for the truncation of fdtd lattices. *IEEE Transactions on Antennas and Propagation*, 44(12):1630–1639, 1996.

[6] Greeshma Pisharody and Daniel S. Weile. Electromagnetic scattering from homogeneous dielectric bodies using time-domain integral equations. *IEEE Transactions on Antennas and Propagation*, 54:687–697, 2006.

[7] D. S. Weile, I. Uluer, J. Li, and D.A. Hopkins. Integration rules and experimental evidences for the stability of time domain integral equations. *International Applied Computational Electromagnetics Society Symposium(ACES)*, 2017.

[8] A. J. Pray, N. V. Nair, and B. Shanker. Stability properties of the time domain electric field integral equationusing a separable approximation for the convolution with the retarded potential. *IEEE Transactions on Antennas and Propagation*, 60:3772–3781, 2012.

[9] M. J. Bluck and S. P. Walker. Time-domain bie analysis of large three-dimensional electromagnetic scattering problems. *IEEE Transactions on Antennas and Propagation*, 45:894–901, 1997.

[10] S. Dodson, S. P. Walker, and M. J. Bluck. Implicitness and stability of time domain integral equation scattering analysis. *Appl. Comput. Electromagn. Soc. J.*, 13:291–301, 1998.

[11] Ying Zhao, Dazhi Ding, and Rushan Chen. A discontinuous galerkin time-domain integral equation method for electromagnetic scattering from pec objects. *IEEE Transactions on Antennas and Propagation*, 64(6):2410–2415, 2016.

[12] Li Huang, Yi-Bei Hou, Hao-Xuan Zhang, Liang Zhou, and Wen-Yan Yin. A discontinuous galerkin time-domain integral equation method for electromagnetic scattering from pec objects. *IEEE Transactions on Electromagnetic Compatibility*, 2018.

[13] D. S. Jones. *The Theory of Electromagnetism*, volume 47 of *International Series of Monographs on Pure and Applied mathematics*. Pergamon Press, 1964.

[14] D. N. Pattanayak and E. Wolf. General form and new interpretation of the ewald-oseen extincition theorem. *Optics communications*, 6(3):217–220, 1972.

[15] Aihua Lin, Anastasiia Kuzmina, and Per Kristen Jakobsen. A boundary integral approach to linear and nonlinear transient wave scattering. *Submitted*, 2018.

[16] Per Jakobsen. Calculating optical forces using the boundary integral method. *Physics Scripta*, 80:35401–9, 2009.

[17] Aihua Lin and Per Kristen Jakobsen. Numerical techniques of solving a 3d nonlinear maxwells equations by the eos formulations: Parallelization, stabilities and singularities. *To appear*, 2018.

4 Paper 3

Submitted to PLOS ONE in the fall of 2018.

On the EOS formulation for light scattering. Stability, Singularity and Parallelization

Aihua Lin and Per Kristen Jakobsen

Department of Mathematics and Statistics, UIT the Arctic University of Norway, 9019 Tromsø, Norway

Abstract

In this paper we discuss some of the mathematical and numerical issues that have to be addressed when calculating wave scattering using the EOS approach. The discussion is framed in context of light scattering by objects whose optical response can be of a nonlinear and/or inhomogeneous nature. The discussions address two issues that, more likely than not, will be part of any investigation of wave scattering using the EOS approach.

1 Introduction

A new hybrid numerical approach for solving linear and nonlinear scattering problems, the Ewald Oseen Scattering(EOS) formulation, has recently been introduced and applied to the cases of 1D transient wave scattering [1] and 3D light scattering [2]. The approach combines a domain-based method and a boundary integral representation in such a way that the wave fields inside the scattering objects are updated in time using the domain-based method, while the integral representation is used to update the boundary values of the fields, which are required by the inside domain-based method. In such a way, for the numerical implementations, no numerical grids outside the scattering objects are needed. This greatly reduces the computational complexity and cost compared to fully domain based methods like the Finite Difference Time Domain(FDTD) method or the Finite Element Methods. The method can handle inhomogeneous and/or nonlinear optical response, and include the time dependent Boundary Element Method(TBEM), as a special case.

For the case of 1D transient wave scattering [1], the method solves the model equations accurately and efficiently, but we don't expect the 1D case to be fully representative for the problems and issues that need to be resolved, while using the EOS formulation to calculate wave scattering. We do, however, expect the case of 3D light scattering [2] to be fairly representative with respect to which problems arise, and also the computational and mathematical severity of these problems. We have seen three types of mathematical and computational issues arise for the case of light scattering which we believe are to be found in any nontrivial application of the EOS formulation to wave scattering.

Firstly, we have the issue of numerical stability. Instabilities in numerical implementations of the EOS formulation can arise from discretization of the domain part of the algorithm but also from discretization of the boundary update part of the algorithm. The numerical instability arising from the boundary part of the algorithm has been noted earlier in the context of transient light scattering from objects that has a linear homogeneous optical response. For this situation, realized for example in antenna theory, the boundary part of the EOS algorithm can be disconnected from the domain part of the algorithm, which in this case can be discarded. The EOS formulation becomes a pure boundary update algorithm which is solving a set integro-differential equations located on the boundary of the scattering objects. These integro-differential equations, which are the defining equations for TBEM, are subject to an instability that, in many common situations, strikes at late times. This late time instability is a major nuisance, and has prevented TBEM from being more widely applied than it is today. The sources of these instabilities are not yet fully understood, but we believe that our investigation of light scattering using the EOS approach, gives some new insight into the origin of these instabilities.

Even without a true understanding of the underlying causes of the late time instability, efforts have been made and several techniques have, over the last several decades, been developed with the goal of improving the stabilities of the numerical schemes designed to solve the integro-differential equations underlying TBEM.

Broadly speaking, there are two different directions that has been pursued. One direction is to delay or remove the late time instability by applying increasing accurate spatial integration schemes [3–9]. For instance Danile. S. Weiler and his co-authors have published a series of articles focused on illustrating the dependence of the stability on the different numerical integration schemes [3–6]. The other direction is aimed at designing more stable time discretization schemes. M. J. Bluck and his co-authors developed a stable, but implicit numerical method, [8, 9] for the integro-differential equations underlying TBEM, for the case when the magnetic response is the dominating one. These are the so called magnetic field integral equations. Some authors have reported some success in mitigating the instability by both making better approximations to the integrals and also applying improved algorithms for the time derivatives [10, 11].

Our work has not been directly aimed at contributing to this discussion, but, as already noted above, the integro-differential equations discussed by these authors can be seen as a special case of our general EOS approach, and we therefore believe that the insights we have gained on how this long time instability depend on the different pieces of the EOS algorithm, in particular how it depends on the material parameters describing the optical response of the scattering object, do have some relevance to the discussion described above.

Secondly, there is the issue of the singular integrals that appear when the integral part of the EOS algorithm is discretized. This issue is very much present in BEM and in TBEM [12–15], but they are more prevalent and severe for the EOS formulation, where we have to tackle both surface integrals and volume integrals. We believe that the type of singular integrals, and how to treat them for the case of light scattering, are fairly representative for the level of complexity one will encounter, while applying the EOS approach to wave scattering problems. For this reason we find it appropriate to include a section in this

paper, where we discuss relevant types of integrals, and how to treat them.

Thirdly, the fundamental equations underlying both the TBEM and our more general EOS approach to transient wave scattering, are retarded in time. This retardation is unavoidable since their underlying equations can only be derived using space-time Green's functions. Thus the solutions at a certain time depend on a values of the solutions from a potentially very long previous interval of time. Computationally this means that the method can be very demanding with respect to memory, and it also means that the updating of the boundary values of the fields, which is done by the boundary part of the EOS algorithm, can be very costly. Parallel processing, either using a computational cluster or a shared memory machine can take on these computational tasks. However, whenever large scale parallel processing is needed, the issue of appropriate partitioning of the problem and load balancing inevitably comes into play. In our work the EOS algorithm was implemented on a large cluster, but we will not in this paper report on any of the parallel issues that our EOS approach for light scattering gave rise to. These kind of considerations, which are important in practical terms, but typically have fairly low generality, are somewhat distinct from the mathematical and numerical issues that are the focus of the current paper, and will therefore be reported elsewhere at a later time.

However, the high memory requirement of the EOS approach to light scattering, is something that should be addressed at this point. On the one hand, the EOS approach represents a large, potentially very large, reduction in memory use, as compared to fully domain based methods, since only the surface and inside of the scattering objects has to be discretized. On the other hand, because of the retardation, there is a large, potentially very large increase in memory use compared to the memory usage needed by the domain part of the algorithm. It is appropriate to ask if anything has been gained with respect to memory usage compared to a fully domain based method like the FDTD method? We don't, as of yet, know the answer to this question, and the answer is almost certainly not going to be a simple one. It will probably depend on the detailed structure of the problems like the nature of the source, the number, shape and distribution of scattering objects etc. However, even if the memory usage for purely domain based methods and our EOS approach are roughly the same for many problems of interest, our approach avoid many of the sources of problems that need to be taken into account while using purely domain based methods. These are problems like stair-casing at sharp interfaces defining the scattering objects, issues of accuracy, stability and complexity associated with the use of multiple grids in order to accommodate the possibly different geometric shapes of the scattering objects and the need to minimize the reflection from the boundary of the finite computational box. The EOS approach is not subject to any of these problems.

In this paper our effort are aimed towards testing the EOS formulations of light scattering with respect to implementation complexity and numerical stability. Thus we illustrate the method by the simplest situation where we have single scattering object in the form of a rectangular box.

In section 2 we analyze the numerical stability of our EOS scheme for light scattering by using eigenvalues of the matrix defining the linearized version of the scheme exactly like for the case of 1D wave scattering [1]. We find, just like for the 1D case, that the internal numerical scheme, Lax-Wendroff for our case determines a stability interval for the time step. In the 1D case, the

stability interval of the EOS formulation is purely determined by the internal numerical scheme. However for the 3D case, there is another lower limit of the stability interval determined by the integral part of the scheme which leads to the situation where the lower limit of the stability interval is determined by the integral equations, and the upper limit is determined by the internal numerical scheme. We find that the late time instability is highly depended on the features of the scattering materials and specifically, it is directly related to the values of the relative magnetic permeability μ_1 and the relative electric permittivity ε_1. Using this we prove that, for the relative permeability and permittivity in a certain range, the numerical scheme for our EOS formulation of light scattering, works well and is without any late time instabilities. The late time instability is only observed for high relative electric permittivity or high relative magnetic permeability. We also observe that the lower limit of the stability interval for the time step is more sensitive to relative differences in magnetic permeability μ_1 than electric permittivity ε_1 between the inside and outside of the scattering objects.

In section 3 we present the singular integrals that appear in our EOS formulation for light scattering and the techniques we use to reduce their calculation to a singular core, which we calculate exactly, and a regular part which we calculate numerically.

2 Stability

In this section we discuss instabilities showing up at late times when we discretize the EOS formulation for light scattering. Whether or not the late time instability show up, depends on the values of the material parameters defining the problem. The overall method is far to complex for an analytical investigation of the stability to be feasible, but using numerical calculation of the eigenvalues of a linearization of the system of difference equations defining the numerical implementation of the EOS formulation, supplemented by running of the full algorithm, we find that the domain part and the boundary part of the algorithm contribute to the instability separately and in different ways. The focus of this section is to disentangle these two contributions to the instability. For the domain part of the algorithm we use Lax-Wendroff, which is an explicit method. The discrete grid inside the scattering object must, for the EOS formulation of light scattering, support both discrete versions of the partial derivatives, and also discretizations of the integrals defining the boundary update part of the algorithm. For this reason the grid is nonuniform close to the boundary. The discretization of the domain part of the algorithm takes the form of a vector iteration

$$Q^{n+1} = MQ^n, \tag{2.1}$$

where Q is a vector containing the components of the electric field and the magnetic field at all points of the grid with a size $6 \times N_x \times N_y \times N_z$, where N_x, N_y and N_z are the number of grid points in the x, y and z directions. The entries of the matrix M are presented in Appendix A. In order to get a stable numerical solution, as discussed in [1], the largest eigenvalues of the matrix M must have a norm smaller than 1. For the non-uniform grids and the discretizations in [2],

we find that the vector iteration (2.1) is stable if

$$0.005 < \tau < 0.48,$$

where $\tau = c_1 \Delta t / \Delta x$.

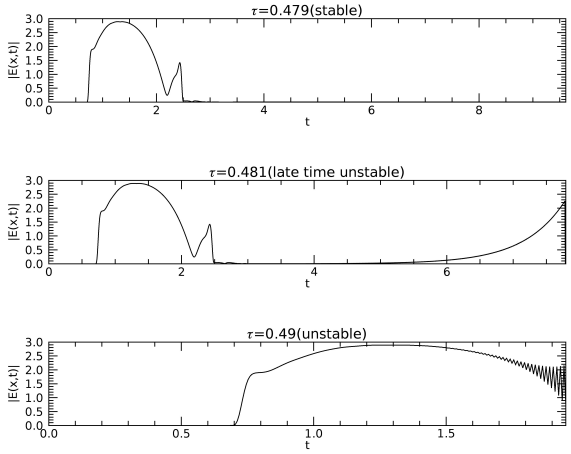

Figure 2.1: Numerical solutions from different values of τ. $\mu_1 = 1.0, \varepsilon_1 = 1.5, \mu_0 = 1.0, \varepsilon_0 = 1.0$.

Figure 2.1 illustrates the intensity of the electric field at a specific point inside the object, as a function of time, for different values of τ. The instability, which in the TBEM literature is called the late time instability, is illustrated in the second panel of figure 2.1. As we mentioned in the introduction in the paper, the term late time instability has been much used in the community that is focused on time dependent boundary element method. We believe that in their domain of application, like antenna theory, the physical parameters are such that the largest eigenvalue for the iteration is always only slightly bigger than 1, like it is in panel two of figure 2.1 . That's why the instability always shows up at late times. In panel three of the figure we are deeper into the unstable domain for τ, and the larges eigenvalue is now so large that it destroys the whole calculation. The late time instability has thus been transformed into an early time instability. Note that the outside source in figure 2.1 is the same as in [2].

In our numerical experiments, we found that the stable range of the EOS formulations is not only restricted by the eigenvalues of the matrix M, but is also restricted by the boundary integral identities through the relative electric permittivity ε_1 and the relative magnetic permeability μ_1. Figure 2.2 shows how the stability depends on the values of ε_1, and figure 2.3 shows how it depends on the values of μ_1. Together, they tell us that increasing the electric permittivity or the magnetic permeability narrows the stable range. Figure 2.3 also tells us that μ_1 and ε_1 don't affect the stability of the full scheme in the same way. It seems that the method is more sensitive to μ_1 than ε_1. After a series of numerical experiments, our conclusion is that, for an explicit numerical method like the one we are using, the lower limit of the stable range of the EOS formulation is restricted by the electric permittivity ε_1 and the magnetic permeability μ_1 while

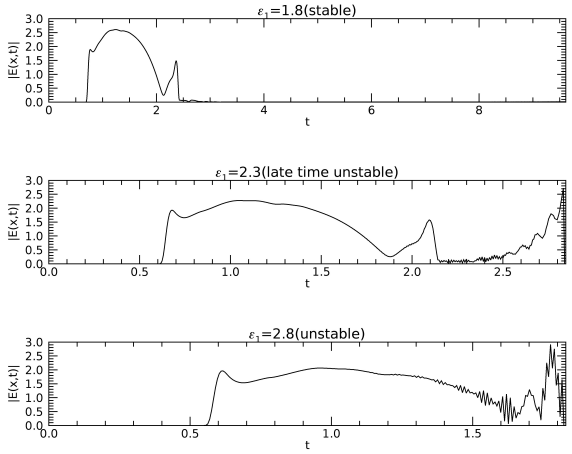

Figure 2.2: Numerical solutions from different values of ε_1. $\tau = 0.45$, $\mu_1 = 1.0, \mu_0 = 1.0, \varepsilon_0 = 1.0$.

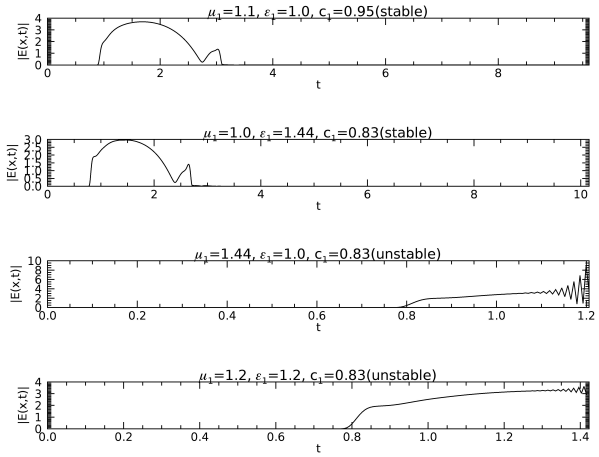

Figure 2.3: Numerical solutions from different values of μ_1. $\tau = 0.45$, $\mu_0 = 1.0, \varepsilon_0 = 1.0$.

the upper limit of the stable range is determined by the inside domain-based method. This conjecture is verified by the following two tests.

2.1 Instabilities coming from the domain-based method

For the first test we consider a homogeneous model without current and charge inside the object which implies $\mu_1 = \mu_0$, $\varepsilon_1 = \varepsilon_0$, $\mathbf{J}_1 = 0$ and $\rho_1 = 0$. Under these assumptions, the electric field and the magnetic field are continuous across the surfaces,

$$\mathbf{E}_- = \mathbf{E}_+,$$
$$\mathbf{B}_- = \mathbf{B}_+,$$

where $\mathbf{E}_{\pm}$and $\mathbf{B}_{\pm}$ are the integral representations of the solutions on the surface by taking the limit from the inside and the outside of the object respectively. The electric field inside the object can be calculated by the outside sources directly

$$\mathbf{E}_1(\mathbf{x},t) = -\partial_t \frac{\mu_0}{4\pi}\int_{V_0} \mathrm{d}V' \frac{\mathbf{J}_0(\mathbf{x}',T)}{|\mathbf{x}'-\mathbf{x}|} - \nabla \frac{1}{4\pi\varepsilon_0}\int_{V_0} \mathrm{d}V' \frac{\rho_0(\mathbf{x}',T)}{|\mathbf{x}'-\mathbf{x}|}, \tag{2.2}$$

where $\mathbf{x} \in V_1$. (2.2) expresses the exact solution for the inside fields. Also from [2] we have the boundary integral identity

$$\mathbf{E}_+(\mathbf{x},t) = -\partial_t \frac{\mu_0}{4\pi}\int_{V_0} \mathrm{d}V' \frac{\mathbf{J}_0(\mathbf{x}',T)}{|\mathbf{x}'-\mathbf{x}|} - \nabla \frac{1}{4\pi\varepsilon_0}\int_{V_0} \mathrm{d}V' \frac{\rho_0(\mathbf{x}',T)}{|\mathbf{x}'-\mathbf{x}|}, \tag{2.3}$$

and

$$\mathbf{B}_+(\mathbf{x},t) = \nabla \times \frac{\mu_0}{4\pi}\int_{V_0} \mathrm{d}V' \frac{\mathbf{J}_0(\mathbf{x}',T)}{|\mathbf{x}'-\mathbf{x}|}, \tag{2.4}$$

for $\mathbf{x} \in S$, $\mathbf{E}_+(\mathbf{x},t)$ and $\mathbf{B}_+(\mathbf{x},t)$ represent the limits by letting $\mathbf{x}$ approach the surface from the inside of the scattering object. On the other hand, [2] gives the integral representations for the inside domain by

$$\begin{aligned}
\mathbf{E}_1(\mathbf{x},t) = \partial_t[&\frac{1}{4\pi}\int_S \mathrm{d}S'\{\frac{1}{c_1|\mathbf{x}'-\mathbf{x}|}(\mathbf{n}'\times\mathbf{E}_+(\mathbf{x}',T))\times\nabla'|\mathbf{x}'-\mathbf{x}| \\
&+ \frac{1}{c_1|\mathbf{x}'-\mathbf{x}|}(\mathbf{n}'\cdot\mathbf{E}_+(\mathbf{x}',T))\nabla'|\mathbf{x}'-\mathbf{x}| + \frac{1}{|\mathbf{x}'-\mathbf{x}|}\mathbf{n}'\times\mathbf{B}_+(\mathbf{x}',T)\}] \\
&- \frac{1}{4\pi}\int_S \mathrm{d}S'\{(\mathbf{n}'\times\mathbf{E}_+(\mathbf{x}',T))\times\nabla'\frac{1}{|\mathbf{x}'-\mathbf{x}|} \\
&+ (\mathbf{n}'\cdot\mathbf{E}_+(\mathbf{x}',T))\nabla'\frac{1}{|\mathbf{x}'-\mathbf{x}|}\}.
\end{aligned} \tag{2.5}$$

Thus the solution for the domain inside the scattering object can now be calculated in three ways. The first is the exact solution expressed by (2.2), the second, Method 2, is the Lax-Wendroff method supplied by the exact boundary values (2.3) and (2.4) , and the third, Method 3, is to calculate the solution using formula (2.5) which expresses the field values inside the scattering object in terms of the values of the fields on the boundary. Note that Method 3 uses the same surface integral expressions as the one that form the boundary part of the full implementation of our EOS formulation of light scattering. Thus, instabilities in the full algorithm originating from the boundary part of the algorithm, should appear as instability in Method 3.

Figure 2.4 compare the solutions calculated in these three ways, where μ_1, ν_1 and τ have been fixed in the stable range. Both Method 2 and Method 3 are stable and give solutions that agree with the exact solution to high accuracy. In Figure 2.5, τ has been set to be 0.49, and is thus is larger than the upper limit of the stable range. The figure shows that Method 2 is now unstable but Method 3 is still stable and equal to the exact solution to high accuracy. The outside source in figure 2.4 and figure 2.5 is as same as in [2] and the values of the parameters are shown under the figure.

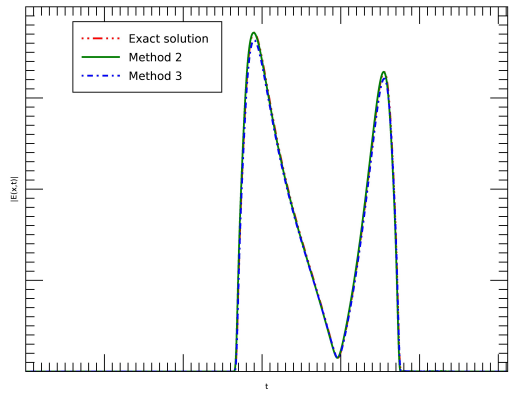

Figure 2.4: Comparison of the intensity of the electric field inside the object at a specific point calculated by three methods. $t_0 = 1.5$, $x_0 = -2.0$, $y_0 = 0.0$, $z_0 = 0.0$, $\tau = 0.45$, $\mu_1 = 1.0$, $\varepsilon_1 = 1.0$, $\mu_0 = 1.0$, $\varepsilon_0 = 1.0$.

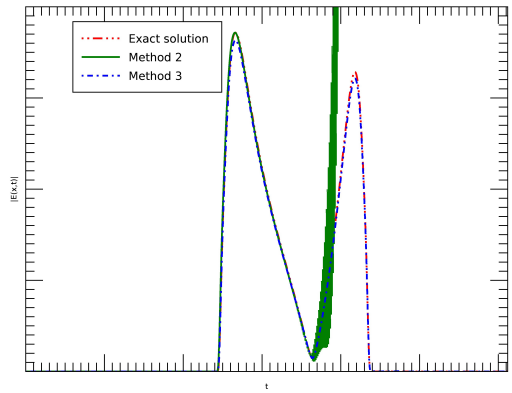

Figure 2.5: Comparison of the intensity of the electric field inside the object at a specific point calculated by three methods. $t_0 = 1.5$, $x_0 = -2.0$, $y_0 = 0.0$, $z_0 = 0.0$, $\tau = 0.49$, $\mu_1 = 1.0$, $\varepsilon_1 = 1.0$, $\mu_0 = 1.0$, $\varepsilon_0 = 1.0$.

2.2 Instabilities coming from the boundary integral identities

In order to investigate the dependence of the stability on μ_1 and ε_1, we set up a test based on the use of artificial sources as in [2]. The idea is to chose functional forms for an electromagnetic field, and then calculate the sources, charge density and current density, needed for making the chosen fields solutions to Maxwell's equations driven by the calculated sources

We now calculate the electromagnetic field inside the scattering object in two

different ways. In Method 1 we use the discretization of the EOS formulation developed in [2], which combines the Lax-Wendroff method for the domain part of the algorithm and our discretization of the integral representations of the boundary fields for the boundary part of the algorithm. Method 2 is to calculate the inside field values by only using the Lax-Wendroff method supplemented by the exact boundary values of the electromagnetic field which are the ones we chose while setting up the artificial sources. Figure 2.6 is the numerical result

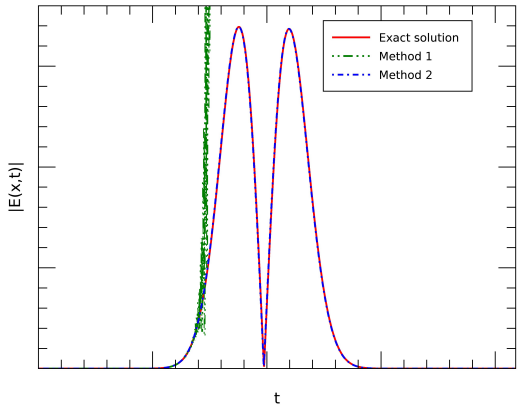

Figure 2.6: Comparison of the intensity of the electric field inside the object at a specific point between the exact solution and the numerical results calculated by two methods. $\tau = 0.45$, $\mu_1 = 1.0$, $\varepsilon_1 = 2.5$, $\mu_0 = 1.0$, $\varepsilon_0 = 1.0$.

where the upper limit of the stable range is kept while the values of μ_1 and ε_1 have been chosen to break the lower limit of the stable range of the EOS formulations. It shows that even though the lower limit of the stable range has been broken, Method 2, which only involves the Lax-Wendroff method works perfectly. 2.5 and 2.6 tell us that the changing of the lower limit does not effect the stability of the Lax-Wendroff method and the changing of upper limit does not effect the stability of the surface integrals. For a general application where the source is located outside the object and there are current density and electric density inside the scattering object, the EOS formulations does have a range for a stable numerical implementation. The upper limit of the range is determined by the Lax-Wendroff method due to the non-uniform grids and the lower limit is determined by the changing μ_1 and ε_1. The setting up of the artificial sources and the values of the parameters in figure 2.6 are the same as the artificial sources in [2]. From figure 2.5 and figure 2.6, we can also see that before the instabilities show up, both the EOS formulations and the Lax-Wendroff method solve the equations accurately.

3 Calculations of the singular integrals

In this section we introduce a technique to accurately calculate integrals with singularities which can be applied for both the singular volume integrals and the

singular surface integrals occurring in the EOS formulations of the 3D Maxwell's equations. Here we illustrate the technique by calculating one type of singular volume integral

$$f_1 = \iiint_{V_{i,j,k}} \frac{1}{|\mathbf{x}' - \mathbf{x}_p|}\,\mathrm{d}V = \iiint_{V_{i,j,k}} \frac{1}{r}\,\mathrm{d}V, \tag{3.1}$$

where the integral domain $V_{i,j,k}$ is adjacent to the surfaces of the scattering object and given by

$$V_{i,j,k} = [x_a, x_a + \Delta x] \times [y_j - \frac{\Delta y}{2}, y_j + \frac{\Delta y}{2}] \times [z_k - \frac{\Delta z}{2}, z_k + \frac{\Delta z}{2}],$$

with surfaces S_m, $m = 1, 2, \cdots, 6$. Here, Δx, Δy and Δz are the grid parameters in x, y and z directions respectively.

The point $\mathbf{x}_p$

$$\mathbf{x}_p = (x_a, y_j, z_k),$$

is centered on one of the surfaces of the scattering object. The geometry is illustrated in figure 3.1, where $\mathbf{n}_m$ is the unit normal vector on surface S_m pointing out of $V_{i,j,k}$.

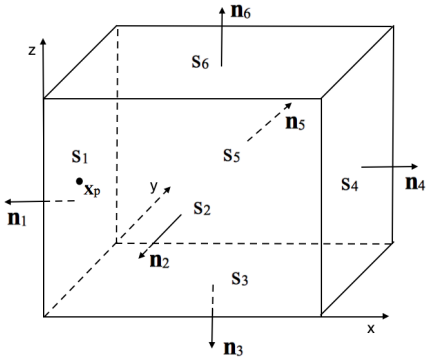

Figure 3.1: The integral domain of the singular integral

The components of the integration variable in (3.1) are given by

$$\mathbf{x}' = (x', y', z'),$$

and let us introduce the quantity

$$\mathbf{r} = \mathbf{x}' - \mathbf{x}_p,$$

with $r = |\mathbf{r}|$.

We want to apply the divergence theorem on (3.1), and therefore need to find a function $\varphi(r)$ that satisfies

$$\nabla \cdot (\mathbf{r}\varphi(r)) = \frac{1}{r},$$

or equivalently

$$3\varphi(r) + r\varphi'(r) = \frac{1}{r}.$$

Solving the above equation, we get

$$\varphi(r) = \frac{1}{2r}.$$

Because of the singularity on S_1, we can not apply the divergence theorem directly, however we can write f_1 as

$$f_1 = \frac{1}{2}(\sum_{m=2}^{6} \iint_{S_m} \frac{1}{r}\mathbf{r}\cdot\mathbf{n}_m \,\mathrm{d}S + \lim_{\epsilon\to 0}\iint_{S_\epsilon} \frac{1}{r}\mathbf{r}\cdot\mathbf{n}_\epsilon \,\mathrm{d}S + \iint_{S_\Omega} \frac{1}{r}\mathbf{r}\cdot\mathbf{n}_1 \,\mathrm{d}S),$$

where S_ϵ is a hemispherical surface of radius ϵ centered at $\mathbf{x}_p$ and S_Ω is the rest of the surface S_1 with a disk of radius ϵ around $\mathbf{x}_p$ has been removed. $\mathbf{n}_\epsilon$ is the unit normal vector on S_ϵ, pointing out of $V_{i,j,k}$. $\mathbf{n}_m$ is the unit normal vector on S_m, pointing out of $V_{i,j,k}$.

For the integral over S_Ω, we have

$$\mathbf{r} = (0, y' - y_j, z' - z_k)$$

and

$$\mathbf{n}_1 = (-1, 0, 0),$$

thus we get

$$\iint_{S_\Omega} \frac{1}{r}\mathbf{r}\cdot\mathbf{n}_1 \,\mathrm{d}S = 0.$$

For the integral over S_ϵ, we use the spherical coordinate system,

$$\mathbf{r} = \epsilon(\cos\theta\sin\varphi, \sin\theta\sin\varphi, \cos\varphi),$$

and

$$\mathbf{n}_\epsilon = (\cos\theta\sin\varphi, \sin\theta\sin\varphi, \cos\varphi),$$

where $\epsilon, \varphi, \theta$ are respectively the radial distance, polar angle and azimuthal angle, so that

$$\begin{aligned}\lim_{\epsilon\to 0}\iint_{S_\epsilon} \frac{1}{r}\mathbf{r}\cdot\mathbf{n}_\epsilon \,\mathrm{d}S &= \lim_{\epsilon\to 0}\frac{1}{\epsilon}\int_0^{2\pi}\int_{-\frac{\pi}{2}}^{\frac{\pi}{2}} \epsilon(\cos\theta\sin\varphi, \sin\theta\sin\varphi, \cos\varphi) \\ &\quad\cdot(\cos\theta\sin\varphi, \sin\theta\sin\varphi, \cos\varphi)\epsilon^2\sin\varphi \,\mathrm{d}\theta\,\mathrm{d}\varphi \\ &= 0.\end{aligned}$$

Defining

$$s_m = \iint_{S_m} \frac{1}{r}\mathbf{r}\cdot\mathbf{n}_m \,\mathrm{d}S,$$

f_1 can be written as

$$f_1 = \frac{1}{2}\sum_{m=2}^{6} s_m. \tag{3.2}$$

(3.2) is not singular any more and can be calculated by 2D Gaussian quadrature. However we will compute f_1 by reducing the surface integral into a line integral, which is also the approach we use to calculate the singular surface integrals appearing in the implementation discussed in this paper.

We first consider the integral over S_2. The geometry is shown in figure 3.2.

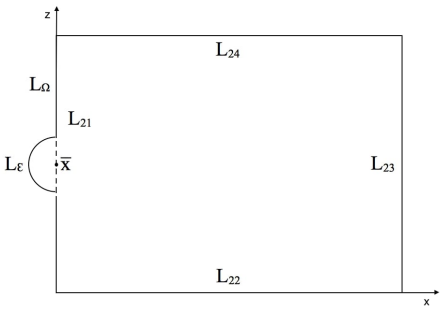

Figure 3.2: Surface S_2

As shown in figure 3.2, the surface S_2 is bounded by the union of four straight lines L_{2n}, $n = 1, 2, 3, 4$. On this surface we have

$$\mathbf{r} = (x' - x_a, \frac{1}{2}\Delta y, z' - z_k)$$

and the unit normal is

$$\mathbf{n}_2 = (0, -1, 0),$$

so that

$$s_2 = \frac{1}{2}\Delta y \iint_{S_2} \frac{1}{\sqrt{(x' - x_a)^2 + \frac{1}{4}\Delta y^2 + (z' - z_k)^2}} \,\mathrm{d}S.$$

The goal is to use the divergence theorem on this surface integral and thereby reduce it to line integrals over the four lines that forms the boundary of S_2. We therefore seek a function $\varphi(\bar{r})$ that satisfies

$$\nabla \cdot (\bar{\mathbf{r}}\varphi(\bar{r})) = \frac{1}{\sqrt{\bar{r}^2 + \frac{1}{4}\Delta y^2}},$$

where $\bar{\mathbf{r}} = (x' - x_a, z' - z_k)$ and $\bar{r} = |\bar{\mathbf{r}}|$. This equation can be rewritten in the form

$$2\varphi(\bar{r}) + r\varphi'(\bar{r}) = \frac{1}{\sqrt{\bar{r}^2 + \frac{1}{4}\Delta y^2}}.$$

Solving the above equation we get

$$\varphi(\bar{r}) = \frac{\sqrt{\bar{r}^2 + \frac{1}{4}\Delta y^2}}{\bar{r}^2}.$$

Using the divergence theorem and taking into account of the singularity at

$$\bar{\mathbf{x}} = (x_a, z_k)$$

on L_{21}, we get

$$s_2 = \frac{1}{2}\Delta y(\sum_{n=2}^{4} \int_{L_{2n}} \varphi(\bar{r})\bar{\mathbf{r}} \cdot \bar{\mathbf{n}}_n \,\mathrm{d}L + \lim_{\epsilon \to 0} \int_{L_\epsilon} \varphi(\bar{r})\bar{\mathbf{r}} \cdot \bar{\mathbf{n}}_\epsilon \,\mathrm{d}L + \int_{L_\Omega} \varphi(\bar{r})\bar{\mathbf{r}} \cdot \bar{\mathbf{n}}_1 \,\mathrm{d}L)$$

where L_ϵ is a semicircle with radius ϵ centered at point $\bar{\mathbf{x}}$ and L_Ω is the rest of L_{21}. Here $\bar{\mathbf{n}}_n$ is the unit normal of L_{2n}, pointing out of S_2, and $\bar{\mathbf{n}}_\epsilon$ is the unit normal of L_ϵ, pointing out of S_2.

For the integral over L_Ω, we have

$$\bar{\mathbf{r}} = (0, z' - z_k),$$

and

$$\bar{\mathbf{n}}_1 = (-1, 0),$$

so that

$$\int_{L_\Omega} \frac{\sqrt{\bar{r}^2 + \frac{1}{4}\Delta y^2}}{\bar{r}^2}(0, z' - z_k) \cdot (-1, 0)\,\mathrm{d}L = 0. \tag{3.3}$$

For the integral over L_ϵ, using the polar coordinates, we have

$$\bar{\mathbf{r}} = \epsilon(\cos\theta, \sin\theta),$$

and

$$\bar{\mathbf{n}}_\epsilon = -(\cos\theta, \sin\theta),$$

so that

$$\begin{aligned}
&\lim_{\epsilon\to 0}\int_{L_\epsilon} \frac{\sqrt{\bar{r}^2 + \frac{1}{4}\Delta y^2}}{\bar{r}^2}\bar{\mathbf{r}} \cdot \bar{\mathbf{n}}_\epsilon\,\mathrm{d}L \\
&= -\lim_{\epsilon\to 0}\int_{-\frac{\pi}{2}}^{\frac{\pi}{2}} \epsilon(\cos\theta, \sin\theta) \cdot (\cos\theta, \sin\theta)\frac{\sqrt{\epsilon^2 + \frac{1}{4}\Delta y^2}}{\epsilon^2}\epsilon\,\mathrm{d}\theta \\
&= -\frac{1}{2}\Delta y\pi.
\end{aligned} \tag{3.4}$$

Summing up (3.3) and (3.4) gives

$$l_{21} = -\frac{1}{2}\Delta y\pi.$$

Thus s_2 is expressed by

$$s_2 = \frac{1}{2}\Delta y \sum_{n=1}^{4} l_{2n},$$

where

$$\begin{aligned}
l_{22} &= \frac{1}{2}\Delta z \int_{x_a}^{x_a+\Delta x} \frac{\sqrt{(x' - x_a)^2 + \frac{1}{4}\Delta y^2 + \frac{1}{4}\Delta z^2}}{(x' - x_a)^2 + \frac{1}{4}\Delta z^2}\,\mathrm{d}x', \\
l_{23} &= \Delta x \int_{z_k - \frac{1}{2}\Delta z}^{z_k + \frac{1}{2}\Delta z} \frac{\sqrt{\Delta x^2 + \frac{1}{4}\Delta y^2 + (z' - z_k)^2}}{\Delta x^2 + (z' - z_k)^2}\,\mathrm{d}z',
\end{aligned}$$

and due to the symmetry of the integrand $\bar{\mathbf{r}}\varphi(\bar{r})$ on xz plane

$$l_{24} = l_{22}.$$

So finally we have

$$s_2 = \frac{1}{2}\Delta y(l_{21} + 2l_{22} + l_{23}).$$

Due to the symmetry of $\mathbf{r}$ in $V_{i,j,k}$ along y direction, we have

$$s_5 = s_2.$$

The calculation of s_3 is similar to the one of s_2 with the final result

$$s_3 = \frac{1}{2}\Delta z(l_{31} + 2l_{32} + l_{33}),$$

where

$$\begin{aligned}
l_{31} &= -\frac{1}{2}\Delta z\pi, \\
l_{32} &= \frac{1}{2}\Delta y \int_{x_a}^{x_a+\Delta x} \frac{\sqrt{(x'-x_a)^2 + \frac{1}{4}\Delta z^2 + \frac{1}{4}\Delta y^2}}{(x'-x_a)^2 + \frac{1}{4}\Delta y^2}\,\mathrm{d}x', \\
l_{33} &= \Delta x \int_{y_j-\frac{1}{2}\Delta y}^{y_j+\frac{1}{2}\Delta y} \frac{\sqrt{\Delta x^2 + \frac{1}{4}\Delta z^2 + (y'-y_j)^2}}{\Delta x^2 + (y'-y_j)^2}\,\mathrm{d}y'.
\end{aligned}$$

Also due to the symmetry of $\mathbf{r}$ in $V_{i,j,k}$ along z direction, we have

$$s_6 = s_3.$$

The only surface integral remaining to be calculated is the one over S_4. On this surface we have

$$\mathbf{r} = (\Delta x, y' - y_j, z' - z_k),$$

and

$$\mathbf{n}_4 = (1, 0, 0),$$

so that

$$s_4 = \Delta x \iint_{S_4} \frac{1}{\sqrt{\Delta x^2 + (y'-y_j)^2 + (z'-z_k)^2}}\,\mathrm{d}S.$$

Defining

$$\bar{\mathbf{r}} = (y' - y_j, z' - z_k)$$

and

$$\bar{r} = |\bar{\mathbf{r}}|,$$

we seek a function $\varphi(\bar{r})$ that satisfies

$$\nabla \cdot (\bar{\mathbf{r}}\varphi(\bar{r})) = \frac{1}{\sqrt{\bar{r}^2 + \Delta x^2}}.$$

This equation can be written in the form

$$2\varphi(\bar{r}) + \bar{r}\varphi'(\bar{r}) = \frac{1}{\sqrt{\bar{r}^2 + \Delta x^2}}.$$

Solving the above equation gives

$$\varphi(\bar{r}) = \frac{\sqrt{\bar{r}^2 + \Delta x^2}}{\bar{r}^2}.$$

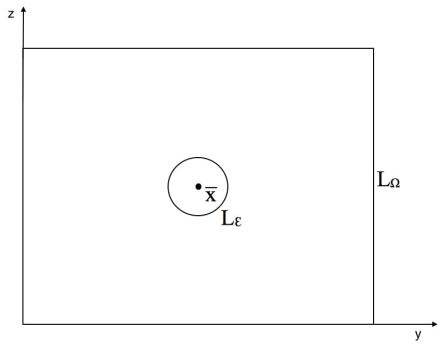

Figure 3.3: Surface S_4

Applying the divergence theorem, we have

$$s_4 = \Delta x \lim_{\epsilon \to 0} \int_{L_\epsilon} \frac{\sqrt{\bar{r}^2 + \Delta x^2}}{\bar{r}^2} \bar{\mathbf{r}} \cdot \bar{\mathbf{n}}_\epsilon \, \mathrm{d}L + \Delta x \int_{L_\Omega} \frac{\sqrt{\bar{r}^2 + \Delta x^2}}{\bar{r}^2} \bar{\mathbf{r}} \cdot \bar{\mathbf{n}}_\Omega \, \mathrm{d}L,$$

where L_ϵ is a circle with radius ϵ centered at point $\bar{\mathbf{x}} = (y_j, z_k)$, and L_Ω is the four edges of surface S_4. $\bar{\mathbf{n}}_\epsilon$ is the unit normal vector of L_ϵ and $\bar{\mathbf{n}}_\Omega$ is the unit normal vector of L_Ω, as shown in figure 3.3.

For the integral over L_ϵ, we write

$$\bar{\mathbf{r}} = \epsilon(\cos\theta, \sin\theta),$$

and

$$\bar{\mathbf{n}}_\epsilon = -(\cos\theta, \sin\theta),$$

then

$$\begin{aligned} &\lim_{\epsilon \to 0} \int_{L_\epsilon} \frac{\sqrt{\bar{r}^2 + \Delta x^2}}{\bar{r}^2} \bar{\mathbf{r}} \cdot \bar{\mathbf{n}}_\epsilon \, \mathrm{d}L \\ &= -\lim_{\epsilon \to 0} \int_0^{2\pi} \epsilon(\cos\theta, \sin\theta) \cdot (\cos\theta, \sin\theta) \frac{\sqrt{\epsilon^2 + \Delta x^2}}{\epsilon^2} \epsilon \, \mathrm{d}\theta \\ &= -2\Delta x \pi. \end{aligned} \tag{3.5}$$

For the integral over L_Ω, there is no singularity anymore and this leads to

$$\begin{aligned} &\int_{l_\Omega} \frac{\sqrt{\bar{r}^2 + \Delta x^2}}{\bar{r}^2} \bar{\mathbf{r}} \cdot \bar{\mathbf{n}}_\Omega \, \mathrm{d}L \\ &= 2l_{41} + 2l_{42}, \end{aligned} \tag{3.6}$$

with

$$l_{41} = \frac{1}{2}\Delta y \int_{z_k - \Delta z}^{z_k + \Delta z} \frac{\sqrt{\Delta x^2 + \frac{1}{4}\Delta y^2 + (z' - z_k)^2}}{\frac{1}{4}\Delta y^2 + (z' - z_k)^2} \, \mathrm{d}z',$$

and

$$l_{42} = \Delta z \int_{y_j - \Delta y}^{y_j + \Delta y} \frac{\sqrt{\Delta x^2 + \frac{1}{4}\Delta z^2 + (y' - y_j)^2}}{\frac{1}{4}\Delta z^2 + (y' - y_j)^2} \, \mathrm{d}y'.$$

Summing up (3.5) and (3.6), we obtain,

$$s_4 = 2\Delta x(l_{41} + l_{42} - \pi\Delta x).$$

We then finally get the following expression for f_1

$$f_1 = \frac{\Delta y}{2}(l_{21} + 2l_{22} + l_{23}) + \frac{\Delta z}{2}(l_{31} + 2l_{32} + l_{33}) + \Delta x(l_{41} + l_{42} - \pi\Delta x).$$

All the line integrals l_{21} etc are non-singular and can be calculated accurately using numerical integration.

4 Summary

In this paper we have, by considering 3D light scattering, discussed some important issues that we believe will be generic for numerical implementations of the EOS formulation for wave scattering. We have shown that the numerical instabilities can be thought as arising separately from the domain part and the boundary update part of the algorithm. We have argued that the instability arising from the boundary part of the algorithm is strongly related to the late time instability noted earlier while solving antenna problems using TBEM. We find that our version of the late time instability can be completely removed by suitably chosen material values, in particular the jump in material values at the boundary of the scattering object should not be too severe. In the limit where the material parameters simulate the properties of highly conductive metallic surfaces, we observe that our version of the late time instability is always present. Thus the instability interval vanishes in this limit. We take this as an indicator that for situations like in antenna theory, the late time instability should always be present, which it is. We are now aware of work where it has been noted that the instability can be removed by manipulating the material parameters defining the scattering objects. The EOS formulation gives thus different window into the late time instability that might be useful.

We have in our discretization used explicit methods. It would not be easy, but we believe that it is possible to do a fully implicit method for the EOS formulation, such an approach might remove all instabilities, which is the ultimate goal both for TBEM and for our EOS formulation.

In this paper we have also discussed how to calculate singular volume and surface integrals for light scattering. The reason for including this discussion is that we think the type of singular integrals we discuss are generic for the singular integrals that will arise while calculating wave scattering using the EOS approach.

Appendices

A Matrix elements

In this section we detail the entries of the updating matrix M in (2.1) where Q is a vector containing the components of the electric field and the magnetic

field at all points of the grid with a size $6 \times N_x \times N_y \times N_z$, where N_x, N_y and N_z are the number of grid points in the x, y and z directions. To simplify the writing, we denote

$$\begin{aligned}
\Lambda_1 &= N_x \times N_y \times N_z, \\
\Lambda_2 &= N_y \times N_z, \\
\Lambda_3 &= 6\Lambda_1, \\
\Gamma_1 &= \Lambda_2 i + N_z j + k, \\
\Gamma_2 &= \Lambda_1 + \Gamma_1, \\
\Gamma_3 &= 2\Lambda_1 + \Gamma_1, \\
\Gamma_4 &= 3\Lambda_1 + \Gamma_1, \\
\Gamma_5 &= 4\Lambda_1 + \Gamma_1, \\
\Gamma_6 &= 5\Lambda_1 + \Gamma_1.
\end{aligned}$$

Thus Q is expressed by

$$Q = \begin{pmatrix} [e_{1,i,j,k}]_{\Lambda_1} \\ [e_{2,i,j,k}]_{\Lambda_1} \\ [e_{3,i,j,k}]_{\Lambda_1} \\ [b_{1,i,j,k}]_{\Lambda_1} \\ [b_{2,i,j,k}]_{\Lambda_1} \\ [b_{3,i,j,k}]_{\Lambda_1} \end{pmatrix}^{n+1} = \begin{pmatrix} [Q_{\Gamma_1}]_{\Lambda_1} \\ [Q_{\Gamma_2}]_{\Lambda_1} \\ [Q_{\Gamma_3}]_{\Lambda_1} \\ [Q_{\Gamma_4}]_{\Lambda_1} \\ [Q_{\Gamma_5}]_{\Lambda_1} \\ [Q_{\Gamma_6}]_{\Lambda_1} \end{pmatrix}^{n+1},$$

where $[e_{1,i,j,k}]_{\Lambda_1}$ represents the vector containing the components of the electric field e_1 at all points of the grid indexing in k, j, i order. $[e_{2,i,j,k}]_{\Lambda_1}$ and so on follow the same rule. Due to the complexity of the matrix, here we only illustrate the entries of the rows of M corresponding to the components $Q_{\Gamma_1}^{n+1}$. Other entries of the matrix can be expressed in the same way.

After applying the Lax-Wendroff method, we have

$$\begin{aligned}
e_{1,i,j,k}^{n+1} = e_{1,i,j,k}^{n} &+ w_1(e_{1,i,j,k}^{n})_{yy} + w_1(e_{1,i,j,k}^{n})_{zz} - w_1(e_{2,i,j,k}^{n})_{xy} \\
&- w_1(e_{3,i,j,k}^{n})_{xz} + w_2(b_{3,i,j,k}^{n})_{y} - w_2(b_{2,i,j,k}^{n})_{z}, \\
&\Downarrow \\
Q_{\Gamma_1}^{n+1} = Q_{\Gamma_1} &+ w_1(Q_{\Gamma_1})_{yy} + w_1(Q_{\Gamma_1})_{zz} - w_1(Q_{\Gamma_2})_{xy} \\
&- w_1(Q_{\Gamma_3})_{xz} + w_2(Q_{\Gamma_6})_{y} - w_2(Q_{\Gamma_5})_{z},
\end{aligned} \tag{A.1}$$

where

$$\begin{aligned}
w_1 &= \frac{c^2 \Delta t^2}{2}, \\
w_2 &= c^2 \Delta t.
\end{aligned}$$

The coefficients of the right side of the equation (A.1) are corresponding to the Γ_1-th row of the matrix M and the values of them are depended on the values of i, j and k. In order to have a compact and uniform expressions, we write

$$
\begin{aligned}
(Q_{\Gamma_6})_y &= \frac{1}{\Delta y}(\xi_{-2}Q_{\kappa_{-2}} + \xi_{-1}Q_{\kappa_{-1}} + \xi Q_{\kappa} + \xi_1 Q_{\kappa_1} + \xi_2 Q_{\kappa_2}),\\
(Q_{\Gamma_1})_{yy} &= \frac{1}{(\Delta y)^2}(\delta_{-2}Q_{\chi_{-2}} + \delta_{-1}Q_{\chi_{-1}} + \delta Q_{\Gamma_1} + \delta_1 Q_{\chi_1} + \delta_2 Q_{\chi_2}),\\
(Q_{\Gamma_2})_{xy} &= \frac{1}{3\Delta x\Delta y}(\omega_{-4}Q_{\Upsilon_{-4}} + \omega_{-3}Q_{\Upsilon_{-3}} + \omega_{-2}Q_{\Upsilon_{-2}} + \omega_{-1}Q_{\Upsilon_{-1}} + \omega Q_{\Upsilon}\\
&\quad + \omega_1 Q_{\Upsilon_1} + \omega_2 Q_{\Upsilon_2} + \omega_3 Q_{\Upsilon_3} + \omega_4 Q_{\Upsilon_4}),
\end{aligned}
$$

where

$$
\begin{aligned}
&\chi_1 = \Gamma_1 + N_z, && \chi_2 = \Gamma_1 + 2N_z, && \chi_{-1} = \Gamma_1 - N_z,\\
&\chi_{-2} = \Gamma_1 - 2N_z, && \kappa = \Gamma_6, && \kappa_1 = \Gamma_6 + N_z,\\
&\kappa_2 = \Gamma_6 + 2N_z, && \kappa_{-1} = \Gamma_6 - N_z, && \kappa_{-2} = \Gamma_6 - 2N_z,\\
&\eta = N_y, && \Upsilon = \Gamma_2, && \Upsilon_{-4} = \Gamma_2 - \Lambda_2 - N_z,\\
&\Upsilon_{-3} = \Gamma_2 - \Lambda_2, && \Upsilon_{-2} = \Gamma_2 - \Lambda_2 + N_z, && \Upsilon_{-1} = \Gamma_2 - N_z,\\
&\Upsilon_1 = \Gamma_2 + N_z, && \Upsilon_2 = \Gamma_2 + \Lambda_2 - N_z, && \Upsilon_3 = \Gamma_2 + \Lambda_2,\\
&\Upsilon_4 = \Gamma_2 + \Lambda_2 + N_z.
\end{aligned}
$$

The expressions for $(Q_{\Gamma_5})_z$, $(Q_{\Gamma_1})_{zz}$ and $(Q_{\Gamma_3})_{xz}$ have the same forms as $(Q_{\Gamma_6})_y$, $(Q_{\Gamma_1})_{yy}$ and $(Q_{\Gamma_2})_{xy}$ respectively, but with

$$
\begin{aligned}
&\chi_1 = \Gamma_1 + 1, && \chi_2 = \Gamma_1 + 2, && \chi_{-1} = \Gamma_1 - 1,\\
&\chi_{-2} = \Gamma_1 - 2, && \kappa = \Gamma_5, && \kappa_1 = \Gamma_5 + 1,\\
&\kappa_2 = \Gamma_5 + 2, && \kappa_{-1} = \Gamma_5 - 1, && \kappa_{-2} = \Gamma_5 - 2,\\
&\eta = N_z, && \Upsilon = \Gamma_3, && \Upsilon_{-4} = \Gamma_3 - \Lambda_2 - 1,\\
&\Upsilon_{-3} = \Gamma_3 - \Lambda_2, && \Upsilon_{-2} = \Gamma_3 - \Lambda_2 + 1, && \Upsilon_{-1} = \Gamma_3 - 1,\\
&\Upsilon_1 = \Gamma_3 + 1, && \Upsilon_2 = \Gamma_3 + \Lambda_2 - 1, && \Upsilon_3 = \Gamma_3 + \Lambda_2,\\
&\Upsilon_4 = \Gamma_3 + \Lambda_2 + 1.
\end{aligned}
$$

After discussing the locations of i, j and k, the values of the coefficients are listed in table 1 and table 2.

Table 1: $(\frac{\partial}{\partial y}, \frac{\partial^2}{\partial y^2})$ or $(\frac{\partial}{\partial z}, \frac{\partial^2}{\partial z^2})$ related coefficients

j or k	δ_{-2}	δ_{-1}	δ	δ_1	δ_2	ξ_{-2}	ξ_{-1}	ξ	ξ_1	ξ_2
0	0	0	-5	2	-1/5	0	0	1/2	2/3	-1/10
η-1	-1/5	2	-5	0	0	1/10	-2/3	-1/2	0	0
[1,η-2]	0	1	-2	1	0	0	-1/2	0	1/2	0

For example, if $i = 0$, $j = 0$ and $k = 0$, the entries of the Γ_1-th row of the

Table 2: $\frac{\partial^2}{\partial x \partial y}$ or $\frac{\partial^2}{\partial x \partial z}$ related coefficients

i	j or k	ω_{-4}	ω_{-3}	ω_{-2}	ω_{-1}	ω	ω_1	ω_2	ω_3	ω_4
0	0	0	0	0	0	9	-5	0	-5	1
	η-1	0	0	0	5	-9	0	-1	5	0
	$[1,\frac{\eta}{2})$	0	0	0	0	3	-3	1	-1	0
	$[\frac{\eta}{2},\eta-2]$	0	0	0	3	-3	0	0	1	-1
N_x-1	0	0	5	-1	0	- 9	5	0	0	0
	η-1	1	-5	0	-5	9	0	0	0	0
	$[1,\frac{\eta}{2})$	-1	1	0	0	- 3	3	0	0	0
	$[\frac{\eta}{2},\eta-2]$	0	-1	1	-3	3	0	0	0	0
[1,N_x-3]	0	0	0	1	0	3	-1	0	-3	0
	η-1	-1	0	0	1	-3	0	0	3	0
	$[1,\eta-2]$	-3/4	0	3/4	0	0	0	3/4	0	-3/4
N_x-2	0	0	3	0	0	-3	1	0	0	-1
	η-1	0	-3	0	-1	3	0	1	0	0
	[1,η-2]	-3/4	0	3/4	0	0	0	3/4	0	-3/4

matrix M are the following

$$
\begin{aligned}
&M_{\Gamma_1,\Gamma_1} = 1 - 5u_1 - 5v_1, && M_{\Gamma_1,\Gamma_1+N_z} = 2u_1, && M_{\Gamma_1,\Gamma_1+2N_z} = -\frac{1}{5}u_1,\\
&M_{\Gamma_1,\Gamma_6} = \frac{1}{2}u_2, && M_{\Gamma_1,\Gamma_6+N_z} = \frac{2}{3}u_2, && M_{\Gamma_1,\Gamma_6+2N_z} = -\frac{1}{10}u_2,\\
&M_{\Gamma_1,\Gamma_2} = 9u_3, && M_{\Gamma_1,\Gamma_2+N_z} = -5u_3, && M_{\Gamma_1,\Gamma_2+\Lambda_2} = -5u_3,\\
&M_{\Gamma_1,\Gamma_2+\Lambda_2+N_z} = u_3, && M_{\Gamma_1,\Gamma_1+1} = 2v_1, && M_{\Gamma_1,\Gamma_1+2} = -\frac{1}{5}v_1,\\
&M_{\Gamma_1,\Gamma_5} = \frac{1}{2}v_2, && M_{\Gamma_1,\Gamma_5+1} = \frac{2}{3}v_2, && M_{\Gamma_1,\Gamma_5+2} = -\frac{1}{10}v_2,\\
&M_{\Gamma_1,\Gamma_3} = 9v_3, && M_{\Gamma_1,\Gamma_3+1} = -5v_3, && M_{\Gamma_1,\Gamma_3+\Lambda_2} = -5v_3,\\
&M_{\Gamma_1,\Gamma_3+\Lambda_2+1} = v_3,
\end{aligned}
$$

otherwise $M_{\Gamma_1,*} = 0$ and where

$$
\begin{aligned}
&u_1 = \frac{w_1}{(\Delta y)^2}, && u_2 = \frac{w_2}{\Delta y}, && u_3 = \frac{w_1}{3\Delta x \Delta y},\\
&v_1 = \frac{w_1}{(\Delta z)^2}, && v_2 = \frac{w_2}{\Delta z}, && v_3 = \frac{w_1}{3\Delta x \Delta z}.
\end{aligned}
$$

B Singular integrals

In this section, we detail the calculations of other types of singular integrals involved in the EOS formulations of 3D Maxwell's equations, denoted by $\mathbf{f}_2$, $\mathbf{f}_3$, g_1, $\mathbf{g}_2$, $\mathbf{g}_3$ in [2]. The techniques are similar with the calculating of f_1 in section 3. The geometry is illustrated in figure 3.1.

B.1 Calculation of $\mathbf{f}_2$

$$\mathbf{f}_2 = \iiint_{V_{i,j,k}} \frac{\mathbf{x}' - \mathbf{x}_p}{|\mathbf{x}' - \mathbf{x}_p|^2} \, \mathrm{d}V. \tag{B.1}$$

The components of the integration variable in (B.1) are given by

$$\mathbf{x}' = (x', y', z'),$$

and let us introduce the quantity

$$\mathbf{r} = \mathbf{x}' - \mathbf{x}_p,$$

with $r = |\mathbf{r}|$.

We want to apply the divergence theorem on (B.1), and therefore need to find a function $\varphi(r)$ that satisfies

$$\nabla \cdot (\mathbf{rr}\varphi(r)) = \frac{\mathbf{r}}{r^2},$$

or equivalently

$$\nabla \cdot (\mathbf{rr})\varphi(r) + \mathbf{rr} \cdot \nabla\varphi(r) = \frac{\mathbf{r}}{r^2}.$$

Solving the above equation, we get

$$\varphi(r) = \frac{1}{2r^2}.$$

Because of the singularity on surface S_1, we can not apply the divergence theorem directly. However we can write

$$\mathbf{f}_2 = \frac{1}{2}\Big(\sum_{m=2}^{6} \iint_{S_m} \frac{\mathbf{rr}}{r^2} \cdot \mathbf{n}_m \, \mathrm{d}S + \lim_{\epsilon \to 0} \iint_{S_\epsilon} \frac{\mathbf{rr}}{r^2} \cdot \mathbf{n}_\epsilon \, \mathrm{d}S + \iint_{S_\Omega} \frac{\mathbf{rr}}{r^2} \cdot \mathbf{n}_1 \, \mathrm{d}S\Big),$$

where S_ϵ is a hemispherical surface of radius ϵ centered at $\mathbf{x}_p$ and S_Ω is the rest of the surface S_1 with a disk of radius ϵ around $\mathbf{x}_p$ has been removed. $\mathbf{n}_\epsilon$ is the unit normal vector on S_ϵ, pointing out of $V_{i,j,k}$. $\mathbf{n}_m$ is the unit normal vector on S_m, pointing out of $V_{i,j,k}$.

For the integral over S_Ω, we have

$$\mathbf{r} = (0, y' - y_j, z' - z_k),$$

and

$$\mathbf{n}_1 = (-1, 0, 0),$$

thus we get

$$\iint_{S_\Omega} \frac{\mathbf{rr}}{r^2} \cdot \mathbf{n} \, \mathrm{d}S = (0, 0, 0).$$

For the integral over surface S_ϵ, we use the spherical coordinate system,

$$\mathbf{r} = \epsilon(\cos\theta \sin\varphi, \sin\theta \sin\varphi, \cos\varphi),$$

and

$$\mathbf{n}_\epsilon = (\cos\theta \sin\varphi, \sin\theta \sin\varphi, \cos\varphi),$$

where $\epsilon, \varphi, \theta$ are respectively the radial distance, polar angle and azimuthal angle, so that

$$\begin{aligned}\iint_{S_\epsilon} \frac{1}{r^2}\mathbf{r}\mathbf{r}\cdot\mathbf{n}_\epsilon \,\mathrm{d}S = \lim_{\epsilon\to 0}\frac{1}{\epsilon^2}\int_0^{2\pi}\int_{-\frac{\pi}{2}}^{\frac{\pi}{2}} &\epsilon(\cos\theta\sin\varphi, \sin\theta\sin\varphi, \cos\varphi)\\ &\epsilon(\cos\theta\sin\varphi, \sin\theta\sin\varphi, \cos\varphi)\\ &\cdot(\cos\theta\sin\varphi, \sin\theta\sin\varphi, \cos\varphi)\\ &\epsilon^2\sin\varphi\,\mathrm{d}\theta\,\mathrm{d}\varphi = (0,0,0).\end{aligned}$$

Defining

$$s_m = \iint_{S_m} \frac{\mathbf{r}\mathbf{r}}{r^2}\cdot\mathbf{n}_m\,\mathrm{d}S,$$

f_2 can be written as

$$\mathbf{f}_2 = \frac{1}{2}\sum_{m=2}^{6} s_m.$$

Due to the symmetry of $\mathbf{r}$ along y and z directions in $V_{i,j,k}$, we have

$$s_5 = s_2$$

and

$$s_6 = s_3.$$

Thus f_2 can be written as,

$$\begin{aligned}\mathbf{f}_2 = \frac{1}{2}\Big(&\iint_{S_2}\Delta y\frac{(x'-x_a, 0, z'-z_k)}{(x'-x_a)^2+(z'-z_k)^2+\frac{1}{4}\Delta y^2}\,\mathrm{d}x'\,\mathrm{d}z'\\ &+\iint_{S_3}\Delta z\frac{(x'-x_a, y'-y_j, 0)}{(x'-x_a)^2+(y'-y_j)^2+\frac{1}{4}\Delta z^2}\,\mathrm{d}x'\,\mathrm{d}y'\\ &+\iint_{S_4}\Delta x^2\frac{(1,0,0)}{\Delta x^2+(y'-y_j)^2+(z'-z_k)^2}\,\mathrm{d}y'\,\mathrm{d}z'\Big).\end{aligned}$$

For computation simplicity, we define

$$\bar{s}_2 = \iint_{S_2}\frac{(x'-x_a, z'-z_k)}{(x'-x)^2+(z'-z_k)^2+\frac{1}{4}\Delta y^2}\,\mathrm{d}x'\,\mathrm{d}z',$$

$$\bar{s}_3 = \iint_{S_3}\frac{(x'-x_a, y'-y_j)}{(x'-x_a)^2+(y'-y_j)^2+\frac{1}{4}\Delta z^2}\,\mathrm{d}x'\,\mathrm{d}y',$$

$$\bar{s}_4 = \iint_{S_4} x^2\frac{1}{\Delta x^2+(y'-y_j)^2+(z'-z_k)^2}\,\mathrm{d}y'\,\mathrm{d}z'.$$

Thus for the calculations of $\bar{s}_2$ and $\bar{s}_3$, we consider a general form

$$\iint_S \frac{\bar{\mathbf{r}}}{\bar{r}^2+A^2}\,\mathrm{d}S, \tag{B.2}$$

where A is a constant, $\bar{\mathbf{r}}$ is a 2-component vector on surface S, and $\bar{r} = |\bar{\mathbf{r}}|$. We want to apply the divergence theorem on (B.2), therefore we need to find a function $\varphi(\bar{r})$ that satisfies

$$\nabla \cdot (\bar{\mathbf{r}}\bar{\mathbf{r}}\varphi(\bar{r})) = \frac{\bar{\mathbf{r}}}{\bar{r}^2 + A^2}.$$

Solving the above equation, we get

$$\varphi(\bar{r}) = -\frac{A\tan^{-1}(\frac{\bar{r}}{A})}{\bar{r}^3} + \frac{1}{\bar{r}^2}.$$

For $\bar{s}_2$,

$$S = S_2,$$
$$A = \frac{1}{2}\Delta y,$$

and

$$\bar{\mathbf{r}} = (x' - x_a, z' - z_k),$$

and because of the singularity on S_2, we can not use the divergence theorem directly, however we can write

$$\bar{s}_2 = \sum_{n=2}^{4} \int_{L_{2n}} \varphi(\bar{r})\bar{\mathbf{r}}\bar{\mathbf{r}} \cdot \bar{\mathbf{n}}_n \, \mathrm{d}L + \lim_{\epsilon \to 0} \int_{L_\epsilon} \varphi(\bar{r})\bar{\mathbf{r}}\bar{\mathbf{r}} \cdot \bar{\mathbf{n}}_\epsilon \, \mathrm{d}L + \int_{L_\Omega} \varphi(\bar{r})\bar{\mathbf{r}}\bar{\mathbf{r}} \cdot \bar{\mathbf{n}}_1 \, \mathrm{d}L,$$

where L_{2n} are edges of S_2. L_ϵ is a semicircle with radius ϵ centered at point $\bar{\mathbf{x}}$ and L_Ω is the rest of L_{21}. $\bar{\mathbf{n}}_\epsilon$ is the unit normal of L_ϵ, pointing out of S_2. $\bar{\mathbf{n}}_n$ is the unit normal of L_{2n}, pointing out of S_2. Geometry is illustrated in figure 3.2.

For the integral over L_Ω, we have

$$\bar{\mathbf{r}} = (0, z' - z_k)$$

and

$$\bar{\mathbf{n}}_1 = (-1, 0),$$

so that

$$\int_{L_\Omega} \varphi(\bar{r})\bar{\mathbf{r}}\bar{\mathbf{r}} \cdot \bar{\mathbf{n}}_1 \, \mathrm{d}L = (0, 0).$$

For the integral over L_ϵ, using the polar coordinates, we have

$$\mathbf{r} = \epsilon(\cos\theta, \sin\theta),$$

and

$$\mathbf{n}_\epsilon = -(\cos\theta, \sin\theta),$$

so that

$$\begin{aligned}\int_{L_\epsilon} \varphi(\bar{r})\bar{\mathbf{r}}\bar{\mathbf{r}} \cdot \bar{\mathbf{n}}_\epsilon \, \mathrm{d}L = &- \lim_{\epsilon \to 0} \int_{-\frac{\pi}{2}}^{\frac{\pi}{2}} -\epsilon^3(\cos\theta, \sin\theta)(\cos\theta, \sin\theta) \\ &(-\frac{\frac{1}{2}\Delta y \tan^{-1}(\frac{\epsilon}{\frac{1}{2}\Delta y})}{\epsilon^3} + \frac{1}{\epsilon^2}) \cdot (\cos\theta, \sin\theta) \, \mathrm{d}\theta \\ &= (0, 0).\end{aligned}$$

There is no singularity on L_{22}, L_{23} and L_{24}, finally,

$$\bar{s}_2 = (I_1, 0),$$

where

$$I_1 = \int_{x_a}^{x_a+\Delta x} \Delta z(x' - x_a)\varphi(r_1)\,\mathrm{d}x' + \int_{z_k-\Delta z}^{z_k+\Delta z} \Delta x^2 \varphi(r_2)\,\mathrm{d}z',$$

with

$$r_1 = \sqrt{(x' - x_a)^2 + \frac{1}{4}\Delta z^2},$$

and

$$r_2 = \sqrt{\Delta x^2 + (z' - z_k)^2}.$$

The calculation of $\bar{s}_3$ is similar to the one of $\bar{s}_2$ with the final result

$$\bar{s}_3 = (I_2, 0),$$

where

$$I_2 = \int_{x_a}^{x_a+\Delta x} \Delta y(x' - x_a)\varphi(r_3)\,\mathrm{d}x' + \int_{y_j-\Delta y}^{y_j+\Delta y} \Delta x^2 \varphi(r_4)\,\mathrm{d}y',$$

with

$$r_3 = \sqrt{(x' - x_a)^2 + \frac{1}{4}\Delta y^2},$$

and

$$r_4 = \sqrt{\Delta x^2 + (y' - y_j)^2}.$$

For the integral $\bar{s}_4$, defining

$$\bar{\mathbf{r}} = (y' - y_j, z' - z_k),$$

and

$$\bar{r} = |\bar{\mathbf{r}}|,$$

we need to find a function $\varphi(\bar{r})$ that satisfies

$$\nabla \cdot (\bar{\mathbf{r}}\varphi(\bar{r})) = \frac{1}{\bar{r}^2 + \Delta x^2}.$$

Solving the above equation gives

$$\varphi(\bar{r}) = \frac{\ln(\bar{r}^2 + \Delta x^2)}{2\bar{r}^2}.$$

Because of the singularity at point $\bar{\mathbf{x}} = (y_j, z_k)$, we write

$$\bar{s}_4 = \lim_{\epsilon \to 0} \int_{L_\epsilon} \varphi(\bar{r})\bar{\mathbf{r}} \cdot \bar{\mathbf{n}}_\epsilon \,\mathrm{d}L + \int_{L_\Omega} \varphi(\bar{r})\bar{\mathbf{r}} \cdot \bar{\mathbf{n}}_\Omega \,\mathrm{d}L,$$

where L_ϵ is a circle with radius ϵ centered at $\bar{\mathbf{x}}$ and L_Ω is the four edges of surface S_4. $\bar{\mathbf{n}}_\epsilon$ is the unit normal vector of L_ϵ, $\bar{\mathbf{n}}_\Omega$ is the unit normal vector of L_Ω, as shown in figure 3.3.

For the integral over L_ϵ, we use the polar coordinates,

$$\bar{\mathbf{r}} = \epsilon(\cos\theta, \sin\theta),$$

and

$$\mathbf{n}_\epsilon = -(\cos\theta, \sin\theta),$$

then

$$\begin{aligned}\lim_{\epsilon\to 0}\int_{L_\epsilon} \varphi(\bar{r})\bar{\mathbf{r}}\cdot\bar{\mathbf{n}}_\epsilon \,\mathrm{d}L &= \lim_{\epsilon\to 0}\int_0^{2\pi} -\epsilon^2(\cos\theta,\sin\theta)\frac{\ln(\epsilon^2+\Delta x^2)}{2\epsilon^2}(\cos\theta,\sin\theta)\,\mathrm{d}\theta \\ &= -\pi\ln(\Delta x^2).\end{aligned}$$

For the integral over L_Ω, there is no singularity any more and this leads to

$$\begin{aligned}\int_{l_\Omega} \varphi(\bar{r})\bar{\mathbf{r}}\cdot\bar{\mathbf{n}}_\Omega \,\mathrm{d}L &= \frac{1}{2}\Delta y\int_{z_k-\Delta z}^{z_k+\Delta z}\frac{\ln(\frac{1}{4}\Delta y^2+\Delta x^2+(z'-z_k)^2)}{\frac{1}{4}\Delta y^2+(z'-z_k)^2}\,\mathrm{d}z' \\ &\quad+\frac{1}{2}\Delta z\int_{y_j-\Delta y}^{y_j+\Delta y}\frac{\ln(\frac{1}{4}\Delta z^2+\Delta x^2+(y'-y_j)^2)}{\frac{1}{4}\Delta z^2+(y'-y_j)^2}\,\mathrm{d}y' \\ &= I_3.\end{aligned}$$

Combining all the above calculations, we finally get,

$$\mathbf{f}_2 = \frac{1}{2}(\Delta y I_1 + \Delta z I_2 + \Delta x^2(I_3 - \pi\ln(\Delta x^2)), 0, 0).$$

All the line integrals I_1, I_2, I_3 are non-singular and can be calculated using numerical integration.

B.2 Calculation of $\mathbf{f}_3$

$$\mathbf{f}_3 = \iiint_{V_{i,j,k}} \frac{\mathbf{x}'-\mathbf{x}_p}{|\mathbf{x}'-\mathbf{x}_p|^3}\,\mathrm{d}V. \tag{B.3}$$

The components of the integration variable in (B.3) are given by

$$\mathbf{x}' = (x', y', z'),$$

and let us introduce the quantity

$$\mathbf{r} = \mathbf{x}' - \mathbf{x}_p,$$

with $r = |\mathbf{r}|$.

We want to apply the divergence theorem on (B.3), and therefore need to find a function $\varphi(r)$ that satisfies

$$\nabla\cdot(\mathbf{r}\mathbf{r}\varphi(r)) = \frac{\mathbf{r}}{r^3},$$

thus we have

$$\nabla\cdot(\mathbf{r}\mathbf{r})\varphi(r) + \mathbf{r}\mathbf{r}\cdot\nabla\varphi(r) = 4\mathbf{r}\varphi(r) + r\mathbf{r}\varphi'(r) = \frac{\mathbf{r}}{r^3}.$$

Solving the above equation gives

$$\varphi(r) = \frac{1}{r^3}.$$

Because of the singularity on surface S_1, we can not apply the divergence theorem directly, however we can write

$$\mathbf{f}_3 = \sum_{m=2}^{6} \iint_{S_m} \frac{\mathbf{rr}}{r^3} \cdot \mathbf{n}_m \,\mathrm{d}S + \lim_{\epsilon \to 0} \iint_{S_\epsilon} \frac{\mathbf{rr}}{r^3} \cdot \mathbf{n}_\epsilon \,\mathrm{d}S + \iint_{S_\Omega} \frac{\mathbf{rr}}{r^3} \cdot \mathbf{n}_1 \,\mathrm{d}S,$$

where S_ϵ is a hemispherical surface of radius ϵ centered at $\mathbf{x}_p$ and S_Ω is the rest of the surface S_1 with a disk of radius ϵ around $\mathbf{x}_p$ has been removed. $\mathbf{n}_\epsilon$ is the unit normal vector on S_ϵ, pointing out of $V_{i,j,k}$. $\mathbf{n}_m$ is the unit normal vector on S_m, pointing out of $V_{i,j,k}$.

For the integral over S_Ω, we have

$$\mathbf{r} = (0, y' - y_j, z' - z_k),$$

and

$$\mathbf{n}_1 = (-1, 0, 0),$$

thus we get

$$\iint_{S_\Omega} \frac{\mathbf{rr}}{r^3} \cdot \mathbf{n} \,\mathrm{d}S = (0, 0, 0).$$

For the integral over surface S_ϵ, we use the spherical coordinate system,

$$\mathbf{r} = \epsilon(\cos\theta \sin\varphi, \sin\theta \sin\varphi, \cos\varphi),$$

and

$$\mathbf{n}_\epsilon = (\cos\theta \sin\varphi, \sin\theta \sin\varphi, \cos\varphi),$$

where $\epsilon, \varphi, \theta$ are respectively the radial distance, polar angle and azimuthal angle, so that

$$\iint_{S_\epsilon} \frac{1}{2r^2} \mathbf{rr} \cdot \mathbf{n}_\epsilon \,\mathrm{d}S = \lim_{\epsilon \to 0} \int_0^{2\pi} \int_{-\frac{\pi}{2}}^{\frac{\pi}{2}} \frac{1}{2r^2} \mathbf{rr} \cdot \mathbf{n}_\epsilon \epsilon^2 \sin\varphi \,\mathrm{d}\theta \,\mathrm{d}\varphi = (0, 0, 0).$$

Defining

$$s_m = \iint_{S_m} \frac{\mathbf{rr}}{r^3} \cdot \mathbf{n}_m \,\mathrm{d}S,$$

$\mathbf{f}_3$ can be written as

$$\mathbf{f}_3 = \sum_{m=2}^{6} s_m.$$

Due to the symmetry of $\mathbf{r}$ in $V_{i,j,k}$ along y and z direction , we have

$$s_2 = s_5$$

and

$$s_3 = s_6.$$

So we have the following,

$$\begin{aligned}\mathbf{f}_3 = &\iint_{S_2} \Delta y \frac{(x'-x_a, 0, z'-z_k)}{((x'-x_a)^2+(z'-z_k)^2+\frac{1}{4}\Delta y^2)^{\frac{3}{2}}}\,\mathrm{d}x'\,\mathrm{d}z' \\ &+ \iint_{S_3} \Delta z \frac{(x'-x_a, y'-y_j, 0)}{((x'-x_a)^2+(y'-y_j)^2+\frac{1}{4}\Delta z^2)^{\frac{3}{2}}}\,\mathrm{d}x'\,\mathrm{d}y' \\ &+ \iint_{S_4} \Delta x \frac{(\Delta x, 0, 0)}{(\Delta x^2+(y'-y_j)^2+(z'-z_k)^2)^{\frac{3}{2}}}\,\mathrm{d}y'\,\mathrm{d}z',\end{aligned}$$

For computation simplicity, we define

$$\bar{s}_2 = \iint_{S_2} \frac{(x'-x_a, z'-z_k)}{((x'-x_a)^2+(z'-z_k)^2+\frac{1}{4}\Delta y^2)^{3/2}}\,\mathrm{d}x'\,\mathrm{d}z',$$

$$\bar{s}_3 = \iint_{S_3} \frac{(x'-x_a, y'-y_j)}{((x'-x_a)^2+(y'-y_j)^2+\frac{1}{4}\Delta z^2)^{3/2}}\,\mathrm{d}x'\,\mathrm{d}y',$$

and

$$\bar{s}_4 = \iint_{S_4} \frac{\Delta x}{(\Delta x^2+(y'-y_j)^2+(z'-z_k)^2)^{3/2}}\,\mathrm{d}y'\,\mathrm{d}z'.$$

Thus for the calculations of $\bar{s}_2$ and $\bar{s}_3$, we consider a general form

$$\iint_S \frac{\bar{\mathbf{r}}}{(\bar{r}^2+A^2)^{3/2}}\,\mathrm{d}S, \tag{B.4}$$

where $\bar{\mathbf{r}}$ is a 2-component vector, A is a constant and $\bar{r} = \bar{\mathbf{r}}$. We want to apply the divergence theorem on (B.4), thus we need to find a function $\varphi(\bar{r})$ that satisfies

$$\nabla \cdot (\bar{\mathbf{r}}\bar{\mathbf{r}}\varphi(\bar{r})) = \frac{\bar{\mathbf{r}}}{(\bar{r}^2+A^2)^{3/2}}.$$

Solving the above equation, we get

$$\varphi(\bar{r}) = \frac{\log(\sqrt{\bar{r}^2+A^2}+\bar{r})}{\bar{r}^3} - \frac{1}{\bar{r}^2\sqrt{\bar{r}^2+A^2}}.$$

For $\bar{s}_2$,

$$S = S_2,$$

$$A = \frac{1}{2}\Delta y,$$

and

$$\bar{\mathbf{x}} = (x'-x_a, z'-z_k),$$

because of the singularity on S_2, we write

$$\bar{s}_2 = \sum_{n=2}^{4} \int_{L_{2n}} \varphi(\bar{r})\mathbf{r}\bar{\mathbf{r}}\cdot\bar{\mathbf{n}}_n\,\mathrm{d}L + \lim_{\epsilon\to 0}\int_{L_\epsilon} \varphi(\bar{r})\bar{\mathbf{r}}\bar{\mathbf{r}}\cdot\bar{\mathbf{n}}_\epsilon\,\mathrm{d}L + \int_{L_\Omega} \varphi(\bar{r})\bar{\mathbf{r}}\bar{\mathbf{r}}\cdot\bar{\mathbf{n}}_1\,\mathrm{d}L,$$

where L_{2n} are edges of S_2. L_ϵ is a semicircle with radius ϵ centered at point $\bar{\mathbf{x}}$ and L_Ω is the rest of L_{21}. $\bar{\mathbf{n}}_\epsilon$ is the unit normal of L_ϵ, pointing out of S_2. $\bar{\mathbf{n}}_n$

is the unit normal of L_{2n}, pointing out of S_2. Geometry is illustrated in figure 3.2.

For the integral over L_Ω, we have

$$\bar{\mathbf{r}} = (0, z' - z_k)$$

and

$$\bar{\mathbf{n}} = (-1, 0),$$

so that

$$\int_{L_\Omega} \varphi(\bar{r})\bar{\mathbf{r}}\bar{\mathbf{r}} \cdot \bar{\mathbf{n}}_1 \, \mathrm{d}L = (0, 0).$$

For the integral over L_ϵ, using the polar coordinates, we have

$$\bar{\mathbf{r}} = \epsilon(\cos\theta, \sin\theta),$$

and

$$\bar{\mathbf{n}}_\epsilon = -(\cos\theta, \sin\theta),$$

then

$$\begin{aligned}
&\int_{L_\epsilon} \varphi(\bar{r})\bar{\mathbf{r}}\bar{\mathbf{r}} \cdot \bar{\mathbf{n}}_1 \, \mathrm{d}L \\
&= \lim_{\epsilon \to 0} \int_{-\frac{\pi}{2}}^{\frac{\pi}{2}} -\epsilon^2(\cos\theta, \sin\theta)^3 \left(-\frac{1}{\epsilon^2(\epsilon^2 + \frac{1}{4}\Delta y^2)^{\frac{1}{2}}} + \frac{\log(\sqrt{\epsilon^2 + \frac{1}{4}\Delta y^2} + \epsilon)}{\epsilon^3}\right) \mathrm{d}\theta \\
&= (-2\log(\frac{1}{2}\Delta y), 0),
\end{aligned}$$

There is no singularity on L_{22}, L_{23} and L_{24} any more, finally,

$$\bar{s}_2 = (I_1 - 2\log(\frac{1}{2}\Delta y), 0),$$

where

$$I_1 = \int_{x_a}^{x_a + \Delta x} \Delta z(x' - x_a)\varphi(r_1) \, \mathrm{d}x' + \int_{z_k - \Delta z}^{z_k + \Delta z} \Delta x^2 \varphi(r_2) \, \mathrm{d}z',$$

with

$$r_1 = \sqrt{(x' - x_a)^2 + \frac{1}{4}\Delta z^2},$$

and

$$r_2 = \sqrt{\Delta x^2 + (z' - z_k)^2}.$$

The calculation of $\bar{s}_3$ is similar to the one of $\bar{s}_2$ with the final result

$$\bar{s}_3 = (I_2 - 2\log(\frac{1}{2}\Delta z), 0),$$

where

$$I_2 = \int_{x_a}^{x_a + \Delta x} \Delta y(x' - x_a)\varphi(r_3) \, \mathrm{d}x' + \int_{y_j - \Delta y}^{y_j + \Delta y} \Delta x^2 \varphi(r_4) \, \mathrm{d}y',$$

with

$$r_3 = \sqrt{(x' - x_a)^2 + \frac{1}{4}\Delta y^2},$$

and

$$r_4 = \sqrt{\Delta x^2 + (y' - y_j)^2}.$$

For the integral $\bar{s}_4$, defining

$$\bar{\mathbf{r}} = (y' - y_j, z' - z_k)$$

and

$$\bar{r} = |\bar{\mathbf{r}}|,$$

we seek a function that satisfies

$$\nabla \cdot (\bar{\mathbf{r}}\varphi(\bar{r})) = \frac{1}{(\bar{r}^2 + \Delta x^2)^{3/2}}.$$

Solving this equation gives

$$\varphi(\bar{r}) = -\frac{1}{\bar{r}^2\sqrt{\bar{r}^2 + \Delta x^2}}.$$

Because of the singularity at point $\bar{\mathbf{x}} = (y_j, z_k)$, we write

$$\bar{s}_4 = \int_{L_\epsilon} \varphi(\bar{r})\bar{\mathbf{r}} \cdot \bar{\mathbf{n}}_\epsilon \, \mathrm{d}L + \int_{L_\Omega} \varphi(\bar{r})\bar{\mathbf{r}} \cdot \bar{\mathbf{n}}_\Omega \, \mathrm{d}L,$$

where L_ϵ is a circle with radius ϵ centered at $\bar{\mathbf{x}}$ and L_Ω is the four edges of surface S_4. $\bar{\mathbf{n}}_\epsilon$ is the unit normal vector of L_ϵ, $\bar{\mathbf{n}}_\Omega$ is the unit normal vector of L_Ω, as shown in figure 3.3.

For the integral over L_ϵ, we use the polar coordinates,

$$\bar{\mathbf{r}} = \epsilon(\cos\theta, \sin\theta),$$

and

$$\mathbf{n}_\epsilon = -(\cos\theta, \sin\theta),$$

then

$$\lim_{\epsilon \to 0} \int_{L_\epsilon} \varphi(\bar{r})\bar{\mathbf{r}} \cdot \bar{\mathbf{n}}_\epsilon \, \mathrm{d}L = \frac{2\pi}{\Delta x}.$$

For the integral on L_Ω, there is no singularity any more and this gives

$$\begin{aligned}
&\int_{L_\Omega} \varphi(\bar{r})\bar{\mathbf{r}} \cdot \bar{\mathbf{n}}_\Omega \, \mathrm{d}L \\
&= -\Delta y \int_{z_k - \Delta z}^{z_k + \Delta z} \frac{1}{(\frac{1}{4}\Delta y^2 + (z' - z_k)^2)\sqrt{\Delta x^2 + \frac{1}{4}\Delta y^2 + (z' - z_k)^2}} \, \mathrm{d}z' \\
&- \Delta z \int_{y_j - \Delta y}^{y_j + \Delta y} \frac{1}{(\frac{1}{4}\Delta z^2 + (y' - y_j)^2)\sqrt{\Delta x^2 + \frac{1}{4}\Delta z^2 + (y' - y_j)^2}} \, \mathrm{d}y' \\
&= I_3.
\end{aligned}$$

Combining all the calculations above, we finally get

$$\begin{aligned}\mathbf{f}_3 = (&\Delta y I_1 + \Delta z I_2 - 2\Delta y \log(\frac{1}{2}\Delta y) - 2\Delta z \log(\frac{1}{2}\Delta z) \\ &+ \Delta x^2 I_3 + 2\pi\Delta x, 0, 0).\end{aligned}$$

All the line integrals I_1, I_2, I_3 are non-singular and can be calculated using numerical integration.

B.3 Calculations of singular surface integrals

When the observing point $\mathbf{x}_p$ and the integrating point are both located on the same integral surface, for instance S_1, as shown in figure 3.1, the surface integrals

$$g_1 = \iint_{S_1} \frac{1}{|\mathbf{x}' - \mathbf{x}_p|}\,\mathrm{d}S, \tag{B.5}$$

$$\mathbf{g}_2 = \iint_{S_1} \frac{\mathbf{x}' - \mathbf{x}_p}{|\mathbf{x}' - \mathbf{x}_p|^2}\,\mathrm{d}S, \tag{B.6}$$

$$\mathbf{g}_3 = \iint_{S_1} \frac{\mathbf{x}' - \mathbf{x}_p}{|\mathbf{x}' - \mathbf{x}_p|^3}\,\mathrm{d}S, \tag{B.7}$$

are singular where

$$\mathbf{x}' - \mathbf{x}_p = (0, y - y', z - z').$$

Defining

$$\bar{\mathbf{r}} = (y' - y_j, z' - z_k),$$

and

$$\bar{r} = |\bar{\mathbf{r}}|,$$

we apply the divergence theorem on (B.5), thus we need to find a function $\varphi(\bar{r})$ that satisfies

$$\nabla_{\bar{\mathbf{r}}}\varphi(\bar{r})) = \frac{1}{\bar{r}},$$

or equivalently

$$2\varphi(\bar{r}) + \bar{r}\varphi'(\bar{r}) = \frac{1}{\bar{r}}.$$

Solving the above equation, we get

$$\varphi(\bar{r}) = \frac{1}{\bar{r}}.$$

Thus g_1 is turned into

$$g_1 = \sum_{n=1}^{4} \int_{L_n} \frac{\mathbf{x}' - \bar{\mathbf{x}}}{|\mathbf{x}' - \bar{\mathbf{x}}|} \cdot \mathbf{n}_n\,\mathrm{d}L,$$

where $\bar{\mathbf{x}} = (y_j, z_k)$, $\mathbf{n}_n$ is the unit normal of L_n. There is no singularity any more and g_1 can be calculated using numerical integration.

For (B.6) and (B.7), due to the symmetry of vector $\mathbf{x}' - \mathbf{x}_p$ on S_1, we have

$$\mathbf{g}_2 = (0, 0, 0),$$

and

$$\mathbf{g}_3 = (0, 0, 0).$$

C Parallelization

This paper closely follows [2] and we therefore directly address the final numerical solving system of the EOS formulations of the 3D Maxwell's equations. For the inside domain, the updating rule follows (2.1). For the boundary part, the discretized boundary integral identities are represented by

$$M_1 \begin{pmatrix} \mathbf{E}_p^n \\ \mathbf{B}_p^n \end{pmatrix} = \begin{pmatrix} \mathbf{E}_R \\ \mathbf{B}_R \end{pmatrix}, \tag{C.1}$$

where $\begin{pmatrix} \mathbf{E}_p^n \\ \mathbf{B}_p^n \end{pmatrix}$ are the solution at the surface point $\mathbf{x}_p$ at time t^n and $\begin{pmatrix} \mathbf{E}_R \\ \mathbf{B}_R \end{pmatrix}$ are the summations of the integrals in the boundary integral representations after moving the unknowns to the left of the equations. From equation (2.1), it is easy to see that the updating for the inside domain at time now will only involve the values that are one time step before. While the solutions on the surface point $\mathbf{x}_p$ in (C.1) require both the historical values of the current density and the charge density and the historical field values of all the surface points due to the retarded integrals involved. Therefore the part of the code calculating the surface solution dominates both the memory usage and the processor usage. The calculations are therefore parallelized based on partitioning the surface into pieces and distributing each piece to separate processors, whereas the inside of the scattering object is residing on each processor. The updating processes are illustrated by the following C code where

p : index of surface point

n : index of time level

es, bs : fields solutions on surface up to time t^{n-1}

e, b : fields solutions of inside domain at time t^n

el, bl : fields solutions of inside domain at time t^{n-1}

J, P : current density and electric density up to time t^{n-1}

UpdateS(p,n,J,P,es,bs) : update surface solutions at $\mathbf{x}_p$ at time t^n

UpdateV(e,b,el,bl,es,bs,J,P,n) : update inside solutions at time t^n

```
1
2  int rank,size;// processor id and number of processors
3
4  MPI_Init(&argc,&argv);
5  MPI_Comm_size(MPI_COMM_WORLD,&size);
6  MPI_Comm_rank(MPI_COMM_WORLD,&rank);
7
8  int Nt,Ns,Nss,lp,lsize;
9  int p,index,indexeb;
10
11 lp=Ns/size;
12 lsize=3*lp;
13 double lse[lsize],lsb[lsize];
14
15 double *esurface,*bsurface;
16 esurface = (double *)malloc(Nss*sizeof(double));
17 bsurface = (double *)malloc(Nss*sizeof(double));
18
```

```
for(n=0;n<Nt;n++){
  for(p=rank*lp;p<(rank+1)*lp;p++){
      gsl_vector *lresult=gsl_vector_alloc(6);
     // update the surface values at each grid point in parallel
      lresult=UpdateS(p,n,J,P,es,bs);
      index=(p%lp)*3;
      for(i=0;i<3;i++){
        indexeb=index+i;
        lse[indexeb]=gsl_vector_get(lresult,i);
        lsb[indexeb]=gsl_vector_get(lresult,i+3);

      }
     gsl_vector_free(lresult);
   }
   //collect data from all processes
    MPI_Allgather( lse, lsize, MPI_DOUBLE, esurface, lsize,
    MPI_DOUBLE, MPI_COMM_WORLD);
    MPI_Allgather( lsb, lsize, MPI_DOUBLE, bsurface, lsize,
    MPI_DOUBLE, MPI_COMM_WORLD);

   //updating the whole surface
    for(p=0;p<Nss;p++){
      gsl_matrix_set(es,p,n,*(esurface+p));
      gsl_matrix_set(bs,p,n,*(bsurface+p));
    }

  //update the inside domain by the domain based method supported
    by the surface values
  UpdateV(e,b,el,bl,es,bs,J,P,n);

}

MPI_Finalize();
```

References

[1] Aihua Lin, Anastasiia Kuzmina, and Per Kristen Jakobsen. A boundary integral approach to linear and nonlinear transient wave scattering. *Submitted*, 2018.

[2] Aihua Lin and Per Kristen Jakobsen. A 3d nonlinear maxwell's equations solver based on a hybrid numerical method. *Submitted*, 2018.

[3] Greeshma Pisharody and Daniel S. Weile. Electromagnetic scattering from homogeneous dielectric bodies using time-domain integral equations. *IEEE Transactions on Antennas and Propagation*, 54:687–697, 2006.

[4] D. S. Weile, I. Uluer, J. Li, and D.A. Hopkins. Integration rules and experimental evidences for the stability of time domain integral equations. *International Applied Computational Electromagnetics Society Symposium(ACES)*, 2017.

[5] Jielin Li, Daniel S. Weile, and D.A. Hopkins. Integral accuracy and experimental evidence for the stability of time domain integral equations. *International Applied Computational Electromagnetics Society Symposium (ACES)*, 2018.

[6] X.Wang, R. A.Wildman, D. S.Weile, and P. Monk. A finite difference delay modeling approach to the discretization of the time domain integral equations of electromagnetics. *IEEE Transactions on Antennas and Propagation*, 56:2442–2452, 2008.

[7] A. J. Pray, N. V. Nair, and B. Shanker. Stability properties of the time domain electric field integral equationusing a separable approximation for the convolution with the retarded potential. *IEEE Transactions on Antennas and Propagation*, 60:3772–3781, 2012.

[8] M. J. Bluck and S. P. Walker. Time-domain bie analysis of large three-dimensional electromagnetic scattering problems. *IEEE Transactions on Antennas and Propagation*, 45:894–901, 1997.

[9] S. Dodson, S. P. Walker, and M. J. Bluck. Implicitness and stability of time domain integral equation scattering analysis. *Appl. Comput. Electromagn. Soc. J.*, 13:291–301, 1998.

[10] Ying Zhao, Dazhi Ding, and Rushan Chen. A discontinuous galerkin time-domain integral equation method for electromagnetic scattering from pec objects. *IEEE Transactions on Antennas and Propagation*, 64(6):2410–2415, 2016.

[11] Li Huang, Yi-Bei Hou, Hao-Xuan Zhang, Liang Zhou, and Wen-Yan Yin. A discontinuous galerkin time-domain integral equation method for electromagnetic scattering from pec objects. *IEEE Transactions on Electromagnetic Compatibility*, 2018.

[12] M. J. Bluck, M. D. Pocock, and S. P. Walker. An accurate method for the calculation of singular integrals arising in time-domain inte- gral equation analysis of electromagnetic scattering. *IEEE Trans. Antennas Propag*, 45(12):1793–1798, 1997.

[13] A. Herschlein, J. V. Hagen, and W. Wiesbeck. Methods for the evalu- ation of regular, weakly singular an d strongly singular surface reaction integrals arising in method of moments. *ACES J*, 17(1):63–73, 2002.

[14] A. G. Polimeridis and T. V. Yioultsis. On the direct evaluation of weakly singular integrals in galerkin mixed p otential integral equa- tion formulations. *IEEE Trans. Antennas Propag*, 56(9):3011–3019, 2008.

[15] MeiSong Tong, Jie Zhang, PengCheng Wang, and Jian Zhang. Electromagnetic analysis for conductive media based on volume integral equations. *IEEE Trans. Antennas Propag*, 62(12):6228–6235, 2014.

5 List of papers and contributions

1. **Aihua Lin**, Anastasiia Kuzmina, Per Kristen Jakobsen. A Boundary Integral Approach to Linear and Nonlinear Transient Wave Scattering.
Submitted.
2. **Aihua Lin**, Per Kristen Jakobsen. A 3D Nonlinear Maxwells Equations Solver Based On A Hybrid Numerical Method.
Submitted.
3. **Aihua Lin**, Per Kristen Jakobsen. On the EOS Formulation for Light Scattering. Stability, Singularity and Parallelization.
Submitted.

Aihua Lin, was responsible for the method derivations, numerical implementations, the analysis and interpretation of the results and the writings of the first draft of all the three papers.

References

[1] Georg Green. An Essay on the Application of mathematical Analysis to the theories of Electricity and Magnetism. Originally published as book in Nottingham, 1828. Reprinted in three parts in Journal f ur die reine und angewandte Mathematik Vol. 39, 1 (1850) p. 7389, Vol. 44, 4 (1852) p. 35674, and Vol. 47, 3 (1854) p. 161221.Transcribed version of the original published in ArXiv under the original title in 2008.

[2] Alexander H. H. Cheng and Daisy T. Cheng. Heritage and early history of the boundary element method. *Engineering Vnalysis with Boundary Elements*, 29:268–302, 2005.

[3] J. Berenger. A perfectly matched layer for the absorption of electromagnetic waves. *Journal of computational physics*, 114(2):185–200, 1994.

[4] S. Gedney. An anisotropic perfectly matched layer absorbing media for the truncation of fdtd lattices. *IEEE Transactions on Antennas and Propagation*, 44(12):1630–1639, 1996.

[5] K. Yee. Numerical solution of initial boundary value problems involving maxwell's equations in isotropic media. *IEEE Transactions on Antennas and Propagation*, 14(3):302–307, May 1966.

[6] A. Taflove. Application of the finite-difference time-domain method to sinusoidal steady state electromagnetic penetration problems. *IEEE Transactions on Electromagnetic Compatibility*, 22(3):191–202, 1980.

[7] A. Taflove et. al. *Computational Electrodynamics: the Finite-Difference Time-Domain Method, 3rd Ed.* Artech House Publishers, 2005.

[8] W. C. Chew and W. H. Weedon. A 3d perfectly matched medium from modified maxwell's equations with stretched coordinates. *Microwave and Optical Tech. Lett.*, 7(13):599–604, 1994.

[9] Steven G. Johnson. Notes on perfectly matched layers. Technical report, MIT, 2007.

[10] S. Ahmed. Finite-element method for waveguide problems. *Electronics Letters*, 4(18):387–389, 1968.

[11] J. P. Webb. Application of the finite-element method to electromagnetic and electric topics. *Rep. Prog. Phys.*, 58:1673–1712, 1995.

[12] J. Jin. *The Finite Element Method in Electromagnetics, 2nd Edition.* Wiley-IEEE Press, 2002.

[13] J. B. Pendry, D. Schurig, and D. R. Smith. Controlling Electromagnetic Fields. *Science*, 312:1780–1782, 2006.

[14] Ulf Leonard. Optical Conformal Mapping. *Science*, 312:1777–1780, 2006.

[15] Jinjie Liu, Moysey Brio, and Jerome V. Moloney. Transformational optics based local mesh refinement for solving Maxwell's equations. *Journal of Computational Physics*, 258:359–370, 2014.

[16] Alexander Hrennikoff. Solution of problems of elasticity by the framework method. *Journal of Applied Mechanics*, 8.4:169–175, 1941.

[17] Alexander Hrennikoff. Variational methods for the solution of problems of equilibrium and vibration. *Bulletin of the American mathematical Society*, 49:1–23, 1943.

[18] D. S. Jones. *The Theory of Electromagnetism*, volume 47 of *International Series of Monographs on Pure and Applied mathematics*. Pergamon Press, 1964.

[19] Greeshma Pisharody and Daniel S. Weile. Electromagnetic scattering from homogeneous dielectric bodies using time-domain integral equations. *IEEE Transactions on Antennas and Propagation*, 54:687–697, 2006.

[20] D. S. Weile, I. Uluer, J. Li, and D.A. Hopkins. Integration rules and experimental evidences for the stability of time domain integral equations. *International Applied Computational Electromagnetics Society Symposium(ACES)*, 2017.

[21] Jielin Li, Daniel S. Weile, and D.A. Hopkins. Integral accuracy and experimental evidence for the stability of time domain integral equations. *International Applied Computational Electromagnetics Society Symposium (ACES)*, 2018.

[22] X.Wang, R. A.Wildman, D. S.Weile, and P. Monk. A finite difference delay modeling approach to the discretization of the time domain integral equations of electromagnetics. *IEEE Transactions on Antennas and Propagation*, 56:2442–2452, 2008.

[23] A. J. Pray, N. V. Nair, and B. Shanker. Stability properties of the time domain electric field integral equationusing a separable approximation for the convolution with the retarded potential. *IEEE Transactions on Antennas and Propagation*, 60:3772–3781, 2012.

[24] M. J. Bluck and S. P. Walker. Time-domain bie analysis of large three-dimensional electromagnetic scattering problems. *IEEE Transactions on Antennas and Propagation*, 45:894–901, 1997.

[25] S. Dodson, S. P. Walker, and M. J. Bluck. Implicitness and stability of time domain integral equation scattering analysis. *Appl. Comput. Electromagn. Soc. J.*, 13:291–301, 1998.

[26] Ying Zhao, Dazhi Ding, and Rushan Chen. A discontinuous galerkin time-domain integral equation method for electromagnetic scattering from pec objects. *IEEE Transactions on Antennas and Propagation*, 64(6):2410–2415, 2016.

[27] Li Huang, Yi-Bei Hou, Hao-Xuan Zhang, Liang Zhou, and Wen-Yan Yin. A discontinuous galerkin time-domain integral equation method for electromagnetic scattering from pec objects. *IEEE Transactions on Electromagnetic Compatibility*, 2018.

[28] D. N. Pattanayak and E. Wolf. General form and new interpretation of the ewald-oseen extincition theorem. *Optics communications*, 6(3):217–220, 1972.

[29] Yong Zeng, Walter Hoyer, Jinjie Liu, Stephan W. Koch, and Jerome V. Moloney. Classical theory for second-harmonic generation from metallic nanoparticles. *Physical Review B*, 79:235109, 2009.